Fit for purpose evapotranspiration measurements: A multi-site comparison of lower-cost approaches across croplands and shrublands

Yeonuk Kim[1,*], Todd Caldwell[1], Justin L Huntington[1], Meetpal Kukal[2], María Isabel Zamora Re[3], Dragomira Zheleva[3], Richard Jasoni[4], Christian Dunkerly[1], Murphy Gardner[1], Clarence Robison[2], Dinesh Gulati[2], Shawn Naylor[5], Christopher Pearson[1], John Volk[1], Bruno Comini de Andrade[6], Robert R. Lotspeich[7]

Affiliations

1. Division of Hydrologic Sciences, Desert Research Institute, Reno, Nevada, USA
2. Department of Soil and Water Systems, University of Idaho, Boise, Idaho, USA
3. Biological and Ecological Engineering, Oregon State University, Corvallis, Oregon, USA
4. Division of Earth and Ecosystem Sciences, Desert Research Institute, Reno, Nevada, USA
5. U.S. Geological Survey, Ohio-Kentucky-Indiana Water Science Center, Indianapolis, IN, USA
6. Independent contractor, Porto Alegre, Rio Grande do Sul, Brazil
7. U.S. Geological Survey, Water Resources Mission Area, Reston, VA, USA

* Correspondence to: Yeonuk Kim (yeonuk.kim@dri.edu)

Abstract

Evapotranspiration (ET) links the water and energy cycles, yet research-grade eddy covariance (EC) systems may not be the best option to deploy operationally for water management. Emerging lower-cost ET approaches may expand fit-for-purpose observations, but their reliability across contrasting ecosystems, climates, and instrumentation configurations remains uncertain. Here, we evaluate lower-cost ET approaches across a heterogeneous network spanning agriculture and shrublands. We assess LI-710 limited-diagnostics 1-D EC, variance Bowen ratio (VBR), and residual energy (RE) ET against collocated benchmark EC, while accounting for systematic uncertainty associated with energy balance non-closure and random uncertainty arising from turbulent sampling.

Raw half-hourly LI-710 fluxes frequently contained spikes, but after quality control they generally agreed well with benchmark EC, with discrepancies at shrubland sites approaching the random uncertainty of EC. LI-710 nevertheless tended to underestimate ET across land covers, including in a replicated sensor experiment where inter-unit precision was high but a common negative bias remained. Energy-balance-closure-derived uncertainty ranges often overlapped between LI-710 and EC, demonstrating the continued value of measured available energy for diagnosing systematic uncertainty. VBR showed relatively low random uncertainty and performed best under intermediate evaporative conditions, but overestimated ET in dry shrublands and underestimated ET in high-ET, advective croplands. A sign-aware commercial VBR implementation partly reduced the latter bias, although departures from the assumed similarity of temperature and water-vapor turbulent transport remained an important limitation. RE performed comparatively well in high-EF irrigated croplands but poorly in shrublands.

These results provide field-based evidence for a fit-for-purpose framework: LI-710 is most useful when paired with rigorous quality control and energy-balance measurements, VBR is most robust under intermediate conditions, and RE is best suited to ET-dominated systems. Overall, the value of lower-cost ET measurements depends not only on sensor cost, but also on post-processing transparency, available energy measurements, ecosystem context, and the intended application.

Keywords: Evapotranspiration; Eddy covariance; LI-710; Variance Bowen ratio; Surface energy balance; Lower-cost

1. Introduction

Evapotranspiration (ET), which integrates plant transpiration with evaporation from soil and intercepted water, plays a central role in agricultural water use, groundwater discharge, ecosystem function, and weather and climate through land–atmosphere exchange (Katul et al., 2012; Wang and Dickinson, 2012; Fisher et al., 2017; Kim and Johnson, 2025). Reliable in situ ET observations are therefore needed for irrigation management, water balance assessment, satellite ET evaluation, and hydrologic research (Scott, 2010; Volk et al., 2024). Despite extensive research and the growing operational use of field-scale satellite ET products across diverse land covers (Melton et al., 2022; Volk et al., 2024; Kim et al., 2026), the limited spatial density of in situ ET observations remains a barrier to their validation and practical adoption for water resource management (Kumar et al., 2024; Huntington et al., 2026).

Eddy covariance (EC) remains the most widely used benchmark for direct ecosystem-scale turbulent flux measurements (Lee et al., 2004; Baldocchi, 2014). Although recent studies have highlighted the benefits of denser observations to better capture spatial heterogeneity in ET (Hill et al., 2017; Callejas-Rodelas et al., 2025; Liu et al., 2026), the high cost, technical complexity, maintenance requirements, and post-processing burden of EC continue to limit the spatial coverage of ET observations (Yi et al., 2024).

A growing number of lower-cost ET sensors and simplified approaches have emerged to help expand observational capacity (Huntington et al., 2026). These approaches include simplified EC systems that replace fast-response gas analyzers for water vapor measurements with slower-response measurements, such as attenuated EC (Dias et al., 2007; Hill et al., 2017), or that use 1-D in place of 3-D sonic anemometers, such as the LI-COR LI-710 (Burba et al., 2024) which also has limited diagnostic capabilities and proprietary processing. Bowen ratio-based approaches have also been simplified using flux variance theory, as in the variance Bowen ratio

(VBR) method (Wang et al., 2023), including commercial implementations such as the METER ATMOS 51 (VBR-A51) (Beverly et al., 2026). Residual energy balance approaches (RE) represent another simplified measurement category, deriving latent heat flux as the residual of available energy and sensible heat flux, with sensible heat flux estimated using either EC or surface renewal theory (Paw U et al., 1995; Wang et al., 2023). Because some commercial systems rely on instrument-specific hardware and proprietary processing, we identify them by instrument model where appropriate to avoid generalizing implementation-specific performance to a broader methodological class.

Collectively, these approaches offer potential advantages in cost, deployment density, and operational simplicity. Yet, because these approaches involve simplifying assumptions, limited diagnostics, and partially opaque processing, their performance may vary across ecosystems, conditions, and time scales (Huntington et al., 2026). Recent intercomparison studies have provided important benchmarks for evaluating lower-cost ET measurement approaches against EC (Markwitz and Siebicke, 2019; Wang et al., 2023; Billesbach et al., 2024; van Ramshorst et al., 2024; Peddinti and Kisekka, 2025; Elsadek et al., 2026; Wang et al., 2026). These studies have shown that lower-cost ET approaches can reproduce aspects of ET variability, but their performance often depends on site conditions, temporal aggregation, and the degree to which underlying assumptions are met. However, many comparisons have focused on a single method class or a limited number of land cover types. Fewer studies have evaluated multiple lower-cost ET approaches across contrasting agricultural and natural ecosystems while explicitly considering the different levels of information needed for different applications. This limits our ability to determine not only whether lower-cost methods agree with EC, but also when they are sufficiently reliable for specific purposes.

The central question is not whether these approaches can replace research-grade EC, but when they provide information that is sufficient for a given application (Huntington et al., 2026). For example, irrigation scheduling may prioritize temporal variability and relative change, whereas watershed water budget closure and satellite validation require stronger constraints on absolute ET values. Furthermore, an approach that performs well in ET-dominated irrigated agriculture may be less reliable in arid shrublands, where ET is a smaller residual of the surface energy balance. These distinctions motivate a fit-for-purpose evaluation of ET measurement techniques, in which method performance is interpreted relative to ecosystem context, measurement configuration, available diagnostics, and intended use.

A further challenge is that measurements of available energy (AE; net radiation minus soil heat flux) are often treated as secondary in benchmark EC, even though uncertainty in AE can dominate uncertainty in ET estimates (Wilson et al., 2002; Fisher et al., 2017). Net radiation and soil heat flux measurements are not required to compute EC latent heat flux, but they are essential for diagnosing energy balance closure. By contrast, Bowen ratio-based and residual energy balance methods are directly affected by AE quality. If AE is poorly measured or estimated from simplified meteorological inputs, the apparent lower costs of new ET systems may come at the expense of reliability (Huntington et al., 2026). Thus, evaluating ET sensors without evaluating surface energy balance measurements can lead to misleading conclusions.

Here, we test these issues using a heterogeneous western United States (U.S.) EC network spanning irrigated agriculture and phreatophyte shrublands. We use research-grade EC as the benchmark and evaluate lower-cost ET configurations that represent distinct simplification pathways: LI-710, two VBR implementations, and a RE approach. The network includes sites with co-located benchmark EC and either LI-710 or VBR-A51 measurements, with some sites supporting multiple evaluated approaches. We compare each lower-cost ET approach against benchmark EC and assess how performance varies with land cover, AE measurements, energy balance closure, and advective conditions.

Specific research questions: (1) what are the uncertainties of lower-cost ET approaches, and how well do they agree with benchmark EC estimates; (2) how do surface energy balance measurements affect the reliability and interpretation of each method; (3) under what conditions does each method provide reliable ET estimates; and (4) for which applications are each method fit for purpose, and where is its use less defensible? By addressing these questions across contrasting agricultural and shrubland ecosystems, this study provides field-based evidence for selecting lower-cost ET measurement approaches according to their reliability, information content, physical constraints, and intended application.

2. Site description

This study used a heterogeneous network of ET measurement sites across the western U.S., spanning irrigated agricultural systems and phreatophyte shrublands. Many of the sites are located in Nevada, including those within the NICE Net network (DRI, 2026), with additional sites in Oregon (Zheleva et al., 2026) and Idaho. Detailed information on data availability is provided in the Data Statement. The site network was designed to evaluate lower-cost ET approaches across contrasting land covers, climate, ET magnitudes, and instrumentation configurations. A summary of site characteristics, measurement periods, and available ET methods is provided in Table 1, and detailed site locations and satellite views are shown in Figure 1.

The Nevada phreatophyte shrubland sites included Railroad Valley phreatophyte shrubland (ERVP), Carson Desert phreatophyte shrubland (ECDP), Desert Valley phreatophyte shrubland (EDVP), Columbus Salt Marsh phreatophyte shrubland (ECSM), and Red Rock Road shrubland (RRR). These sites represent both groundwater-dependent vegetation and sagebrush shrublands with relatively low to moderate ET and strong seasonal variability.

The agricultural sites included Diamond Valley grass/hay (EDVG) and Railroad Valley alfalfa (ERVA) in Nevada, one alfalfa site (S2), and two orchard sites (OSU-T1 and OSU-T2) in Oregon, and three cropland sites (SnakeFlux: SF1, SF2, and SF3) in Idaho. The agricultural sites are actively managed and irrigated and span a gradient of advective influence. This gradient allows us to evaluate lower-cost ET methods across varying degrees of advection and associated violations of assumptions related to negligible horizontal transport, surface energy balance closure, and scalar similarity.

All sites were instrumented with benchmark EC systems, net radiometers, soil heat flux plates, and soil temperature and moisture probes installed between the plates and the soil surface (Table S1). Surface soil heat flux was estimated by applying a calorimetric correction for heat storage above the plates (Gao et al., 2017), with plate depths varying among sites. The study sites were also equipped with low-cost ET sensors, including either LI-710 sensor (LI-COR, Lincoln, NE) and/or commercial VBR-A51 sensor (Meter Group, Pullman, WA). At the RRR site, multiple LI-710 sensors were deployed simultaneously during part of the study period, allowing sensor-level intercomparison (Section 5.4.1). As described later in the Methods section, we also estimated VBR using high-frequency sonic temperature from the EC measurements (VBR-Ts), independently of the VBR estimates from the A51 sensor. The residual-energy approach was calculated using EC-measured sensible heat flux and measured available energy.

Table 1. Site characteristics used for evaluating lower-cost ET approaches.

Site ID	Location (latitude, longitude; elevation)	Land Cover	ET Instruments	Study Period	Operating Institution
ERVP	Railroad Valley, NV (38.355, -115.758; 1449 m)	Shrubland (phreatophyte)	IRGASON LI-710	10/22/2024 - 6/17/2026	DRI (DRI, 2026)
ECDP	Carson Desert, NV (39.578, -118.862; 1214 m)	Shrubland (phreatophyte)	IRGASON LI-710	11/26/2025 - 6/17/2026	DRI (DRI, 2026)
EDVP	Desert Valley, NV (41.452, -118.127; 1256 m)	Shrubland (phreatophyte)	IRGASON LI-710	12/22/2025 - 6/17/2026	DRI (DRI, 2026)
ECSM	Columbus Salt Marsh, NV (38.020, -117.972; 1384 m)	Shrubland (phreatophyte)	IRGASON LI-710	4/9/2026 - 7/16/2026	DRI (DRI, 2026)
RRR	Red Rock Road, NV (39.801, -119.920; 1720 m)	Shrubland (Sagebrush)	LI7500 CSAT LI-710 ATMOS 51	11/13/2024 - 3/20/2026	DRI
EDVG	Diamond Valley, NV (39.684, -115.999; 1798 m)	Cropland (grass/alfalfa mix)	IRGASON LI-710	10/26/2024 - 6/17/2026	DRI (DRI, 2026)
ERVA	Railroad Valley, NV (38.266, -115.773; 1460 m)	Cropland (alfalfa)	IRGASON LI-710	10/8/2024 - 6/17/2026	DRI (DRI, 2026)
S2	Harney County, OR (43.417, -118.614; 1254 m)	Cropland (alfalfa)	LI7500 CSAT LI-710	11/5/2024-11/6/2025	DRI
OSU_T1	Willamette Valley, OR (45.093, -123.311; 62 m)	Cropland (hazelnut orchard with cover crops)	IRGASON LI-710	4/1/2025-10/8/2025	OSU (Zheleva et al., 2026)
OSU_T2	Willamette Valley, OR (45.098, -123.311; 62 m)	Cropland (hazelnut orchard with bare ground)	IRGASON LI-710	4/1/2025-10/8/2025	OSU (Zheleva et al., 2026)
SnakeFlux 1 (SF1)	Treasure Valley, ID (43.706, -116.964; 703 m)	Cropland (Potatoes)	LI7500DS	5/8/2025-10/9/2025	UI

			WindMaster ATMOS 51		
SnakeFlux 2 (SF2)	Raft River Valley, ID (42.469, -113.258; 1348 m)	Cropland (Sugarbeets)	LI7500DS WindMaster ATMOS 51	5/14/2025-10/5/2025	UI
SnakeFlux 3 (SF3)	Raft River Valley, ID (42.447, -113.257; 1362 m)	Cropland (Wheat)	LI7500DS WindMaster	5/1/2025-8/7/2025	UI

DRI, Desert Research Institute; OSU, Oregon State University; UI, University of Idaho

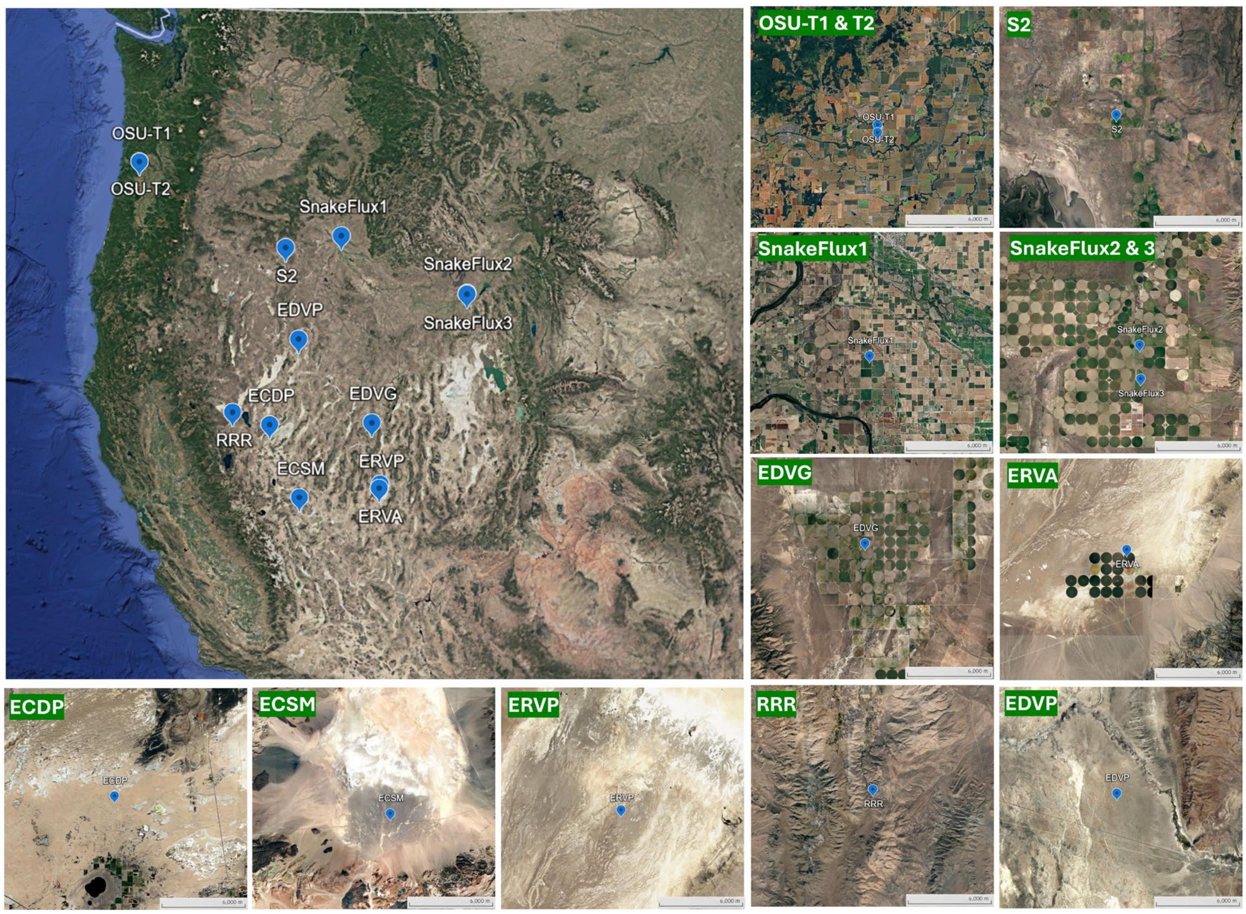

Figure 1. Locations of ET measurement sites used to evaluate lower-cost ET approaches across the western United States. The regional map shows the full study network, while inset panels provide site-scale satellite imagery for individual sites or nearby site clusters. The sites span irrigated agricultural fields and phreatophyte shrublands across Nevada, Oregon, and Idaho. Map and satellite imagery: Google Earth. Regional map data © Google, Landsat/Copernicus, SIO, NOAA, U.S. Navy, NGA, GEBCO, LDEO-Columbia, NSF, NOAA, and INEGI. Inset imagery includes Google, Airbus, and Vexcel Imaging US, Inc.

3. Methods

This study evaluated four ET observation approaches: research-grade EC, the LI-710 ET sensor, two VBR implementations, and RE. The LI-710 represents a limited-diagnostics, one-dimensional EC implementation, but because its reported fluxes depend on instrument-specific hardware and proprietary processing, we refer to this implementation throughout as LI-710. For VBR, we distinguish between two implementations: VBR-Ts, derived in this study from high-frequency EC sonic-temperature and water-vapor measurements, and VBR-A51, the implementation provided by the ATMOS 51 sensor. This notation distinguishes differences in implementation while retaining VBR as the underlying methodological framework.

These approaches differ in whether latent heat flux is measured directly or inferred from surface energy partitioning, as well as in their required measurements and underlying assumptions. Table 2 summarizes the measurement principle, required inputs, key assumptions, and implementation of each approach. Sections 3.1–3.4 provide further details for each method.

Table 2. Principles and measurement requirements of the evaluated ET approaches including eddy covariance (EC), LI-710 limited diagnostic eddy covariance, variance Bowen ratio (VBR) and residual energy (RE).

	EC	LI-710	VBR	RE
Principle	Direct covariance of vertical wind with temperature and water vapor	Direct covariance of 1-D vertical wind with water vapor	Partitions AE using a variance-based Bowen ratio	Calculate latent heat flux as residual energy (AE - H)
Required inputs	3-D sonic and fast-response gas analyzer; AE optional for diagnostics	1-D sonic and water vapor analyzer; AE optional for diagnostics	Temperature and humidity variances; measured or estimated AE	Measured or estimated AE and independent H
Key assumptions	Turbulence and footprint are well represented; required coordinate, density, and spectral corrections are valid	1-D wind and water vapor measurements adequately capture turbulent covariance; internal flow, lag, and flux-processing procedures are sufficient	Temperature and water vapor follow the scalar-similarity; AE is adequately quantified; flux direction is correctly represented when sign information is used	AE and H are adequately quantified; minor energy terms are negligible or accounted for

AE, available energy; H, sensible heat flux; 3-D, three-dimensional; 1-D, one-dimensional.

3.1. Benchmark ET measurement: eddy covariance

High-frequency EC data were processed into half-hourly turbulent fluxes using block averaging. The half-hourly turbulent latent and sensible heat fluxes were defined conceptually as:

$$\lambda E = \lambda \bar{\rho} \overline{w'q'} \quad (1)$$

$$H = c_p \bar{\rho} \overline{w'T'} \quad (2)$$

where the overbar denotes a half-hour average, primes denote deviations from the half-hour mean, c_p is specific heat of air (J kg^{-1} K^{-1}), ρ is the moist air density (kg m^{-3}), λ is latent heat of vaporization (J kg^{-1}), w is the vertical wind velocity (m s^{-1}), T is air temperature (K), q is specific humidity (kg kg^{-1}). As such, the covariance between vertical wind velocity and temperature or humidity, calculated as the mean product of their deviations from their respective means, represents the turbulent flux of heat or water vapor, respectively. λE is latent heat flux (W m^{-2}), representing ET in energy units, and H is sensible heat flux (W m^{-2}).

Strictly, turbulent water vapor flux should be formulated using a water vapor mixing ratio (Webb et al., 1980). However, for notational simplicity, Eq. (1) is written in terms of specific humidity and moist air density to parallel the sensible heat flux expression as in Wang et al. (2023), and should be interpreted as fully-corrected latent heat flux.

Raw EC data were processed using EddyPro for EDVG, ERVA, ERVP, ECDP, EDVP, ECSM, RRR, S2, SF1, SF2, and SF3 sites and EasyFlux for OSU-T1 and OSU-T2 sites. Core corrections included double coordinate rotation (Tanner and Thurtell, 1969), WPL density corrections (Webb et al., 1980), high- and low-frequency spectral corrections (Moncrieff et al., 1997; Moncrieff et al., 2004), footprint modeling (Kljun et al., 2015), and standard SSITC quality control flagging (Foken and Wichura, 1996; Mauder and Foken, 2004), although specific processing settings varied slightly among sites.

Half-hourly EC fluxes and supplementary meteorological measurements were further post-processed using a consistent workflow across sites. Quality control included SSITC quality-flag filtering where appropriate (Mauder and Foken, 2004), physical range checks using ecosystem-specific thresholds (Chu et al., 2023), median absolute deviation (MAD)-based despiking (Papale et al., 2006), and footprint-based filtering for irrigated agricultural sites (McGloin et al., 2018). MAD-based despiking was applied iteratively, and both despiking and footprint-based filtering were implemented using the openeddy R package (Šigut, 2023). A single-height storage correction was applied to EC latent and sensible heat fluxes at low-canopy sites, whereas no storage correction was applied at the high-canopy orchard sites, where a single-height correction was considered less appropriate (Burba, 2013).

Gap filling was performed using the marginal distribution sampling (MDS) method (Reichstein et al., 2005), implemented in REddyProc R package, with continuous gaps longer than 60 days left unfilled (Wutzler et al., 2018). Key meteorological observations, including net radiation, soil heat flux, air temperature, air pressure, humidity, precipitation, soil temperature and soil moisture were similarly quality controlled using physical range checks and despiking, and gap-filled where appropriate, primarily using nearby site observations.

3.2. Lower-cost ET 1: LI-710

The LI-COR LI-710 is a limited diagnostic EC sensor that applies 1-D EC principles using measurements of vertical wind speed and water vapor concentration. According to LI-COR documentation, the instrument uses 10 Hz vertical wind and water vapor measurements and reports fully processed ET and turbulent flux outputs at 30-min intervals (Table S2). The LI-710 draws ambient air through an inlet and filter to an onboard 10 Hz fast-response temperature and relative humidity sensor. The sampled ambient air is not heated or otherwise modified before measurement. A separate temperature and relative humidity sensor monitor conditions inside the instrument housing and is used only for system protection (e.g., cell temperature and humidity, Table S2). The LI-710 shuts down when the internal cell temperature falls below 5°C or the internal cell relative humidity exceeds 90% to protect the pump and electronics from condensation and water intrusion.

The LI-710 system provides fewer diagnostic variables and less processing transparency than conventional EC. Specifically, users do not have the same access to high-frequency raw covariance data or complete correction workflows available from research-grade EC systems. This places the LI-710 in the limited-diagnostics EC category (Huntington et al., 2026).

LI-710 data were processed at the half-hourly scale using the sensor-reported fluxes and flow and instrument diagnostics. Preliminary inspection identified frequent spikes in the reported ET at several sites; therefore, we applied an additional post-processing workflow rather than using the unfiltered output directly. The workflow followed the same general structure used for benchmark EC data. First, iterative MAD–based despiking and ecosystem-specific physical-range filters were applied using the openeddy R package (Papale et al., 2006; Šigut, 2023). Second, observations were also removed when available flow diagnostics indicated instrument malfunction or unreliable measurements.

More recent LI-710 firmware allows diagnostic flags to be combined with a data-quality percentage for additional filtering and provides standard deviations of measured variables that can help identify low-turbulence periods (Barker, 2025). These outputs were unavailable for most instruments used in this study because they operated with older firmware. Diagnostic flags alone were therefore not used as exclusion criteria, and quality control relied primarily on flow diagnostics, physical-range screening, and statistical despiking.

Gap filling of LI-710 ET was performed using the same MDS approach applied to benchmark EC, implemented in REddyProc (Reichstein et al., 2005; Wutzler et al., 2018). This allowed direct comparison of raw and gap-filled ET totals between LI-710 and EC where co-located measurements were available.

Except at the SnakeFlux sites, LI-710 instruments were installed at heights comparable to those of the co-located EC systems, and these paired measurements formed the primary basis of the analysis. We also evaluated instrument-to-instrument reproducibility to better characterize LI-710 measurement uncertainty. At the RRR site, six LI-710 units were temporarily deployed in a collocated cluster 10 m from the permanent EC tower for 17 days. The six units were mounted on crossarms on two separate towers with a sonic-to-sonic separation of 1.4 m. Inter-unit precision was assessed by comparing each unit against the leave-one-out mean of the other units at concurrent timestamps. This replicated comparison provides a direct measure of LI-710 repeatability that complements the MDS-based random-uncertainty estimates derived across the network. Accuracy is assessed against EC for fluxes (H and λE), and separately for flux partitioning via evaporative fraction (EF). See Section 5.4.1 and Supplementary Information Text S2 for more details.

3.3. Lower-cost ET 2: Variance Bowen Ratio

Unlike EC, which directly estimates turbulent fluxes from covariances between vertical wind velocity and scalar fluctuations, Bowen-ratio methods partition AE between sensible and latent heat fluxes. The Bowen ratio, β, is defined as the ratio of sensible to latent heat flux:

$$\beta = \frac{H}{\lambda E} = \frac{c_p \bar{\rho}\overline{w'T'}}{\lambda \bar{\rho}\overline{w'q'}} = \frac{c_p}{\lambda}\frac{\overline{w'T'}}{\overline{w'q'}} \tag{3a}$$

and latent heat flux is subsequently estimated as

$$\lambda E_\beta = \frac{R_n - G}{1+\beta} \tag{3b}$$

where R_n is net radiation (W m^{-2}), G is surface soil heat flux (W m^{-2}), and $R_n - G = AE$ is referred to as total available energy.

Whereas conventional Bowen-ratio energy-balance systems estimate β from vertical temperature and humidity gradients, the VBR method uses the ratio of scalar variances. In the VBR formulation of Wang et al. (2023),

$$\beta_{VBR} = \frac{c_p}{\lambda}\frac{r_{wT}\sigma_w\sigma_T}{r_{wq}\sigma_w\sigma_q} = \frac{c_p}{\lambda}\frac{r_{wT}}{r_{wq}}\frac{\sigma_T}{\sigma_q} \approx \frac{c_p}{\lambda}\frac{\sigma_T}{\sigma_q} \tag{4}$$

where r is the correlation coefficient, and σ is the standard deviation. In other words, VBR estimates the Bowen ratio from the ratio of temperature to humidity variability, then uses it to partition AE into sensible and latent heat fluxes. The key assumption is that the correlations of vertical velocity with temperature and water vapor are approximately equal due to scalar similarity, such that $r_{wT} \approx r_{wq}$ (Katul et al., 1995).

Although some implementations have tested the use of low-frequency temperature and humidity observations for VBR (Wang et al., 2026), the scalar variances should, in principle, be derived from high-frequency measurements, such as 10-Hz observations, to remain consistent with the theoretical derivation. All EC systems in this study provided high-frequency sonic temperature (T_s) and water-vapor measurements that could potentially be used for VBR estimation. Because sonic temperature is affected by water-vapor fluctuations, air-temperature variance should ideally be derived after correcting T_s for humidity effects. At sites equipped with an IRGASON, sonic temperature and water vapor were measured synchronously within the same integrated measurement system, allowing high-frequency air temperature to be reconstructed and its standard deviation (σ_T) to be calculated directly. At other sites, however, sonic anemometers and gas analyzers were spatially separated and differed in path averaging and high-frequency response, making an equivalent pointwise reconstruction difficult.

Nevertheless, previous studies have shown that the standard deviations of sonic and air temperature are generally similar (Liu et al., 2001). We therefore evaluated the approximation $\sigma_T \approx \sigma_{T_s}$ at sites equipped with IRGASON systems, where high-frequency air temperature could be reconstructed from synchronous sonic-temperature and water-vapor measurements. VBR estimates calculated using reconstructed air-temperature variance were compared with those obtained using sonic-temperature variance (Table S3). Because differences between the two implementations were small relative to the differences among the ET methods evaluated in this study, sonic-temperature standard deviation was used as a practical proxy for air-temperature standard deviation for the common network-wide VBR implementation.

$$\beta_{VBR-Ts} = \frac{c_p}{\lambda}\frac{\sigma_{T_s}}{\sigma_q} \quad (5)$$

We hereafter denote this approach as VBR-Ts. See Supplementary Information Text S3 for more details.

A structural limitation of VBR estimates is that standard deviations are nonnegative. Consequently, this ratio alone cannot identify flux direction, i.e., advective conditions when latent heat flux is positive but sensible heat flux becomes negative. Such conditions commonly occur under strong advection, commonly around dryland irrigation (Brakke et al., 1978; Todd et al., 2000; Tolk et al., 2006), when warm and dry air supplies additional energy for evaporation and λE may exceed locally available energy. A positive-only VBR would assign the wrong Bowen-ratio sign under these conditions and consequently underestimate λE.

The sign of the temperature–humidity covariance can be used to address this limitation (METER, 2026). When warm and humid fluctuations occur together, $\mathrm{Cov}(T, q) > 0$, whereas negative covariance can indicate a daytime inversion in which warm fluctuations are relatively dry and cool fluctuations are relatively humid. The commercial METER ATMOS 51 (VBR-A51) sensor applies this approach by assigning the sign of the measured temperature–humidity covariance to the otherwise nonnegative variance ratio (METER, 2026):

$$\beta_{VBR-A51} = sign[\mathrm{Cov}(T, q)]\,\frac{c_p}{\lambda}\frac{\sigma_T}{\sigma_q} \quad (6)$$

In the ATMOS 51 implementation, $\beta_{VBR-A51}$ is internally constrained to a minimum of -0.5, preventing unrealistically large ET estimates as $\beta_{VBR-A51}$ approaches -1.

VBR-Ts from Eq. (5) was applied consistently across the full study network to evaluate VBR behavior across ecosystems. VBR-A51 measurements were additionally available at three sites (RRR, SF1, and SF2). At these sites, VBR-Ts from Eq. (5) were compared with VBR-A51 in Eq. (6) to assess how the network-wide findings translated to a purpose-built lower-cost VBR sensor.

3.4. Lower-cost ET 3: Energy balance residual

The energy balance residual approach estimates λE as the remaining component of the surface energy balance after accounting for available energy and sensible heat flux (Amiro and Wuschke, 1987). In this approach, λE is calculated as:

$$\lambda E_{RE} = R_n - G - H \tag{7}$$

Unlike VBR, which partitions available energy using an inferred Bowen ratio, the residual approach relies directly on an independent estimate of H. Therefore, uncertainty in R_n, G, and H propagates directly into λE and ET.

Several lower or intermediate-cost ET approaches can be interpreted within this residual-energy framework because they first estimate H and then calculate λE as the residual of the surface energy balance. For example, surface renewal methods estimate H from temperature ramp structures associated with turbulent surface renewal events using fine-wire thermocouples (Paw U et al., 1995), while some VBR-based implementations combine scalar variance information with sonic temperature-based sensible heat flux estimates to consider humidity effects (Wang et al., 2023).

In this study, Eq. (7) was calculated using H from the fully processed EC workflow (details in section 3.1), which we treated as the best available estimate of sensible heat flux. This implementation was intended to evaluate the potential performance of a residual-energy approach under favorable H measurement conditions. Other implementations, such as surface renewal, may provide more lower-cost alternatives but would introduce additional uncertainty associated with estimating H.

4. Evaluation

We evaluated the lower-cost ET measurement methods across multiple complementary dimensions, primarily using EC-based ET as the benchmark. However, EC-based ET are also subject to both systematic uncertainty, including incomplete surface energy balance closure (Mauder et al., 2013), and random uncertainty associated with turbulent sampling and measurement noise (Hollinger and Richardson, 2005). We therefore evaluated the performance of the lower-cost methods while explicitly accounting for uncertainty in the EC benchmark.

4.1. Surface energy balance closure and systematic uncertainty

The EC technique is widely known to exhibit incomplete surface energy balance closure, with the measured turbulent heat fluxes, ($\lambda E + H$), typically falling below the measured available energy, (R_n - G) (Wilson et al., 2002). When minor energy terms, including changes in heat storage within the soil, vegetation, and canopy air space, are adequately quantified, the remaining energy balance residual may reflect unresolved sensible and latent heat transport associated with mesoscale circulations or horizontal and vertical advective flux divergence (Foken et al., 2006; Leuning et al., 2012; Mauder et al., 2020). This source of systematic uncertainty is particularly relevant during daytime, when convective boundary-layer processes contribute most strongly to energy balance non-closure (Stoy et al., 2013; Mauder et al., 2020).

Mauder et al. (2013) proposed quantifying the systematic uncertainty of EC turbulent heat fluxes using the daytime energy balance ratio and an energy balance closure correction that preserves the daytime Bowen ratio, following the general approach of Twine et al. (2000). While the original approach of Mauder et al. (2013) has been widely used to correct EC latent heat fluxes (e.g., Peddinti and Kisekka, 2025), it may overcorrect ET when nighttime energy imbalance is appreciable but not explicitly accounted for (Supplementary Text S1 and Figure S1).

Here, we adopted a similar framework but modified the daytime closure constraint to account for unresolved sub-daily heat storage. For each day, we assumed that the nighttime energy imbalance primarily represented unresolved changes in heat storage and the net change in unresolved heat storage cancels over a complete diurnal cycle. As such, the nighttime imbalance can be used to adjust the amount of available energy assigned to the daytime turbulent fluxes. The daytime energy balance ratio, (EBR_d), was therefore calculated as:

$$EBR_d = \frac{\sum_d(\lambda E + H)}{\sum_d(R_n - G) - S_d} \tag{8}$$

where the subscript d denotes "daytime", and S_d is the apparent daytime storage term which cannot be directly measured. S_d was assumed to be equal in magnitude and opposite in sign to the apparent nighttime storage term:

$$S_d = -S_n \tag{9}$$

where the subscript n denotes "nighttime", and the apparent nighttime storage term (S_n) was defined as:

$$S_n = \sum\nolimits_n (R_n - G) - \sum\nolimits_n (\lambda E + H) \tag{10}$$

by assuming nighttime turbulent fluxes are reliable.

We calculated EBR_d based on gap-filled λE, H, R_n, and G. To prevent unrealistically large closure corrections, EBR_d was constrained to the range 0.3-1.7. The resulting daily EBR_d was used to quantify the systematic uncertainty in each daytime half-hourly λE and H (Mauder et al., 2013).

$$\delta_{\lambda E} = \begin{cases} \lambda E \cdot (\frac{1}{EBR_d} - 1), & daytime \\ 0, & nighttime \end{cases} \tag{11a}$$

$$\delta_{H} = \begin{cases} H \cdot (\frac{1}{EBR_d} - 1), & daytime \\ 0, & nighttime \end{cases} \tag{11b}$$

where $\delta_{\lambda E}$ and δ_H represent the systematic error of EC-derived λE and H, respectively. The surface energy balance-corrected turbulent heat fluxes were then calculated by applying these adjustments during daytime while leaving nighttime turbulent fluxes unchanged (Mauder et al., 2018):

$$\lambda E_{CORR} = \lambda E + \delta_{\lambda E} \tag{12a}$$

$$H_{CORR} = H + \delta_H \tag{12b}$$

where λE_{CORR} and H_{CORR} are surface energy balance corrected latent and sensible heat fluxes, respectively (W m^{-2}).

In principle, this method preserves the daytime Bowen ratio, but the magnitude of the correction was constrained from nighttime imbalance so that the daily sum of corrected turbulent fluxes matched the daily sum of available energy (Supplementary Text S1 and Figure S1). This formulation avoids forcing closure based solely on daytime available energy, which can lead to overcorrection because unresolved heat storage effects potentially make daytime-only EBR lower than EBR calculated over the full daily cycle (Reed et al., 2018).

We did not use a multi-day window-based energy balance closure correction, such as the ONEFlux approach (Pastorello et al., 2020; Volk et al., 2023), because preserving the Bowen ratio over multi-day windows may smooth short-lived advective signals, particularly periods with negative sensible heat flux (Bambach et al., 2025). We also found that the half-hourly ONEFlux correction produced overclosure after daily aggregation, consistent with the overcorrection of ONEFlux-corrected turbulent fluxes reported by Zhang et al. (2024) (further details are provided in Supplementary Text S1 and Figure S2).

Both energy balance-corrected and uncorrected EC-derived ET were used as benchmarks when evaluating the lower-cost ET methods, thereby representing the plausible range associated with EC energy balance non-closure. We also evaluated surface energy balance characteristics using fluxes measured by both the EC systems and the LI-710 sensors. These diagnostics were used to determine the extent to which incomplete energy balance closure contributed to systematic uncertainty in the resulting ET estimates. We did not conduct an analogous systematic uncertainty analysis for the VBR-Ts or RE methods because both methods inherently impose surface energy balance closure.

4.2. Random uncertainty and replicated measurements

We quantified random uncertainty using a gap-filling residual approach (Moffat et al., 2007; Lasslop et al., 2008; Richardson et al., 2008; Kim et al., 2020). Specifically, we assumed that flux measurements (x) obtained under similar meteorological conditions represent the same underlying flux (F) (Richardson et al., 2006; Lasslop et al., 2008):

$$x_1 = F + \delta + \varepsilon_1 \tag{13a}$$

$$x_2 = F + \delta + \varepsilon_2 \tag{13b}$$

where δ is a systematic error and ε is a random error. Here, x_1 is the observed flux, whereas x_2 is the corresponding flux estimated by the gap-filling model using observations from similar meteorological conditions. Because the systematic error is assumed to be common to both estimates, it cancels when their difference is calculated. Assuming that ε_1 and ε_2 are independent and have equal variance, the standard deviation of the random error can be estimated as (Richardson et al., 2006):

$$\sigma(\varepsilon) = \frac{\sigma(x_1 - x_2)}{\sqrt{2}} \tag{14}$$

For each method, MDS gap-filling was applied while retaining all available observations, and residual variability was calculated from the difference between each original flux estimate and its corresponding MDS-estimated value (Moffat et al., 2007; Lasslop et al., 2008). Only high-quality MDS predictions with a quality-control flag of 1 were used to estimate random uncertainty. This procedure provided a consistent estimate of random uncertainty for EC, LI-710, VBR-Ts, and RE ET estimates.

4.3. Comparison with benchmark EC

We evaluated the performance of each low-cost ET method relative to benchmark EC. Comparisons were conducted at half-hourly and daily timescales using both uncorrected and energy-balance-corrected EC, as benchmark references. Method agreement was quantified using regression slope, coefficient of determination (r^2), root mean square deviation (RMSD), and mean bias error (MBE). We also examined whether sensor or method performance varied across sites, land cover types, and environmental conditions, with particular attention to periods when assumptions related to energy-balance partitioning or closure may be challenged.

We further evaluated whether each method captured temporal patterns in ET. Mean diurnal cycles were compared to assess whether each method reproduced sub-daily timing and amplitude, including peak daytime ET and nighttime behavior. Seasonal dynamics were evaluated using daily and monthly aggregated ET to assess whether each method captured longer-term variations in water use. We also compared cumulative ET through time because small biases in half-hourly or daily ET can accumulate into substantial seasonal ET differences.

All half-hourly analyses were based exclusively on quality-controlled fluxes, with MDS gap-filled values excluded. Daily-scale analyses used gap-filled ET only for days in which at least 80% of the half-hourly records consisted of measured values or high-quality MDS estimates. For time-series, cumulative-flux, and frequency-domain analyses, all gap-filled values were retained because these analyses required continuous datasets.

5. Results

5.1. Seasonal flux dynamics and energy partition gradient across sites

Before evaluating the lower-cost ET approaches, we characterized site-level energy partitioning using uncorrected benchmark EC fluxes. Daily latent and sensible heat fluxes showed distinct seasonal patterns across sites (Figure 2). Irrigated croplands were generally dominated by latent heat flux, with negative sensible heat flux occurring at the most strongly advective sites. In contrast, shrublands were dominated by sensible heat flux and had substantially lower ET.

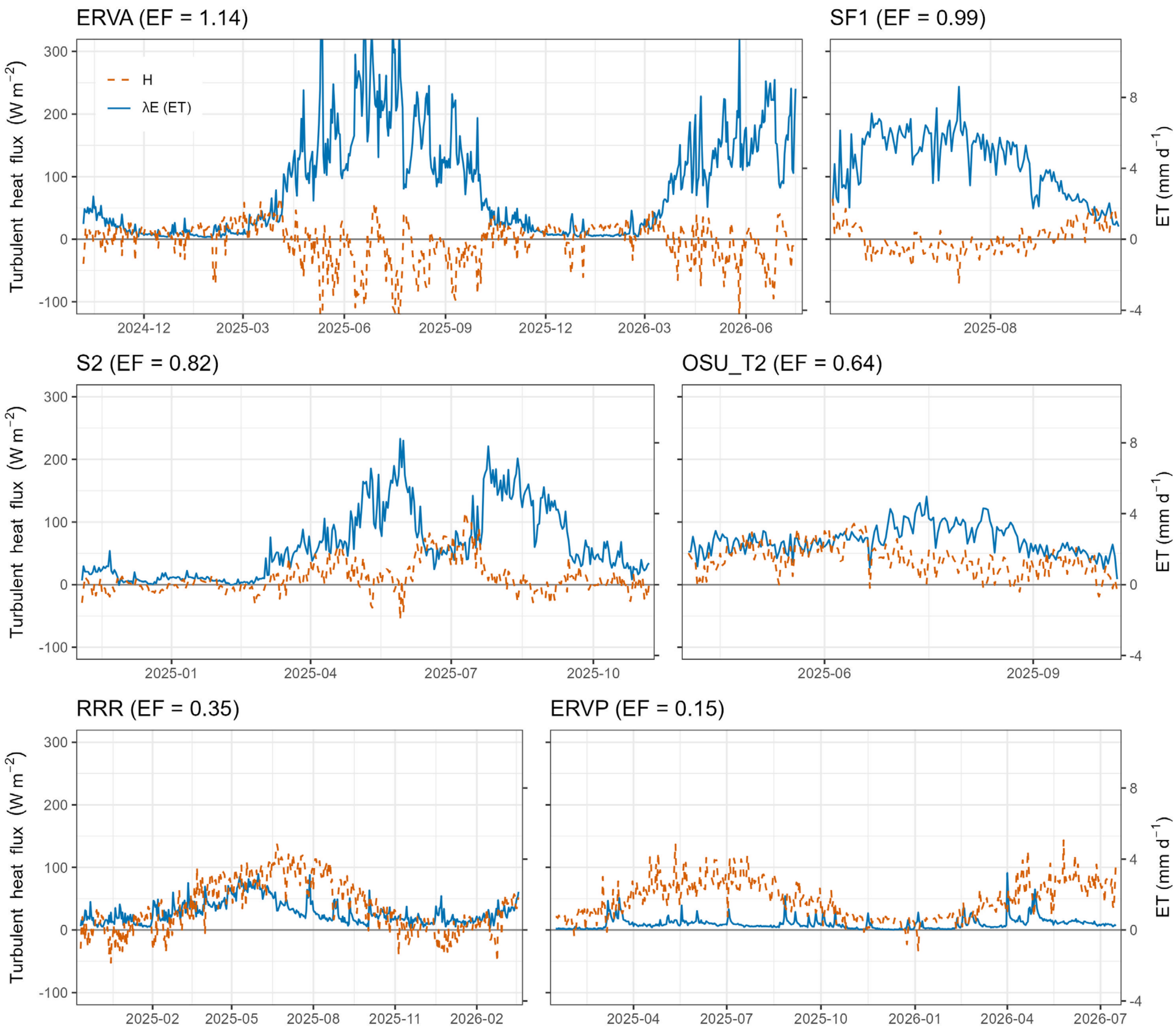

Figure 2. Seasonal dynamics of benchmark EC latent and sensible heat fluxes at selected sites spanning the observed energy partition gradient. Blue solid lines show daily latent heat flux (λE), and orange dashed lines show daily sensible heat flux (H). The secondary axis expresses λE as equivalent ET. Sites are ordered from high to low growing season (April – Oct.) evaporative fraction (EF), calculated as the ratio of summed λE to summed λE+H.

Growing season (April – Oct.) evaporative fraction (EF) was calculated as

$$EF = \frac{\sum \lambda E}{\sum(\lambda E + H)} \tag{15}$$

using uncorrected benchmark EC fluxes. Growing season EF ranged from 0.14 to 1.14 across sites (Table 3). Table 3 also summarizes the occurrence of negative sensible heat flux and unstable atmospheric conditions (i.e., atmospheric stability parameter $\xi < -0.04$) across the growing season. Across sites, EF was strongly positively correlated with the occurrence of negative sensible heat flux ($r = 0.94$) and negatively correlated with the occurrence of unstable conditions ($r = -0.85$; Figure S3). Thus, EF captured a broad site-level gradient from conditions characterized by more frequent atmospheric instability at low EF to conditions with more frequent negative sensible heat flux, indicative of advective influence, at high EF. These gradients are summarized here because the performance of some low-cost ET methods can be affected by atmospheric stability and advective conditions, as examined in the following sections.

Although not a strict threshold, EF values above the approximate theoretical value of 0.8 can indicate advective enhancement of latent heat flux, often accompanied by negative sensible heat flux (Milly and Dunne, 2016; Kim et al., 2023). Consistent with this expectation, negative sensible heat flux occurrence increased markedly between S2 (EF = 0.82; 54%) and EDVG (EF = 0.96; 64%; Table 3 and Figure S3a). ERVA had the highest EF (1.14), and negative sensible heat flux was particularly evident during periods of high ET (Figure 2), consistent with a pronounced oasis effect at the irrigated alfalfa field surrounded by arid desert vegetation (Figure 1). However, ERVA had the second-highest overall occurrence of negative sensible heat flux (68%), whereas SF2 had the highest occurrence (72% of growing season observations). Negative sensible heat flux occurrence below approximately 50%, as observed primarily at the shrubland sites, is consistent with negative fluxes being largely confined to nighttime conditions, whereas the substantially higher occurrence at several cropland sites indicates that negative sensible heat flux also occurred frequently during daytime.

Shrubland sites had much lower EF and smaller latent heat fluxes than croplands and generally experienced unstable conditions more frequently (Table 3; Figure S3). RRR, an evergreen sagebrush site, had the highest shrubland EF (0.35), with latent and sensible heat fluxes becoming similar until spring and then diverging during summer. In contrast, the phreatophyte shrubland sites were drier overall and had substantially lower EF values (0.14–0.20), with sensible heat flux dominating surface energy partitioning. These sites also had relatively high unstable-condition occurrence (41–47%), consistent with stronger sensible heating under lower-EF conditions. Because nighttime conditions are generally neutral to stable, unstable conditions occurring during more than 40% of all growing season observations suggest that unstable conditions prevailed through much of the daytime period at these phreatophyte shrubland sites. In contrast, the lower unstable-condition occurrence at most irrigated cropland sites suggests a greater prevalence of neutral or stable conditions during daytime, consistent with weaker sensible heating and, at the more strongly advective sites, frequent negative sensible heat flux.

Table 3. Growing season evaporative fraction (EF) and micrometeorological characteristics at each study site using observations available from April through October. Negative H occurrence represents the percentage of half-hourly observations with negative sensible heat flux, and unstable occurrence represents the percentage of half-hourly observations with the atmospheric

stability parameter $\boldsymbol{\xi = (z - d)/L < -0.04}$, where z is the measurement height, d is the displacement height, and L is the Monin–Obukhov length.

Land cover	Site	EF	Negative H occurrence (%)	Unstable occurrence (%)
Croplands	EDVG	0.96	64	29
	ERVA	1.14	68	28
	OSU_T1	0.59	51	33
	OSU_T2	0.64	52	33
	S2	0.82	54	39
	SF1	0.99	65	32
	SF2	1.03	72	21
	SF3	1.01	68	22
Shrublands	ECDP	0.14	46	43
	ECSM	0.20	43	47
	EDVP	0.19	43	47
	ERVP	0.15	47	41
	RRR	0.35	46	34

5.2. Uncertainty characteristics of lower-cost ET methods

5.2.1. Energy balance ratio and systematic uncertainty

Figure 3a shows the distributions of daily daytime EBR_d derived from EC and LI-710 measurements using Eq. (8). Median EC EBR_d ranged from 0.68 to 1.00 across sites, with most sites exhibiting median values near 0.8. LI-710 EBR_d was generally lower than EC EBR_d, although the magnitude of the difference varied considerably among sites. The two systems showed similar median closure at six of the ten sites with paired measurements, whereas LI-710 exhibited markedly lower closure at OSU_T1, OSU_T2, S2, and RRR.

RRR had the lowest median EBR_d for both EC and LI-710, suggesting that turbulent flux measurements were particularly challenging at this site. Unlike the other shrubland sites, which were located on relatively broad valley floors, RRR was more directly influenced by surrounding mountainous terrain (Figure 1). Terrain-induced advection may therefore have contributed to the low closure observed by both systems. These effects may have been more pronounced for the LI-710. However, the relative contributions of terrain, advection, and instrument configuration could not be isolated from the present measurements. The two orchard sites, OSU_T1 and OSU_T2, also showed substantially lower EBR_d for the LI-710 than for EC. These sites had the tallest canopies and measurement towers in the network, potentially increasing the effects of canopy heat storage, limited representation of G under drip irrigation, and differences in flux footprint. In addition, frequent declines in LI-710 flow rate were observed at these sites and may have contributed to the lower LI-710 EBR_d. S2 also exhibited a pronounced difference between EC and LI-710 closure, although no single characteristic was identified as its dominant cause.

Incomplete energy balance closure translated into systematic uncertainty in ET (Figure 3b). Mean daily systematic uncertainty varied from 0.01 to 1.33 mm d^{-1} for EC and from 0.09 to 1.03 mm d^{-1} for the LI-710. Absolute systematic uncertainty was generally greater at cropland sites than at shrubland sites, because the magnitude of the systematic uncertainty depended on both EBR_d and the magnitude of ET. Consequently, sites with relatively high ET could have large absolute uncertainty even when their EBR_d was not exceptionally low. At cropland sites where the LI-710 showed a pronounced closure deficit (i.e., OSU_T1, OSU_T2, and S2), the corresponding LI-710 ET uncertainty was substantially greater than that estimated for EC. Interestingly, however, the largest difference in systematic uncertainty between the LI-710 and EC occurred at ERVA, despite their similar median EBR_d at this site.

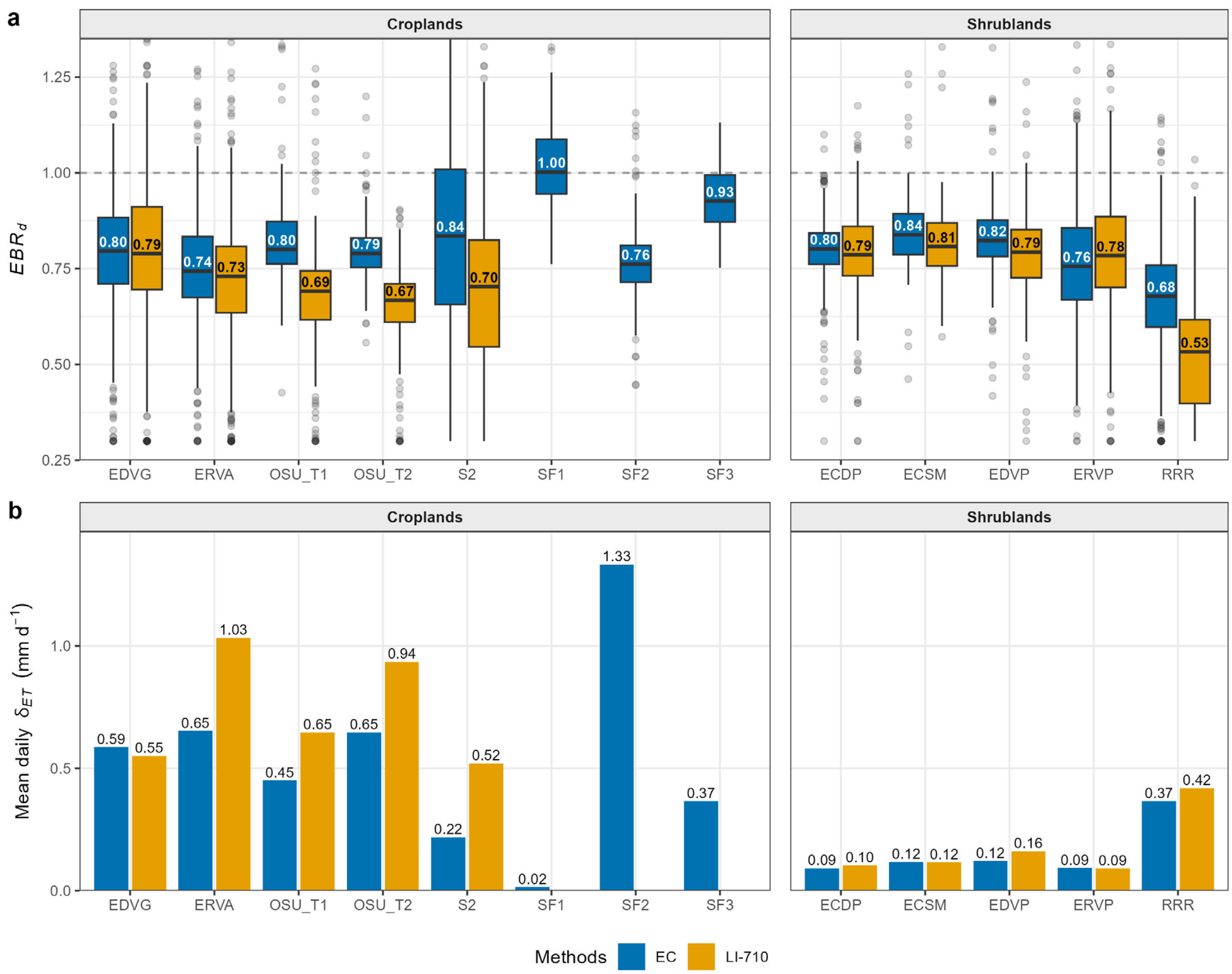

Figure 3. Surface energy balance ratio and closure-derived systematic uncertainty for EC and LI-710 measurements across sites. (a) Distributions of daily daytime EBR_d. Boxes show the interquartile range, medians, 1.5× IQR whiskers, and outliers. Numbers within the boxes indicate median EBR_d, and the horizontal dashed line represents complete energy balance closure

($\boldsymbol{EBR_d = 1}$). (b) Mean daily systematic uncertainty in ET ($\boldsymbol{\delta_{ET}}$), expressed as water depth (mm d^{-1}). Blue and orange bars indicate EC and LI-710 measurements, respectively.

5.2.2. Random uncertainty

Random uncertainty varied substantially among methods and sites and was generally greater in croplands (12 to 39 W m^{-2}) than in shrublands (6 to 14 W m^{-2}), particularly for EC and LI-710 (Figure 4a). The site-to-site variation in LI-710 uncertainty closely followed that of EC (Figure 4b). The fitted relationship was near the 1:1 line, with $R^2 = 0.97$. This indicates that conditions associated with greater random variability in EC estimates generally produced a similar increase in LI-710 uncertainty, which is expected because LI-710 is also based on turbulent flux measurements using the eddy covariance method.

VBR-Ts uncertainty exhibited a narrower range, approximately 14–20 W m^{-2} in croplands and 11–16 W m^{-2} in shrublands, than either EC or LI-710. Consequently, VBR-Ts generally had lower uncertainty than EC at cropland sites with large EC uncertainty but moderately greater uncertainty than EC at shrubland sites. RE uncertainty ranged from approximately 19 to 32 W m^{-2} in croplands and 18 to 26 W m^{-2} in shrublands. RE therefore tended to have greater uncertainty than EC at sites where EC uncertainty was relatively low, particularly in shrublands, but was comparable to or lower than EC at several cropland sites.

These contrasting patterns reflect differences in how random variability propagates through each method. VBR-Ts variability is largely controlled by variability in available energy, which is generally less affected by random noise than turbulent flux measurements. VBR-Ts therefore tended to exhibit relatively low random uncertainty when ET was moderate to high. Under low-ET conditions, however, EC and LI-710 uncertainty decreased with flux magnitude, whereas VBR-Ts uncertainty did not decline to the same extent. RE uncertainty was influenced by variability in both available energy and turbulent sensible heat flux, resulting in greater uncertainty than VBR at most sites. Moreover, low ET in the RE framework generally coincides with a larger sensible heat flux contribution, allowing RE uncertainty to remain relatively high even when EC and LI-710 uncertainty is small.

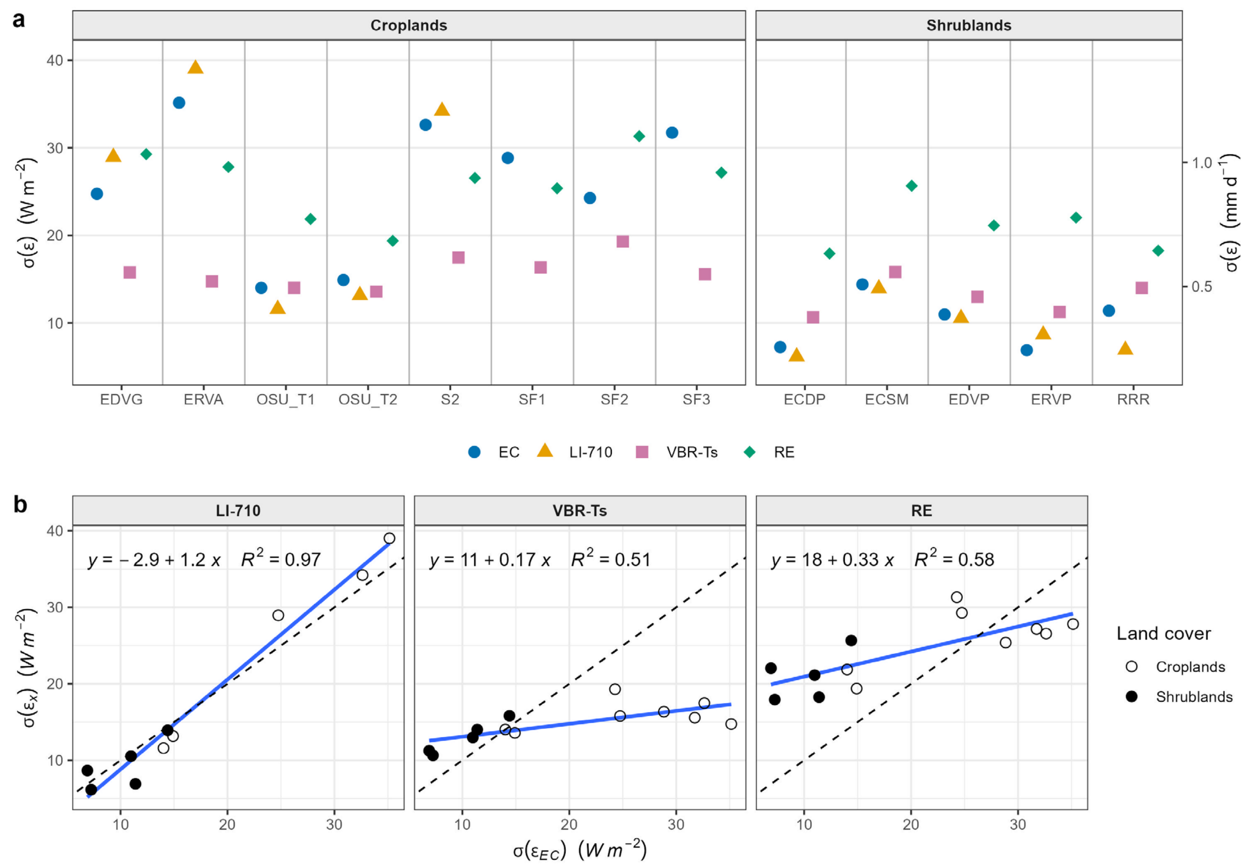

Figure 4. Site-level random uncertainty from EC, LI-710, VBR-Ts, and RE methods. Random uncertainty, $\boldsymbol{\sigma(\varepsilon)}$, was estimated as the standard deviation of the difference between each observed flux estimate and its corresponding high-quality MDS prediction, divided by $\sqrt{\mathbf{2}}$. (a) Site-level random uncertainty for cropland and shrubland sites. The secondary y-axis expresses the corresponding uncertainty as an equivalent daily ET rate. (b) Site-level random uncertainty of LI-710, VBR-Ts, and RE plotted against that of EC. Open and filled symbols represent cropland and shrubland sites, respectively. Solid blue lines show ordinary least-squares regressions, with the fitted equations and R^2 shown in each panel. Dashed lines indicate the 1:1 relationship.

We further examined how random uncertainty varied with measured ET by pooling observations within each land cover class (Figure 5); corresponding site-specific relationships are shown in Figure S4. Random uncertainty generally increased with EC λE, although the strength and shape of this dependence differed substantially among methods. At near-zero fluxes, uncertainties in EC, LI-710, and VBR-Ts estimates were relatively small, whereas RE uncertainty remained appreciable. This behavior reflects the residual formulation of RE: near-zero ET can result from the difference between two substantially larger and independently variable terms, available energy and sensible heat flux, such that their variability does not necessarily diminish as the resulting latent heat flux approaches zero. SnakeFlux sites (SF1, SF2, and SF3) were excluded because LI-710 measurements were unavailable at these sites, thereby ensuring that all methods were evaluated using the same set of sites.

Consequently, RE generally exhibited the greatest random uncertainty at low to moderate EC λE, up to approximately 150–200 W m^{-2} in both croplands and shrublands. At higher fluxes, however, uncertainties in the turbulent flux methods increased more rapidly. In croplands, EC uncertainty increased to approximately 50–60 W m^{-2} and then largely plateaued, whereas LI-710 uncertainty continued to increase linearly beyond approximately 300 W m^{-2}, reaching more than 130 W m^{-2} in the highest-flux bin (800 W m^{-2}). The site-specific results indicate that this strong increase was most evident at EDVG and ERVA, while EC and LI-710 uncertainties remained more comparable at the OSU sites (Figure S4). In shrublands, EC and LI-710 uncertainties remained below uncertainties of RE and VBR-Ts over most of the observed flux range, although LI-710 increased rapidly in the highest-flux bin and slightly exceeded VBR-Ts.

VBR-Ts displayed the weakest dependence on flux magnitude in croplands. Its uncertainty increased at low fluxes but then remained near approximately 20–30 W m^{-2}, making it the least uncertain method under moderate- to high-ET cropland conditions. In shrublands, VBR-Ts uncertainty increased more consistently with EC λE, but it generally remained intermediate between the turbulent flux methods and RE. Overall, these results demonstrate that the relative random uncertainty of the methods depends strongly on ET magnitude: RE is particularly uncertain when small latent heat flux is obtained as the residual of larger energy-balance terms, whereas LI-710 becomes increasingly uncertain under very high-flux conditions.

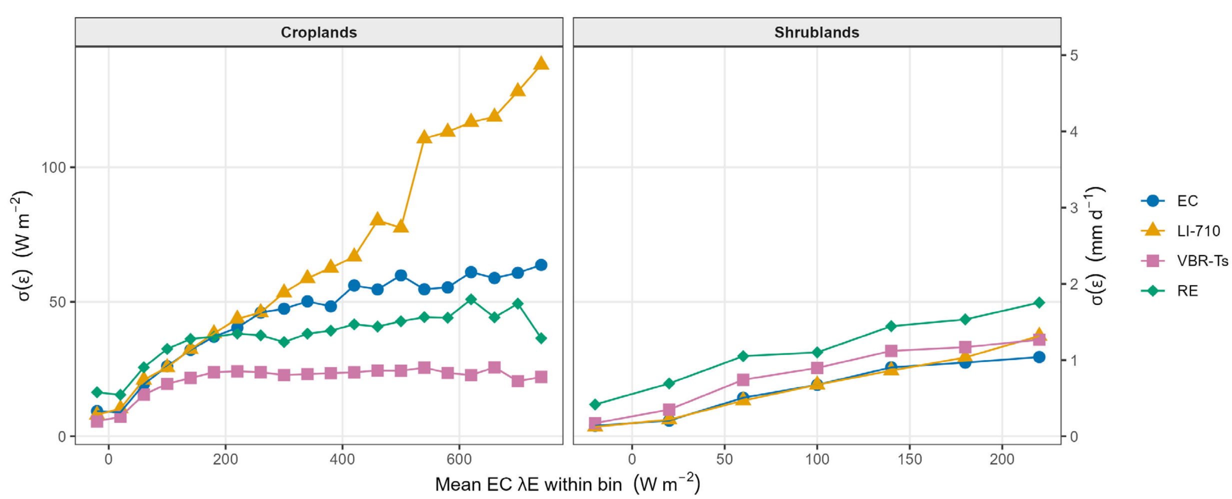

Figure 5. Dependence of random uncertainty on flux magnitude. Observations were pooled across sites within each land cover class and grouped into equal-width bins according to measured EC latent heat flux (λE). Individual colored symbols indicate random uncertainty, $\boldsymbol{\sigma(\varepsilon)}$, for the respective method calculated within each bin for EC, LI-710, VBR-Ts, and RE. The

x-coordinate represents the mean EC λE within each bin. The secondary y-axis expresses uncertainty as an equivalent ET rate.

5.3. Agreement of lower-cost ET methods with EC benchmarks

5.3.1. Root-mean-square difference relative to EC benchmarks

At the half-hourly scale, the LI-710 generally showed the closest agreement with EC, although its apparent performance depended on whether closure correction was applied to either system (Figure 6 for RMSD; Figure S5 for percent RMSD normalized by mean ET magnitude). Relative to measured EC, uncorrected LI-710 had the lowest or among the lowest RMSD at nearly all sites. ERVA was the main exception, consistent with the large closure-related systematic uncertainty and high LI-710 random uncertainty identified at this site (Figures 3 and 4). When uncorrected LI-710 was compared directly with EBR-corrected EC, RMSD increased, particularly in croplands, because the benchmark ET increased while the LI-710 closure deficit remained unresolved. When both EC and LI-710 were EBR-corrected, however, RMSD was again among the lowest of the evaluated methods.

To interpret these differences relative to uncertainty in the EC benchmark, Figure 6 also shows the site-specific value of $\sqrt{2}\sigma(\varepsilon_{\mathrm{EC}})$, where $\sigma(\varepsilon_{\mathrm{EC}})$was estimated from the MDS residual analysis. This value represents the expected RMSD between two independent measurements having random uncertainty equal to that of EC and therefore provides a reference for EC-equivalent random performance. At most shrubland sites, RMSD between LI-710 and measured EC approached this reference level, indicating disagreement comparable to that expected between two measurements with EC-like random uncertainty. In croplands, by contrast, RMSD for all lower-cost methods remained above this reference, indicating additional effects of method-specific uncertainty, energy balance closure, and greater turbulent variability.

VBR-Ts generally had intermediate half-hourly RMSD. In shrublands, it provided the second-closest agreement after LI-710, although its RMSD remained above the EC-equivalent random-uncertainty reference. In croplands, VBR-Ts performance was more condition dependent. It showed relatively low RMSD at the OSU orchard sites, where sensible heat flux was predominantly positive and ET was largely constrained by local available energy. VBR-Ts agreement weakened at more strongly advective sites, where negative sensible heat flux allowed ET to approach or exceed locally measured available energy.

RE showed the strongest contrast between land-cover classes. In shrublands, it consistently had the highest half-hourly RMSD relative to both EC benchmarks. In croplands, however, RE showed relatively low RMSD against EBR-corrected EC at several high-EF and strongly advective sites, including ERVA, SF2, and SF3. This indicates that the residual framework can represent high ET supported by negative sensible heat flux but becomes unreliable where ET is small relative to available energy and sensible heat flux.

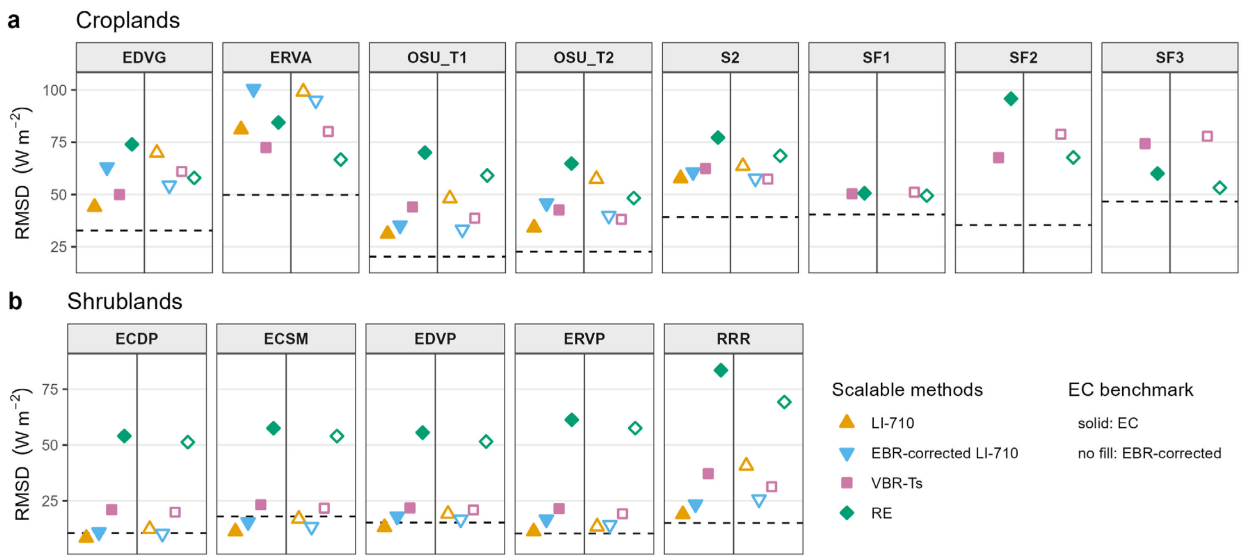

Figure 6. Site-level agreement of lower-cost ET methods with EC benchmarks at the half-hourly timescale. Root-mean-square difference (RMSD) was calculated from paired half-hourly λE estimates for (a) cropland and (b) shrubland sites. Filled symbols show RMSD relative to measured EC, whereas open symbols show RMSD relative to EBR-corrected EC. The horizontal dashed lines indicate $\sqrt{2}\sigma(\varepsilon_{\mathrm{EC}})$, where $\sigma(\varepsilon_{\mathrm{EC}})$ is the random uncertainty of site-specific EC.

Representative time series further illustrated these method-specific differences (Figure 7). At both the ECSM shrubland and ERVA cropland sites, LI-710 reproduced much of the short-term variability and timing observed by EC. In contrast, VBR-Ts exhibited smoother diurnal patterns because it was strongly constrained by available energy, which generally varied more smoothly than turbulent latent heat flux. RE also showed a relatively smooth daytime cycle but greater variability during nighttime. At ECSM, RE remained above the EC uncertainty range during daytime, whereas VBR-Ts was generally closer to the EBR-corrected EC estimate. At ERVA, VBR-Ts and RE largely followed the diurnal cycle of available energy, while EC and LI-710 exhibited greater short-term variability and some differences in the timing and shape of daytime fluxes. These offsets may partly reflect heat-storage terms and transient turbulent processes that temporarily decouple measured available energy from turbulent fluxes.

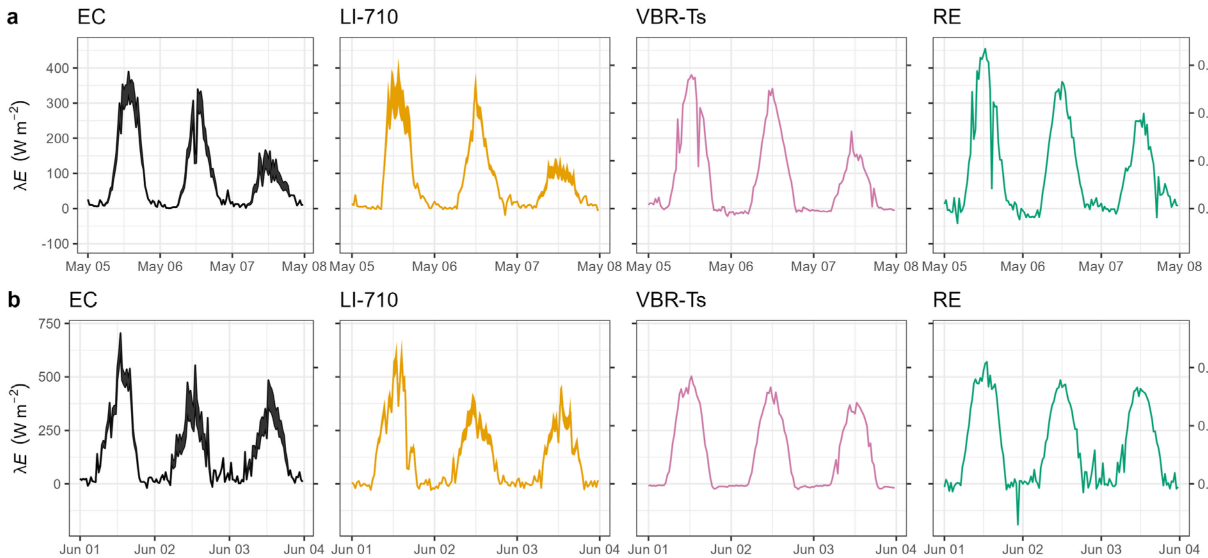

Figure 7. Representative half-hourly time series of ET. (a) three-day period following rainfall at the ECSM shrubland site (5–7 May 2026) and (b) three-day irrigated period at the ERVA cropland site (1–3 June 2026). Columns show EC, LI-710, VBR-Ts, and RE estimates, respectively. Shading around EC and LI-710 represents the range between measured and EBR-corrected EC latent heat flux, reflecting systematic uncertainty.

After aggregation to the daily scale, LI-710 was no longer uniformly the lowest-RMSD method (Figure 8 for RMSD; Figure S6 for percent RMSD normalized by mean ET magnitude). Its half-hourly advantage was partly attributable to the ability of two turbulent-flux systems to reproduce similar sub-daily timing and variability. Daily integration reduced this advantage by allowing short-term positive and negative differences to cancel. It also reduced the importance of the smoother response and phase offsets observed for VBR-Ts and RE.

Daily LI-710 RMSD nevertheless remained low in shrublands, particularly when compared using consistent closure treatments. In croplands, uncorrected LI-710 was less consistently superior to VBR-Ts or RE, and ERVA continued to show relatively large disagreement. Applying EBR correction to both EC generally improved daily agreement, although some differences remained at sites with substantial LI-710 closure deficits.

After daily aggregation, the daily RMSD for VBR-Ts was comparable to, or lower than, that of uncorrected LI-710 at several cropland sites, indicating that part of its half-hourly disagreement arose from smoothing and timing differences rather than errors in integrated daily ET. VBR-Ts continued to perform well in the lower-EF OSU orchards but showed larger errors relative to EBR-corrected EC at strongly advective sites.

RE exhibited the largest improvement after daily aggregation, but primarily in croplands. Relative to EBR-corrected EC, RE produced the lowest or among the lowest daily RMSD at

EDVG, ERVA, S2, SF1, SF2, and SF3. Sub-daily discrepancies associated with phase offsets, heat storage, and turbulent variability therefore largely canceled over the daily cycle. RE remained less successful in the OSU orchards, where unresolved canopy or biomass heat storage may be important, and daily aggregation did not resolve its large errors in shrublands. Thus, temporal aggregation reduced errors arising from sub-daily dynamics but did not eliminate ecosystem-dependent limitations in the underlying method formulations.

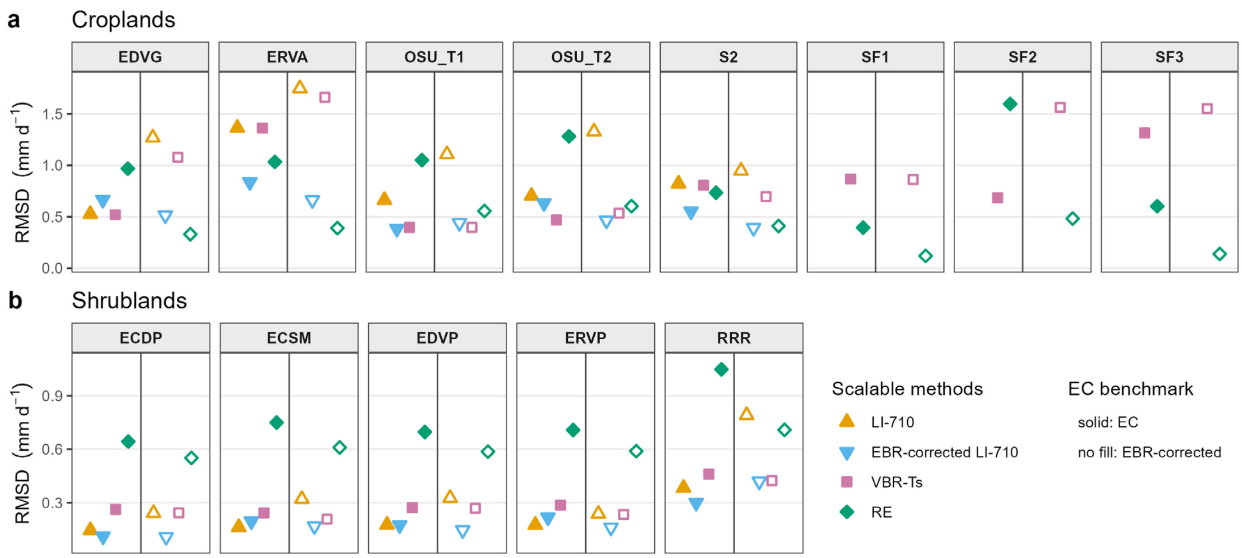

Figure 8. Site-level agreement of lower-cost ET methods with EC benchmarks at the daily timescale. Root-mean-square error (RMSD) was calculated from paired daily ET estimates for (a) cropland and (b) shrubland sites. Filled symbols show RMSD relative to measured EC, whereas open symbols show RMSD relative to EBR-corrected EC.

5.3.2. Mean bias error relative to EC systematic uncertainty

Daily mean bias error (MBE) was evaluated relative to uncorrected EC, which was treated as the primary benchmark (Figure 9). Absolute MBE is shown in Figure 9a, while Figure 9b expresses the same bias relative to the mean daily uncorrected EC ET. Positive values indicate overestimation and negative values indicate underestimation. The gray shaded regions represent the mean increase in EC ET that would result from applying the EBR correction. Thus, a method falling within the shaded range produced ET between the uncorrected and EBR-corrected EC estimates. The shaded range represents closure-related systematic uncertainty in the EC benchmark rather than a statistical confidence interval.

Uncorrected LI-710 estimates showed little bias at most shrubland sites but generally underestimated EC ET in croplands. The negative PBIAS was particularly evident at ERVA, the OSU orchard sites, S2, and RRR where LI-710 systematic uncertainty was relatively large.

Applying EBR correction to the LI-710 shifted its bias upward and generally brought the estimates within or closer to the EC systematic-uncertainty range. This indicates that much of the apparent LI-710 to EC bias was associated with differences in energy balance closure. Nevertheless, EBR-corrected LI-710 remained below the upper closure-corrected EC bound at most sites.

VBR-Ts bias was more dependent on ecosystem, atmospheric stability, and advective conditions (Figure 9). At the OSU orchards, VBR-Ts estimates fell within the EC systematic-uncertainty range, indicating agreement with the plausible range between uncorrected and corrected EC. At more strongly advective cropland sites, however, VBR-Ts generally underestimated uncorrected EC or remained near its lower bound. In shrublands, the absolute VBR-Ts bias appeared modest because daily ET was small. When normalized by mean EC ET, however, VBR-Ts biases were commonly approximately 20–50%, demonstrating that these errors were not negligible relative to the magnitude of shrubland ET.

RE generally overestimated EBR-corrected EC (upper bound), but the interpretation differed sharply between croplands and shrublands (Figure 9). At several high-EF cropland sites, particularly the SnakeFlux sites, RE estimates near the EC systematic-uncertainty range. At the lower-EF orchard sites, RE remained above the upper uncertainty bound. In shrublands, RE substantially exceeded the EC systematic-uncertainty range.

The relationship between relative MBE and growing season EF further clarified these method-specific patterns (Figure 10). LI-710 bias showed no significant relationship with EF, either before or after EBR correction, indicating comparatively consistent performance across the observed EF gradient. At most sites, LI-710 systematically underestimated ET but EBR-corrected LI-710 fell within the EC systematic-uncertainty range. In contrast, VBR-Ts bias declined strongly with increasing EF ($R^2 = 0.83, p < 0.01$). This relationship followed the micrometeorological gradient associated with EF (Table 3; Figure S3): VBR-Ts tended to overestimate ET at low-EF sites with more frequent unstable conditions, while bias became increasingly negative toward high-EF sites characterized by more frequent negative sensible heat flux. VBR-Ts performed best at the lower-EF OSU orchard sites, modestly overestimated ET in dry shrublands, and modestly underestimated ET as EF increased and sensible heat flux became negative. RE showed a more rapid decline in bias with increasing EF ($R^2 = 0.76, p < 0.01$).

Pooled daily comparisons further demonstrated that these bias patterns varied systematically with growing season evaporative fraction (Figure 11). The LI-710 provided the most consistent agreement across the EF gradient when energy balance diagnostics were used, although uncorrected estimates tended to underestimate EC under high-EF conditions. VBR-Ts performed best at the lower-EF OSU orchard sites, but increasingly underestimated ET as EF increased and sensible heat flux became negative, while modestly overestimating ET in dry shrublands. RE agreement improved at high EF because ET became large relative to unmeasured storage and other minor energy-balance terms. At low EF, particularly in shrublands, ET represented a small residual between substantially larger available-energy and sensible-heat-flux components, amplifying errors in the RE estimate. Thus, comparison with the EC systematic-uncertainty range helps distinguish apparent disagreement caused by benchmark closure uncertainty from method-specific biases that persist beyond the plausible EC range.

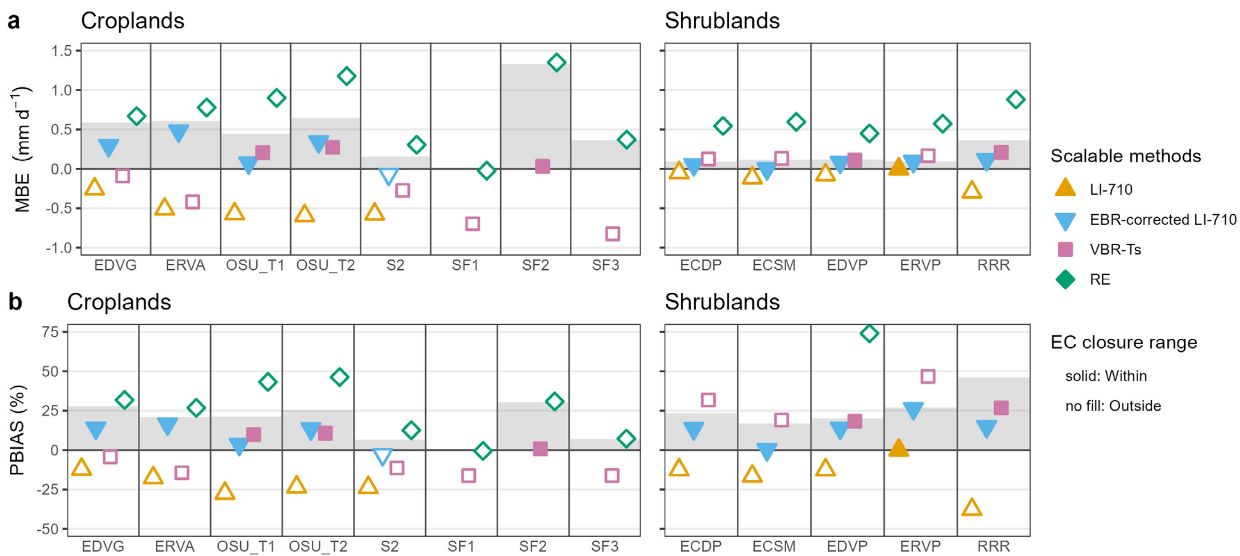

Figure 9. Site-level bias of lower-cost ET methods with EC benchmarks at the daily timescale. Mean bias error (MBE) was calculated from paired daily ET estimates for cropland and shrubland sites and is shown as (a) mean bias (MBE) (mm d^{-1}) and (b) percent relative bias (PBIAS) normalized by mean daily measured EC ET (%). Positive values indicate overestimation and negative values indicate underestimation relative to measured EC. Gray shaded areas represent the EBR-derived systematic uncertainty of the EC benchmark, extending from zero to the mean difference between EBR-corrected and measured EC. Filled symbols indicate that the bias falls within the EBR-derived systematic uncertainty range of EC, whereas open symbols indicate bias outside this range. In panel (b), relative MBE values exceeding 100%, including RE at several shrubland sites, are outside the displayed range and are omitted.

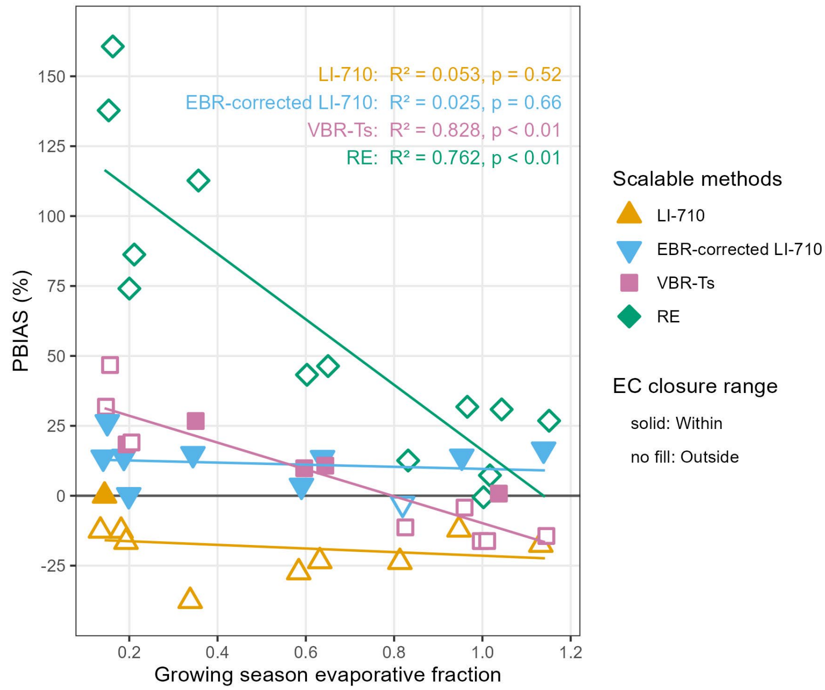

Figure 10. Relationship between growing-season evaporative fraction and MBE of lower-cost ET methods. Each symbol represents the site-level PBIAS of a lower-cost ET method relative to uncorrected EC, normalized by the mean daily EC ET and expressed as a percentage. Positive values indicate overestimation and negative values indicate underestimation. Colors and shapes distinguish LI-710, EBR-corrected LI-710, VBR-Ts, and RE. Filled symbols indicate that the bias falls within the EBR-derived systematic uncertainty range of EC, whereas open symbols indicate bias outside this range. Solid lines show ordinary least-squares regressions for each method. Corresponding coefficients of determination (R^2) and p-values are shown in matching colors.

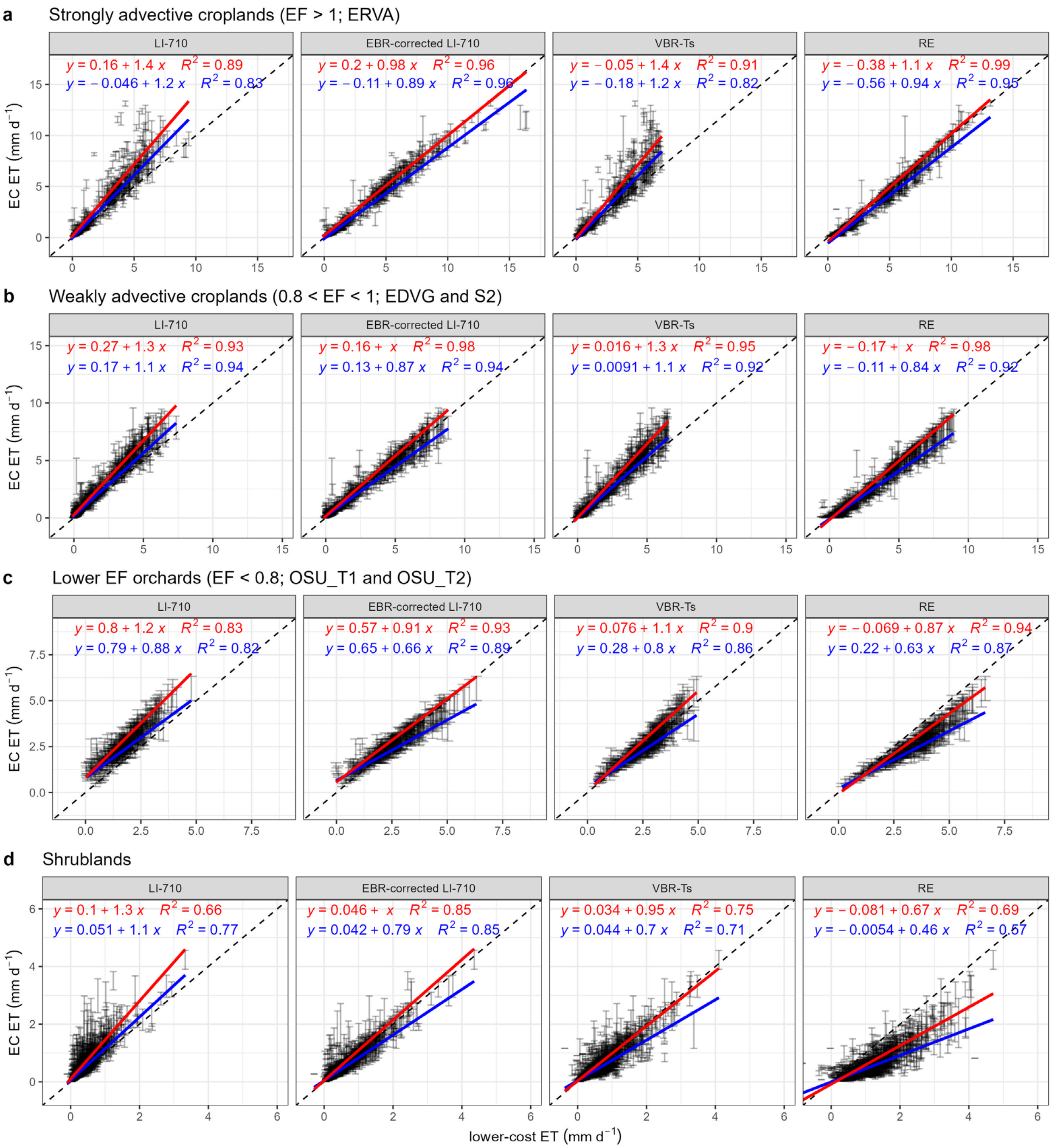

Figure 11. Daily agreement between lower-cost ET and EC ET across land-cover and growing season evaporative fraction (EF) regimes. Paired daily ET estimates are shown for (a) strongly advective cropland with EF greater than 1 (ERVA), (b) weakly advective croplands with 0.8 < EF < 1 (EDVG and S2), (c) lower-EF orchards with EF < 0.8 (OSU-T1 and OSU-T2), and (d) shrublands. Each vertical gray segment connects the measured EC and its EBR-corrected value. Blue and red lines show ordinary least-squares regressions against measured and EBR-corrected EC ET, respectively, with the corresponding regression equations and R^2 shown in

each panel. Dashed lines indicate the 1:1 relationship. SF1, SF2, and SF3 were excluded for this analysis.

5.4. Additional method-specific evaluations

To evaluate aspects of method performance that were not fully captured by the network-wide uncertainty and EC-agreement analyses, we conducted targeted evaluations of the LI-710 sensor and VBR implementation sensitivity.

5.4.1. LI-710 side-by-side evaluation

A six LI-710 sensor cluster was temporarily collocated with the permanent RRR EC and LI-710 at RRR (see Text S2). The quality-controlled time series and cumulative flux are shown in Figure S7 and S8 for the 17-day period. The six units were installed with a minimum sonic-to-sonic separation of 1.4 m, and analysis by wind direction showed no detectable neighbor-induced wake bias (Figure S9). One sensor was identified as an outlier against the group mean with ambient temperature biased +6.9 °C and its humidity slope of 0.622. It was removed. Precision was assessed between the 5 units and accuracy against the EC.

Over 732 concurrent half-hours, the five-unit cluster agreed on λE to within a slope of 0.973 to 1.044 and a bias of -1.28 to +1.17 W m^{-2}, with residual standard deviation (SD) of 6.2–9.6 W m^{-2} and 2.6–4.0 W m^{-2} (median absolute deviation, MAD) (Table 4). This direct replicate-based precision is conceptually consistent with, but distinct from, the MDS-based random uncertainty evaluated across sites in Section 5.2.2. H agreed comparably in slope (0.933 to 1.065) but with roughly 2 times the scatter (14.8–24.7 W m^{-2} SD), reflecting the larger magnitude of H at this site and the arid conditions experienced during the test period, rather than a difference in sensor precision. Individual sensor precision was a function of flux magnitude and was proportional (Figure S10).

Each LI-710 also reports ambient air temperature, relative humidity and barometric pressure. Comparing these across units separates a flux-processing disagreement from a sensor calibration fault. Among the five units the agreement is close: temperature biases span -0.15 to +0.18 °C with 0.15 °C typical scatter, humidity slopes span 0.980 to 1.046 with 0.36 %RH scatter, and pressure slopes span 0.996 to 1.003 with 0.009 kPa scatter.

Table 4. LI-710 precision against the leave-one-out mean, for every measured variable (n = 732 half-hours). Every column gives the minimum and maximum across the five-unit reference pool, so the width of each entry is the unit-to-unit spread in that quantity.

Variable	Units	Slope	Bias	Residual SD	Residual MAD
Latent heat flux	W m^{-2}	0.973–1.044	-1.28 to +1.17	6.2–9.6	2.6–4.0
Sensible heat flux	W m^{-2}	0.933–1.065	-1.69 to +0.72	14.8–24.7	9.9–18.0

Air temperature	°C	0.995–1.004	-0.15 to +0.18	0.13–0.18	0.12–0.20
Relative humidity	%	0.980–1.046	-0.48 to +0.58	0.30–0.42	0.26–0.42
Barometric pressure	kPa	0.996–1.003	-0.351 to +0.422	0.005–0.015	0.005–0.015

Sensor accuracy was assessed against the collocated EC. Over 731 concurrent half-hours and with unclosed energy balance, the LI-710 underestimates both λE and H. The five-unit ensemble gives an λE slope of 0.868 with a mean bias of -4.40 W m^{-2} and RMSD 14.6 W m^{-2}, and an H slope of 0.914 with mean bias -9.98 W m^{-2} and RMSD 22.5 W m^{-2}. The direction and magnitude of the λE underestimate are consistent with Peddinti and Kisekka (2025).

Although the LI-710 underestimates both fluxes in absolute terms, the energy partition is preserved. The five-unit ensemble reproduces the EC evaporative fraction with a slope of 1.009 and a mean bias of -0.0003 EF units (n = 300); the six-unit ensemble is equivalent (1.000, -0.0047). The RRR LI-710, the permanent installation on the EC tower 6 m from the cluster, is reported alongside the ensemble in Table 5. It is biased lower than the cluster with an λE slope of 0.746 and mean bias -8.34 W m^{-2}, and an H slope of 0.840 with mean bias -7.55 W m^{-2}, over 480 periods; however, the partitioning (EF slope 1.072) is consistent.

Table 5. LI-710 accuracy against EC for both fluxes and for evaporative fraction, as measured (unclosed). The ensemble is the cluster of five collocated units; RRR LI-710 is the permanent installation at the EC-tower. It is evaluated over its own valid period, hence the smaller n. Bias is the mean bias error (MBE); flux bias and RMSD are in W m^{-2}; EF is unitless and its final column is the SD of the difference.

Variable	Series	n	Slope	MBE	RMSD or SD
Latent heat flux	five-unit ensemble	731	0.868	-4.40	14.59
Latent heat flux	RRR LI-710	480	0.746	-8.34	17.82
Sensible heat flux	five-unit ensemble	731	0.914	-9.98	22.49
Sensible heat flux	RRR LI-710	480	0.840	-7.55	22.06
Evaporative fraction	five-unit ensemble	300	1.009	-0.0003	0.0668
Evaporative fraction	RRR LI-710	158	1.072	-0.0204	0.0651

Both precision and accuracy were strongly dependent on daylight (shortwave radiation >0 W m^{-2}) versus nighttime. The between-unit residual scatter is 10.4 W m^{-2} by day against 4.2 at night for λE, and 23.5 against 11.4 for H (Table 6). Precision degrades with flux magnitude rather than with time of day as such; the diel signal is largely the magnitude dependence. The accuracy against EC is almost entirely a daytime phenomenon. Mean λE bias is -8.97 W m^{-2} during the day but +0.81 W m^{-2} at night, and mean H bias -17.41 against -1.54 W m^{-2}. The pooled mean biases therefore understate the daytime disagreement and overstate the nighttime.

Table 6. Residual statistics (W m^{-2}) split between day and night. Pooled between-unit mean residuals are omitted as they are zero carry no information (see Supplemental Text 2).

Comparison	Flux	Day SD	Night SD	Day mean	Night mean
Between units (precision)	λE	10.41	4.22		
Between units (precision)	H	23.55	11.42		
Unit - EC (accuracy)	λE	17.96	8.73	-8.97	+0.81
Unit - EC (accuracy)	H	28.04	18.50	-17.41	-1.54

5.4.2. VBR-A51 evaluation

The comparison between VBR-Ts and VBR-A51 is summarized in Figure 12. It should be noted that this comparison was restricted to periods with concurrent VBR-A51 observations and therefore does not necessarily reproduce the site-level evaluations presented in the preceding multi-method analysis.

During periods when VBR-A51 assigned a positive Bowen-ratio sign, VBR-Ts and VBR-A51 produced nearly identical half-hourly latent heat flux estimates at all three sites, with regression slopes of 1.06 at RRR, 1.06 at SF1, and 1.05 at SF2 (Figure 12a). This close agreement further supports the use of sonic-temperature variance as a practical proxy for air-temperature variance, consistent with the comparison between humidity-corrected and sonic-temperature-based VBR estimates presented in Supplementary Text S3.

In contrast, when VBR-A51 assigned a negative sign, it produced larger positive latent heat flux when $R_n - G > 0$ and more negative latent heat flux when $R_n - G < 0$, with regression slopes of 2.62, 1.21, and 1.23 at RRR, SF1, and SF2, respectively. Thus, the primary divergence between the two implementations occurred when covariance-derived sign information allowed VBR-A51 to represent negative Bowen ratios. Under positive available energy, this allowed latent heat flux to exceed $R_n - G$, whereas under negative available energy it increased the magnitude of negative latent heat flux.

The effect of this sign-aware treatment on agreement with EC depended strongly on site conditions (Figure 12b). At RRR, VBR-A51 had substantially higher RMSD relative to EBR-corrected EC than VBR-Ts, while bias was reduced only slightly. The increase in RMSD was largely associated with the more negative latent heat flux produced by VBR-A51 during periods with $R_n - G < 0$, which increased the magnitude of individual errors despite a small reduction in overall bias. VBR-A51 nevertheless remained strongly positively biased at RRR. Because VBR assumes $\frac{r_{wT}}{r_{wq}} = 1$, with VBR-A51 using covariance information primarily to determine the sign (i.e., $\frac{r_{wT}}{r_{wq}} = -1$), this remaining discrepancy indicates that departure of the covariance ratio magnitude from unity, rather than sign assignment alone, was an important source of error at this low-EF shrubland site.

At SF1 and SF2, representing negative Bowen ratios increased latent heat flux during periods with $R_n - G > 0$, while producing more negative latent heat flux when $R_n - G < 0$. At SF1, these opposing effects shifted the overall bias closer to zero, but RMSD increased, indicating that the improvement in mean bias was offset by larger deviations during individual periods, particularly when available energy was negative. At SF2, the sign-aware formulation reduced RMSD and shifted VBR estimates toward the EBR-corrected EC benchmark. Although this shift corresponded to a larger positive bias relative to uncorrected EC, it represented improved agreement once EC energy-balance non-closure was accounted for. The stronger benefit at SF2 is consistent with the greater occurrence of negative sensible heat flux at SF2 than at SF1 (Table 3), indicating a larger fraction of periods in which negative Bowen ratios were physically plausible and allowing latent heat flux to exceed available energy improved agreement with the closure-corrected EC reference.

Overall, covariance-derived sign information was most beneficial where negative sensible heat flux occurred frequently and negative Bowen ratios were therefore more prevalent. However, its effect depended on both the Bowen-ratio sign and the sign of available energy. In particular, applying the negative Bowen-ratio formulation when $R_n - G < 0$ produced more negative latent heat flux and increased RMSD at all three sites, partially offsetting the benefit of representing negative Bowen ratios during daytime advective conditions. These results suggest that treatment of negative-Bowen-ratio periods under negative available energy warrants further consideration in the sign-aware VBR implementation.

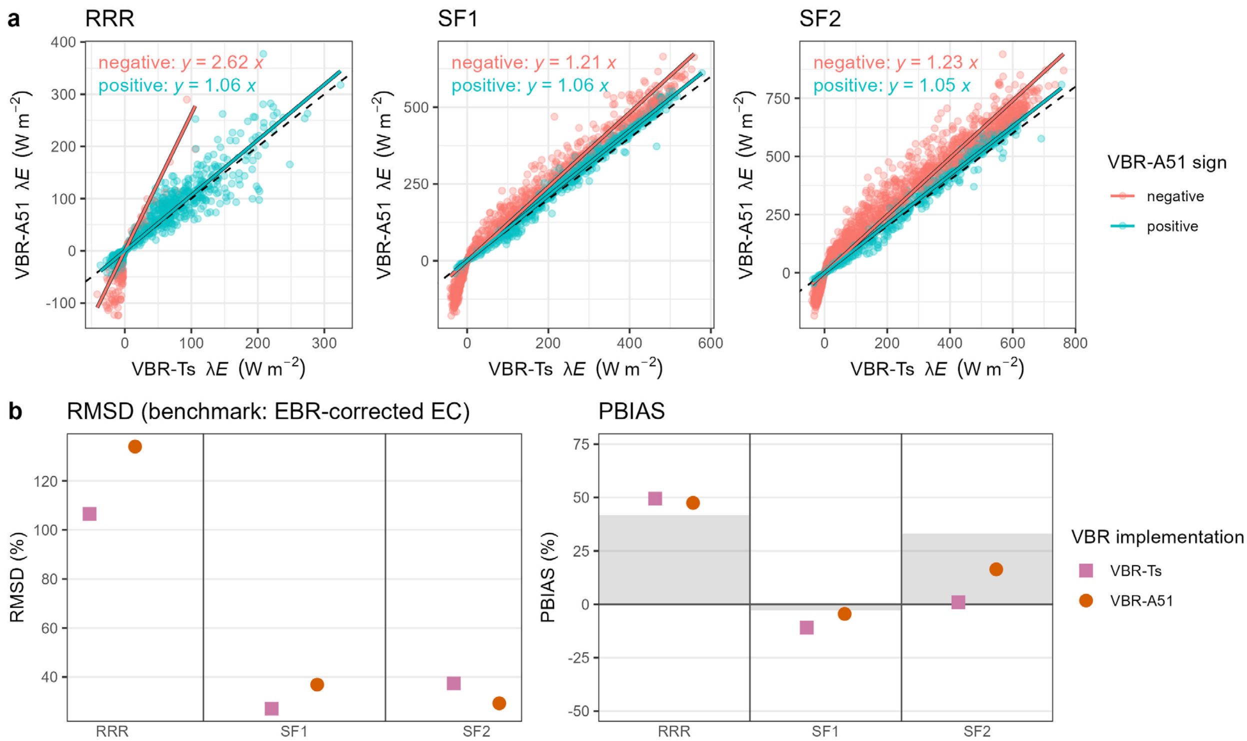

Figure 12. Comparison of VBR-Ts and the sign-aware VBR-A51 implementation. (a) Half-hourly latent heat flux estimated using VBR-Ts and VBR-A51 at RRR, SF1, and SF2. Colors indicate the VBR-A51 sign, which was based on the temperature-humidity correlation when AE is positive. Solid lines show regressions through the origin for each sign, and dashed lines indicate the 1:1 relationship. (b) percent RMSD relative to EBR-corrected EC and PBIAS of VBR-Ts and VBR-A51 relative to EBR-uncorrected EC. Gray shading in the PBIAS panels represents the EBR-derived systematic uncertainty range of the EC benchmark.

6. Discussion

The performance of lower-cost ET methods depended on which physical measurements were retained and which quantities were inferred. LI-710 retained direct turbulent flux measurement and showed the most consistent performance across sites. In contrast, VBR and RE approaches depended more strongly on surface energy partitioning, available energy, and advective conditions. These methods should therefore be evaluated according to ecosystem conditions, temporal scale, supporting measurements, and intended application rather than ranked using a single performance metric (Huntington et al., 2026).

Growing season EF provided a useful indicator of these differences. Biases from both VBR and RE ET decreased with increasing EF, but the rates and implications differed. VBR modestly overestimated ET in low-EF shrublands, performed best at intermediate EF, and increasingly underestimated ET at high EF. RE bias declined much more steeply with EF. It substantially overestimated ET in shrublands and became most comparable to EC only at the highest-EF cropland sites. LI-710 bias showed less systematic dependence on EF. These patterns indicate that VBR is most favorable under intermediate energy partition conditions, whereas RE ET becomes more defensible only when λE represents a dominant energy balance component.

Interpretation of all methods depended on uncertainty in the EC benchmark. The difference between measured and EBR-corrected EC was often comparable to the biases of the lower-cost methods. This was especially relevant for VBR and RE approaches, which inherently impose energy balance closure, but it was also necessary for diagnosing systematic uncertainty in LI-710. Comparisons with uncorrected EC alone can therefore make closure-constrained methods appear positively biased and can obscure closure differences between independent turbulent flux systems (Mauder et al., 2024).

Temporal aggregation reduced short-term differences among all methods. LI-710 reproduced much of the turbulent variability and timing measured by EC, resulting in relatively close half-hourly agreement. VBR and RE estimates were smoother and sometimes showed phase offsets because of their dependence on available energy. These differences were reduced after daily aggregation as short-term timing and storage effects partly canceled.

6.1. LI-710 retains broad applicability but requires quality control and energy balance diagnostics

LI-710 generally agreed more closely with EC than the other lower-cost approaches at the half-hourly scale. Its random uncertainty varied among sites in close correspondence with EC uncertainty, indicating that both systems responded similarly to environmental and turbulent-sampling conditions. Agreement was particularly close in shrublands, while larger differences occurred in croplands under high-flux conditions. The overall agreement with EC is consistent with the crop-based evaluation of Peddinti and Kisekka (2025).

LI-710 can provide an ET estimate that is independent of AE. Nevertheless, without AE measurements, it can be difficult to determine whether the system is underestimating turbulent flux or to quantify its systematic uncertainty (Mauder et al., 2013; Mauder et al., 2024). Across most sites, LI-710 generally estimated lower ET than EC. The side-by-side evaluation at RRR further illustrates the distinction between precision and systematic accuracy. The five retained LI-710 units showed close agreement with one another, with small inter-unit biases and relatively low residual scatter, indicating good sensor-to-sensor precision. However, the units consistently underestimated latent heat flux relative to the EC benchmark. This indicates that the dominant uncertainty was not primarily associated with unit-to-unit precision, but rather with a systematic component shared across sensors. Measurements of AE are therefore particularly valuable for diagnosing this type of bias and distinguishing sensor repeatability from agreement with the surface energy budget.

However, the uncertainty ranges derived from energy balance closure overlapped substantially, and much of the difference was reduced when closure correction was applied consistently to both systems. Corrected LI-710 generally remained lower than corrected EC, but the remaining difference was reasonable relative to the systematic uncertainty of the measurements. AE measurements should therefore accompany limited-diagnostics EC, particularly when absolute ET magnitude or cumulative water flux is important.

The reason for the generally lower LI-710 fluxes remains unclear. Plausible contributing factors include the limited ability of one-dimensional wind measurements to diagnose and correct flow tilt or distortion, as well as attenuation or imperfect time-lag compensation in the closed-path water-vapor signal. Either effect could reduce the measured covariance between vertical wind and water vapor (Burba, 2013). Because high-frequency observations and the full internal processing workflow were unavailable (i.e., limited diagnostics), these possibilities could not be evaluated directly. Differences may also result from the limited ability to apply post-processing procedures routinely used for research-grade EC, including footprint filtering and filtering of low-turbulence conditions (e.g., SSITC flag or friction velocity threshold). However, the relative importance of these factors could not be determined. Raw LI-710 outputs also contained frequent spikes at several sites and required physical range filtering, statistical despiking, and screening using available flow diagnostics. Simplified instrumentation therefore does not remove the need for external QA/QC. Limited diagnostic access may allow anomalous records to be identified without allowing their causes to be fully resolved.

With appropriate QA/QC, AE measurements, and ancillary wind measurements for flux footprint characterization, LI-710 appears suitable for half-hourly and daily ET monitoring across both croplands and shrublands. It may also support irrigation monitoring, satellite ET evaluation, and seasonal water-use assessment. Greater caution is required for cumulative or annual applications when data gaps are extensive or systematic underestimation cannot be independently evaluated.

6.2. VBR provides stable estimates across a broad EF range but remains sensitive to scalar similarity and advection

VBR-Ts had relatively stable random uncertainty across sites. Its uncertainty increased less strongly with flux magnitude than that of EC and LI-710, and its relative performance improved after daily aggregation. These characteristics make VBR useful for applications that prioritize daily variability, or relative temporal change rather than exact reproduction of half-hourly turbulent fluctuations. Similar advantages for temporally aggregated ET monitoring have been reported in previous VBR evaluations (Wang et al., 2026).

VBR bias showed a significant decline with increasing EF. It tended to overestimate ET in dry, low-EF shrublands, performed best at intermediate EF, and underestimated ET at high EF. The modest overestimation relative to uncorrected EC can partly be explained by incomplete EC energy balance closure because VBR partitions the full measured available energy. At the driest shrubland sites, however, VBR estimates exceeded even the EC closure-corrected uncertainty range. This suggests that energy balance non-closure alone was insufficient to explain the bias.

The low-EF overestimation likely reflects limitations in the scalar similarity assumption under unstable conditions. VBR assumes that vertical velocity is similarly correlated with temperature and water vapor ($\frac{r_{wT}}{r_{wq}} \approx 1$) (Katul et al., 1995; Assouline et al., 2016; Wang et al., 2023). Under very dry conditions, the correlation between vertical velocity and temperature may exceed that between vertical velocity and water vapor. Previous studies have shown that $\frac{r_{wT}}{r_{wq}}$ frequently exceeds unity under unstable and dry conditions (Katul and Hsieh, 1999; Lamaud and Irvine, 2006) and can increase with Bowen ratio (Wang et al., 2016; Martí et al., 2025). Assuming equal correlations would then underestimate the Bowen ratio and overestimate ET. The relatively frequent unstable conditions at the low-EF shrubland sites (Table 3; Figure S3) are therefore physically consistent with the positive VBR biases observed here. These effects may explain why VBR remained biased even when AE uncertainty was considered in the benchmark EC.

At high EF, VBR underestimation appears to reflect both flux-sign ambiguity under advection and departures from scalar similarity. Consistent with this interpretation, negative sensible heat flux occurred during 64–72% of growing season observations at the near-unity and high-EF cropland sites, indicating that negative was not confined to nighttime cooling (Table 3). When sensible heat flux becomes negative, λE can approach or exceed AE (Brakke et al., 1978). A positive-only VBR formulation cannot represent these conditions (Assouline et al., 2016). The VBR-A51 comparison showed that covariance-derived sign information can partly address this limitation when AE is positive: during negative-sign periods, VBR-A51 produced higher latent heat flux than VBR-Ts, allowing λE to exceed AE. Its agreement with closure-corrected EC improved most clearly at SF2, where negative sensible heat flux was most frequent. Although this shift increased positive bias relative to uncorrected EC, it moved VBR estimates closer to the closure-corrected EC benchmark.

However, the same sign-aware treatment was not beneficial when AE was negative. During negative-sign periods with negative AE, VBR-A51 produced more negative latent heat flux than VBR-Ts and increased RMSD at all three sites. Thus, poorer performance during negative-AE periods partly offset the benefit of representing negative Bowen ratios under positive-AE advective conditions. This contrast suggests that the usefulness of covariance-derived sign information depends not only on the Bowen-ratio sign but also on the energetic regime in which it occurs.

Also, flux sign alone did not explain the high-EF bias. Even when the Bowen ratio remained positive, the original VBR assumption requires not only the correct sign but also $\frac{r_{wT}}{r_{wq}} \approx 1$. If $\frac{r_{wT}}{r_{wq}} < 1$, the variance ratio overestimates the magnitude of the Bowen ratio and consequently underestimates ET even without negative sensible heat flux. This provides a potential explanation for the persistent VBR underestimation at SF1, where covariance-derived sign information reduced bias but did not improve RMSD. Thus, covariance-derived sign information can correct one important failure mode of VBR under advection, but it does not account for differences in the magnitude of temperature and water-vapor coupling to vertical motion.

Despite these limitations, VBR agreed reasonably well with EC across a broad EF range while requiring relatively simple and low-cost instrumentation. VBR may therefore still have merit when the primary objective is to capture temporal patterns at low cost, but it is less suitable when high relative accuracy is required, such as for evaluating groundwater-derived ET in dry phreatophyte shrublands (Beamer et al., 2013).

VBR remains a relatively new approach. Future improvements may require constraining not only flux direction but also departures from the assumed equality of temperature and water-vapor correlations with vertical velocity. Approaches that account for both the sign and magnitude of scalar dissimilarity may therefore improve VBR performance across the full EF gradient. Evaluation with estimated rather than measured AE will also be needed before comparable performance can be assumed in more simplified deployments.

6.3. Residual-energy ET should be restricted primarily to high-EF croplands

RE ET performance reflected the combined effects of surface energy balance closure and energy partitioning. Agreement was closest at SF1, where EC energy balance closure was near complete, leaving little residual energy to be incorrectly assigned to latent heat flux. More generally, RE performed comparatively well at high-EF croplands even when energy balance closure was incomplete, because latent heat flux represented a large fraction of the turbulent energy flux. The same closure residual therefore constituted a smaller fraction of ET than it did at low-EF sites.

The method can also represent λE greater than locally available energy because negative sensible heat flux increases the residual estimate (Brakke et al., 1978; Amiro and Wuschke, 1987). This gives it an advantage over positive-only VBR formulations under advective conditions. However, RE ET generally remained above the EC systematic-uncertainty range even at high-EF cropland sites. The magnitude of overestimation decreased with increasing EF, but the method did not become unbiased under its most favorable conditions. RE estimates should therefore be interpreted cautiously even in strongly evaporative croplands and may provide an upper estimate rather than an independent absolute ET measurement.

Among the evaluated approaches, RE ET was most directly affected by assumptions about energy balance closure. The method assigns the full difference between AE and measured sensible heat flux to λE. Any energy balance residual arising from unmeasured storage, horizontal or vertical advection, AE error, or sensible heat flux underestimation is therefore transferred directly into ET. In contrast, the EC closure correction used here partitioned the estimated imbalance between sensible and latent heat according to the measured Bowen ratio (Twine et al., 2000; Mauder et al., 2013). The residual approach can consequently overestimate ET even relative to closure-corrected EC.

This problem became severe in low-EF shrublands. ET was calculated as a small difference between much larger AE and sensible heat flux terms, causing small component errors to produce large relative ET errors. RE uncertainty remained substantial even when EC λE approached zero, and daily aggregation did not resolve the large positive bias. Within the ecosystems evaluated here, the results do not support the use of RE ET for absolute ET estimation outside croplands. RE ET also performed poorly at the orchard sites. This result is consistent with unresolved heat storage in canopy biomass, within-canopy air, or other components not represented by net radiation and surface soil heat flux. Complex agricultural canopies may therefore remain unsuitable even when EF is moderate.

The present analysis used fully processed EC sensible heat flux and thus represents favorable conditions for the residual framework. Lower-cost sensible heat flux methods, including surface renewal (Paw U et al., 1995), would introduce additional H uncertainty that would propagate directly into ET. RE ET should therefore be limited to high-EF, relatively simple agricultural systems where sensible heat flux and all major available-energy components are well measured. Even under these conditions, the tendency toward overestimation should be evaluated independently.

6.4. Limitations and future needs

Several limitations should be considered when interpreting these results. First, EC was used as the primary benchmark but does not provide an error-free estimate of ET. The energy balance correction used to define the systematic uncertainty range is also assumption dependent (Mauder et al., 2013; Mauder et al., 2024). The comparisons therefore evaluate agreement with a plausible EC range rather than absolute measurement accuracy.

Second, the evaluated implementations do not represent all possible configurations of each method. VBR-Ts was applied across the full network to provide a consistent comparison, whereas VBR-A51 observations were available at only three sites. The residual-energy analysis used fully processed EC sensible heat flux and therefore represents favorable conditions compared with implementations that estimate H using more lower-cost sensors. Measurement periods and available instrument combinations also differed among sites.

Finally, VBR and residual-energy ET were evaluated using measured net radiation and soil heat flux. Their performance may differ when available energy is estimated from simplified meteorological or remotely sensed inputs. The study was also limited to irrigated croplands and shrublands in the western United States. Additional evaluation across other ecosystems, climates, and independent ET benchmarks will be needed to determine how broadly the observed EF-dependent patterns apply.

7. Conclusion

The evaluated lower-cost ET methods were useful under different ecosystem and energy-partition conditions but were not interchangeable. Limited diagnostic LI-710 ET sensor showed the most consistent performance across the observed EF range. LI-710 generally underestimated EC, but much of the difference fell within closure-related uncertainty when both systems were evaluated consistently. It appears suitable for half-hourly to seasonal ET monitoring when external QA/QC and AE measurements are included.

VBR provided stable, low-cost estimates across a broad range of conditions and performed best at intermediate EF. Relative overestimation remained important in dry shrublands, while strong advection caused underestimation at high EF. Sign-aware formulations may reduce this limitation. RE ET improved as EF increased but generally remained positively biased and performed poorly in shrublands. Its use should therefore be limited mainly to croplands with accurate measurements of sensible heat flux and available energy.

Overall, method selection should reflect the intended application, ecosystem energy regime, and required accuracy. Supporting measurements, data recovery, QA/QC, and processing transparency are part of the complete ET observation system and should be considered together with sensor cost.

Data statement

The in situ data used in this study are expected to be archived on Zenodo before publication, subject to project-specific data-release requirements. Any data that cannot be included in the public archive will be available upon request. In addition, raw half-hourly flux data from the Oregon orchard sites (OSU-T1 and OSU-T2) are publicly available through Zenodo (Zheleva et al., 2026; https://doi.org/10.5281/zenodo.19740895), and raw half-hourly flux data from the ERVP, ECDP, EDVP, ECSM, EDVG, and ERVA sites are publicly available through NICE Net (DRI, 2026; https://www.dri.edu/nicenet/). High-frequency IRGASON data used for the VBR calculations are available upon reasonable request.

The quality-control and post-processing workflows used for eddy-covariance and meteorological data are maintained in a GitHub repository (https://github.com/DRI-RAD/DRI-RAD-EC_Proc_operational). The manuscript-specific post-processing and analysis code used to calculate the lower-cost ET estimates and reproduce the statistical analyses and figures presented in this manuscript will be archived together on Zenodo before publication.

Acknowledgements

The work at the Desert Research Institute (DRI) was supported by the U.S. Geological Survey Next Generation Water Observing System (NGWOS) Research and Development. The DRI-managed field sites were additionally supported by Nevada Division of Water Resources (NICE NET sites: ERVP, ECDP, EDVP, ECSM, EDVG, and ERVA), Oregon Department of Water Resources, Oregon State University (S2 site), and National Science Foundation under grant Grant No. OIA-2148788 (RRR site).

The work conducted in Idaho was supported by funding from Idaho Agricultural Experiment Station (IAES)- University of Idaho College of Agricultural and Life Sciences, USDA-NIFA Research Capacity Fund (Hatch) Accession Number 7010874, Idaho Wheat Commission (Grant No. AW9295), and Idaho Potato Commission and Northwest Potato Research Consortium (Grant No. AW9173). The authors thank Sage McClintick of J.R. Simplot Company (cooperator for site SF1), and Hannah Sanders, Braylund Sanders, and Rulon Spear of S&H Farms (cooperators for sites SF2 and SF3) for their stewardship as well as support and collaboration for on-farm research and sharing management information related to their farming operations.

The work conducted in Oregon was supported by Western Sustainable Agriculture Research and Education (Western SARE; Grant MU-ID G273-24-WA509), and the OSU Agricultural Research Foundation (Grant No. 25183A), and OSU Hatch/Nexus funds. The authors thank Walter Mahafee at the USDA and Chad Higgins at OSU for providing access to existing eddy covariance towers, instrumentation, and associated research infrastructure that supported this study. We also thank Jeff Newton and Zach Christensen of Christensen Farms for facilitating access to the hazelnut orchard and supporting field activities at the site.

We thank METER Group for providing prototype ATMOS 51 sensors for evaluation in this study. We are also grateful to the researchers, technicians, and field personnel who contributed to field deployment and maintenance, data collection, data production, quality control, and processing across the study sites.

Author contributions

Yeonuk Kim: Conceptualization, Data curation, Formal analysis, Investigation, Methodology, Software, Validation, Visualization, Writing – original draft. **Todd Caldwell**: Conceptualization, Data curation, Formal analysis, Investigation, Methodology, Resources, Supervision, Validation, Visualization, Writing – original draft. **Justin L Huntington**: Conceptualization, Funding acquisition, Investigation, Methodology, Resources, Supervision, Writing – review and editing. **Meetpal Kukal**: Conceptualization, Funding acquisition, Investigation, Resources, Writing – review and editing. **María Isabel Zamora Re**: Conceptualization, Funding acquisition, Investigation, Resources, Writing – review and editing. **Dragomira Zheleva**: Data curation, Investigation, Resources, Writing – review and editing. **Richard Jasoni**: Data curation, Investigation, Resources, Writing – review and editing. **Christian Dunkerly**: Data curation, Resources. **Murphy Gardner**: Data curation, Resources. **Clarence Robison**: Data curation, Investigation. **Dinesh Gulati**: Data curation. **Shawn Naylor**: Conceptualization, Resources, Supervision, Writing – review and editing. **Christopher Pearson**: Writing – review and editing. **John Volk**: Writing – review and editing. **Bruno Comini de Andrade**: Writing – review and editing. **Robert R. Lotspeich**: Resources, Supervision.

References

Amiro, B.D., Wuschke, E.E., 1987. Evapotranspiration from a boreal forest drainage basin using an energy balance/eddy correlation technique. *Bound.-Layer Meteorol.* 38, 125-139. https://doi.org/10.1007/BF00121560

Assouline, S., Li, D., Tyler, S., Tanny, J., Cohen, S., Bou-Zeid, E., Parlange, M., Katul, G.G., 2016. On the variability of the Priestley-Taylor coefficient over water bodies. *Water Resour. Res.* 52, 150-163. https://doi.org/10.1002/2015wr017504

Baldocchi, D., 2014. Measuring fluxes of trace gases and energy between ecosystems and the atmosphere—the state and future of the eddy covariance method. *Glob. Change Biol.* 20, 3600-3609. https://doi.org/10.1111/gcb.12649

Bambach, N.E., Miksch, M., Oldroyd, H.J., Knipper, K., Kustas, W.P., McElrone, A.J., Alfieri, J.G., Hipps, L., Prueger, J., Bustamante, S.C., 2025. Environmental Challenges for Eddy Covariance Measurements over Irrigated Croplands. In, Chapman Conference on the Energy Balance Closure Problem: AGU

Barker, T., 2025. A Summary of a Multistage Data Processing Pipeline for the LI-710 and LI-720 Sensors on LI-COR Cloud [website]. Application Note. LI-COR, Inc. https://www.licor.com/support/Cloud/topics/multistage-data-processing-pipeline.html

Beamer, J.P., Huntington, J.L., Morton, C.G., Pohll, G.M., 2013. Estimating Annual Groundwater Evapotranspiration from Phreatophytes in the Great Basin Using Landsat and Flux Tower Measurements. *J. Am. Water Resour. Assoc.* 49, 518-533. https://doi.org/10.1111/jawr.12058

Beverly, D., Campbell, C., Cobos, D., Campbell, G., Kukal, M., 2026. Expanding direct evapotranspiration (ET) measurements with accessible and low-cost Variance Bowen Ratio instruments. In, EGU General Assembly 2026. Vienna, Austria. https://doi.org/10.5194/egusphere-egu26-2333

Billesbach, D.P., Arkebauer, T.J., Sullivan, R.C., 2024. Intercomparison of sensible and latent heat flux measurements from combined eddy covariance, energy balance, and Bowen ratio methods above a grassland prairie. *Sci. Rep.* 14, 21866. https://doi.org/10.1038/s41598-024-67911-z

Brakke, T.W., Verma, S.B., Rosenberg, N.J., 1978. Local and Regional Components of Sensible Heat Advection. *J. Appl. Meteorol.* 17, 955-963. https://doi.org/10.1175/1520-0450(1978)017<0955:LARCOS>2.0.CO;2

Burba, G., 2013. Eddy Covariance Method for Scientific, Industrial, Agricultural and Regulatory Applications: A Field Book on Measuring Ecosystem Gas Exchange and Areal Emission Rates. LI-Cor Biosciences

Burba, G., Miller, B., Fratini, G., Inkenbrandt, P.C., Xu, L., 2024. Simple direct evapotranspiration measurements with a new cost-optimized ET flux Sensor. In, 104th Annual AMS Meeting 2024 (p. 431027)

Callejas-Rodelas, J.Á., Knohl, A., Mammarella, I., Vesala, T., Peltola, O., Markwitz, C., 2025. Does increased spatial replication above heterogeneous agroforestry improve the representativeness of eddy covariance measurements? *Biogeosciences* 22, 4507-4529. https://doi.org/10.5194/bg-22-4507-2025

Chu, H., Christianson, D.S., Cheah, Y.-W., Pastorello, G., O'Brien, F., Geden, J., Ngo, S.-T., Hollowgrass, R., Leibowitz, K., Beekwilder, N.F., Sandesh, M., Dengel, S., Chan, S.W., Santos, A., Delwiche, K., Yi, K., Buechner, C., Baldocchi, D., Papale, D., Keenan, T.F., Biraud, S.C., Agarwal, D.A., Torn, M.S., 2023. AmeriFlux BASE data pipeline to support network growth and data sharing. *Sci. Data* 10, 614. https://doi.org/10.1038/s41597-023-02531-2

Dias, N.L., Duarte, H.F., Maggiotto, S.R., Grodzki, L., 2007. An attenuated eddy covariance method for latent heat flux measurements. *Water Resour. Res.* 43, W04415. https://doi.org/10.1029/2006WR005259

DRI, 2026. NICE Net: Nevada Integrated Climate and Evapotranspiration Network [website]. Desert Research Institute. https://www.dri.edu/nicenet.

Elsadek, E.A., Attalah, S., Williams, C., Thorp, K.R., Wang, D., Elshikha, D.E.M., 2026. Comparing Cotton ET Data from a Satellite Platform, In Situ Sensor, and Soil Water Balance Method in Arizona. *Agriculture* 16, 228. https://doi.org/10.3390/agriculture16020228

Fisher, J.B., Melton, F., Middleton, E., Hain, C., Anderson, M., Allen, R., McCabe, M.F., Hook, S., Baldocchi, D., Townsend, P.A., Kilic, A., Tu, K., Miralles, D.D., Perret, J., Lagouarde, J.-P., Waliser, D., Purdy, A.J., French, A., Schimel, D., Famiglietti, J.S., Stephens, G., Wood, E.F., 2017. The future of evapotranspiration: Global requirements for ecosystem functioning, carbon and climate feedbacks, agricultural management, and water resources. *Water Resour. Res.* 53, 2618-2626. https://doi.org/10.1002/2016WR020175

Foken, T., Wichura, B., 1996. Tools for quality assessment of surface-based flux measurements. *Agric. For. Meteorol.* 78, 83-105. https://doi.org/10.1016/0168-1923(95)02248-1

Foken, T., Wimmer, F., Mauder, M., Thomas, C., Liebethal, C., 2006. Some aspects of the energy balance closure problem. *Atmos. Chem. Phys.* 6, 4395-4402. https://doi.org/10.5194/acp-6-4395-2006

Gao, Z., Russell, E.S., Missik, J.E.C., Huang, M., Chen, X., Strickland, C.E., Clayton, R., Arntzen, E., Ma, Y., Liu, H., 2017. A novel approach to evaluate soil heat flux calculation: An analytical review of nine methods. *J. Geophys. Res. Atmos.* 122, 6934-6949. https://doi.org/10.1002/2017jd027160

Hill, T., Chocholek, M., Clement, R., 2017. The case for increasing the statistical power of eddy covariance ecosystem studies: why, where and how? *Glob. Change Biol.* 23, 2154-2165. https://doi.org/10.1111/gcb.13547

Hollinger, D.Y., Richardson, A.D., 2005. Uncertainty in eddy covariance measurements and its application to physiological models. *Tree Physiol.* 25, 873-885. https://doi.org/10.1093/treephys/25.7.873

Huntington, J., Kim, Y., Caldwell, T.G., Kukal, M., Naylor, S., de Andrade, B.C., Pearson, C., Jasoni, R., Volk, J., Gardner, M., 2026. Toward Fit-for-Purpose Evapotranspiration Observations. *EarthArXiv (preprint)*. https://doi.org/10.31223/X5RZ0W

Katul, G., Goltz, S.M., Hsieh, C.-I., Cheng, Y., Mowry, F., Sigmon, J., 1995. Estimation of surface heat and momentum fluxes using the flux-variance method above uniform and non-uniform terrain. *Bound.-Layer Meteorol.* 74, 237-260. https://doi.org/10.1007/BF00712120

Katul, G.G., Hsieh, C.-I., 1999. A note on the flux-variance similarity relationships for heat and water vapour in the unstable atmospheric surface layer. *Bound.-Layer Meteorol.* 90, 327-338. https://doi.org/10.1023/A:1001747925158

Katul, G.G., Oren, R., Manzoni, S., Higgins, C., Parlange, M.B., 2012. Evapotranspiration: A process driving mass transport and energy exchange in the soil-plant-atmosphere-climate system. *Rev. Geophys.* 50, RG3002. https://doi.org/10.1029/2011rg000366

Kim, Y., Garcia, M., Johnson, M., 2023. Land-atmosphere coupling constrains increases to potential evaporation in a warming climate: Implications at local and global scales. *Earth's Futur.* 11, e2022EF002886. https://doi.org/10.1029/2022EF002886

Kim, Y., Huntington, J.L., Comini de Andrade, B., Johnson, M.S., Volk, J.M., Majumdar, S., Morton, C., ReVelle, P., 2026. Thermodynamically constrained surface energy balance using medium-resolution remote sensing for efficient evapotranspiration mapping. *Remote Sens. Environ.* 344, 115510. https://doi.org/10.1016/j.rse.2026.115510

Kim, Y., Johnson, M.S., 2025. Deciphering the role of evapotranspiration in declining relative humidity trends over land. *Commun. Earth Environ.* 6, 105. https://doi.org/10.1038/s43247-025-02076-9

Kim, Y., Johnson, M.S., Knox, S.H., Black, T.A., Dalmagro, H.J., Kang, M., Kim, J., Baldocchi, D., 2020. Gap-filling approaches for eddy covariance methane fluxes: A comparison of three machine learning algorithms and a traditional method with principal component analysis. *Glob. Change Biol.* 26, 1499-1518. https://doi.org/10.1111/gcb.14845

Kljun, N., Calanca, P., Rotach, M.W., Schmid, H.P., 2015. A simple two-dimensional parameterisation for Flux Footprint Prediction (FFP). *Geosci. Model Dev.* 8, 3695-3713. https://doi.org/10.5194/gmd-8-3695-2015

Kumar, S., Imen, S., Sridharan, V.K., Gupta, A., McDonald, W., Ramirez-Avila, J.J., Abdul-Aziz, O.I., Talchabhadel, R., Gao, H., Quinn, N.W.T., Weiss, W.J., Poulose, T., Palmate, S.S., Lee, C.M., Baskaran, L., 2024. Perceived barriers and advances in integrating earth observations with water resources modeling. *Remote Sens. Appl. Soc. Environ.* 33, 101119. https://doi.org/10.1016/j.rsase.2023.101119

Lamaud, E., Irvine, M., 2006. Temperature–humidity dissimilarity and heat-to-water-vapour transport efficiency above and within a pine forest canopy: The role of the Bowen ratio. *Bound.-Layer Meteorol.* 120, 87-109. https://doi.org/10.1007/s10546-005-9032-6

Lasslop, G., Reichstein, M., Kattge, J., Papale, D., 2008. Influences of observation errors in eddy flux data on inverse model parameter estimation. *Biogeosciences* 5, 1311-1324. https://doi.org/10.5194/bg-5-1311-2008

Lee, X., Massman, W., Law, B. (Eds.), 2004. Handbook of Micrometeorology: A Guide for Surface Flux Measurement and Analysis. Kluwer Academic Publishers, Dordrecht. https://doi.org/10.1007/1-4020-2265-4

Leuning, R., van Gorsel, E., Massman, W.J., Isaac, P.R., 2012. Reflections on the surface energy imbalance problem. *Agric. For. Meteorol.* 156, 65-74. https://doi.org/10.1016/j.agrformet.2011.12.002

Liu, H., Peters, G., Foken, T., 2001. New Equations For Sonic Temperature Variance And Buoyancy Heat Flux With An Omnidirectional Sonic Anemometer. *Bound.-Layer Meteorol.* 100, 459-468. https://doi.org/10.1023/A:1019207031397

Liu, Y., Stoy, P., Chu, H., Hollinger, D.Y., Ollinger, S.V., Ouimette, A.P., Durden, D.J., Sturtevant, C., Lucas, B., Richardson, A.D., 2026. A tale of two towers: comparing NEON and AmeriFlux data streams at Bartlett Experimental Forest. *Agric. For. Meteorol.* 378, 110939. https://doi.org/10.1016/j.agrformet.2025.110939

Markwitz, C., Siebicke, L., 2019. Low-cost eddy covariance: a case study of evapotranspiration over agroforestry in Germany. *Atmos. Meas. Tech.* 12, 4677-4696. https://doi.org/10.5194/amt-12-4677-2019

Martí, B., Martínez-Villagrasa, D., Price, J.D., Cuxart, J., 2025. Revisiting Stability Functions of Surface Heat Fluxes in Semi-arid Environments. *Bound.-Layer Meteorol.* 192, 4. https://doi.org/10.1007/s10546-025-00947-4

Mauder, M., Cuntz, M., Drüe, C., Graf, A., Rebmann, C., Schmid, H.P., Schmidt, M., Steinbrecher, R., 2013. A strategy for quality and uncertainty assessment of long-term eddy-covariance measurements. *Agric. For. Meteorol.* 169, 122-135. https://doi.org/10.1016/j.agrformet.2012.09.006

Mauder, M., Foken, T., 2004. Documentation and instruction manual of the eddy-covariance software package TK2. Arbeitsergebnisse 26, Universität Bayreuth, Abteilung Mikrometeorologie, Bayreuth.

Mauder, M., Foken, T., Cuxart, J., 2020. Surface-Energy-Balance Closure over Land: A Review. *Bound.-Layer Meteorol.* 177, 395-426. https://doi.org/10.1007/s10546-020-00529-6

Mauder, M., Genzel, S., Fu, J., Kiese, R., Soltani, M., Steinbrecher, R., Zeeman, M., Banerjee, T., De Roo, F., Kunstmann, H., 2018. Evaluation of energy balance closure adjustment methods by independent evapotranspiration estimates from lysimeters and hydrological simulations. *Hydrol. Process.* 32, 39-50. https://doi.org/10.1002/hyp.11397

Mauder, M., Jung, M., Stoy, P., Nelson, J., Wanner, L., 2024. Energy balance closure at FLUXNET sites revisited. *Agric. For. Meteorol.* 358, 110235. https://doi.org/10.1016/j.agrformet.2024.110235

McGloin, R., Šigut, L., Havránková, K., Dušek, J., Pavelka, M., Sedlák, P., 2018. Energy balance closure at a variety of ecosystems in Central Europe with contrasting topographies. *Agric. For. Meteorol.* 248, 418-431. https://doi.org/10.1016/j.agrformet.2017.10.003

Melton, F.S., Huntington, J., Grimm, R., Herring, J., Hall, M., Rollison, D., Erickson, T., Allen, R., Anderson, M., Fisher, J.B., Kilic, A., Senay, G.B., Volk, J., Hain, C., Johnson, L., Ruhoff, A., Blankenau, P., Bromley, M., Carrara, W., Daudert, B., Doherty, C., Dunkerly, C., Friedrichs, M., Guzman, A., Halverson, G., Hansen, J., Harding, J., Kang, Y., Ketchum, D., Minor, B., Morton, C., Ortega-Salazar, S., Ott, T., Ozdogan, M., ReVelle, P.M., Schull, M., Wang, C., Yang, Y., Anderson, R.G., 2022. OpenET: Filling a Critical Data Gap in Water Management for the Western United States. *J. Am. Water Resour. Assoc.* 58, 971-994. https://doi.org/10.1111/1752-1688.12956

METER Group, Inc., 2026. ATMOS 51 User Manual. METER Group, Inc., Pullman, WA

Milly, P.C.D., Dunne, K.A., 2016. Potential evapotranspiration and continental drying. *Nat. Clim. Change* 6, 946-949. https://doi.org/10.1038/nclimate3046

Moffat, A.M., Papale, D., Reichstein, M., Hollinger, D.Y., Richardson, A.D., Barr, A.G., Beckstein, C., Braswell, B.H., Churkina, G., Desai, A.R., Falge, E., Gove, J.H., Heimann, M., Hui, D., Jarvis, A.J., Kattge, J., Noormets, A., Stauch, V.J., 2007. Comprehensive comparison of gap-filling techniques for eddy covariance net carbon fluxes. *Agric. For. Meteorol.* 147, 209-232. https://doi.org/10.1016/j.agrformet.2007.08.011

Moncrieff, J., Clement, R., Finnigan, J., Meyers, T., 2004. Averaging, detrending, and filtering of eddy covariance time series. In: Lee, X., Massman, W., Law, B. (Eds.), Handbook of Micrometeorology: A Guide for Surface Flux Measurement and Analysis. Kluwer Academic Publishers, Dordrecht, pp. 7–31. https://doi.org/10.1007/1-4020-2265-4_2

Moncrieff, J.B., Massheder, J.M., de Bruin, H., Elbers, J., Friborg, T., Heusinkveld, B., Kabat, P., Scott, S., Soegaard, H., Verhoef, A., 1997. A system to measure surface fluxes of momentum, sensible heat, water vapour and carbon dioxide. *J. Hydrol.* 188-189, 589-611. https://doi.org/10.1016/S0022-1694(96)03194-0

Papale, D., Reichstein, M., Aubinet, M., Canfora, E., Bernhofer, C., Kutsch, W., Longdoz, B., Rambal, S., Valentini, R., Vesala, T., 2006. Towards a standardized processing of Net Ecosystem Exchange measured with eddy covariance technique: algorithms and uncertainty estimation. *Biogeosciences* 3, 571-583. https://doi.org/10.5194/bg-3-571-2006

Pastorello, G., Trotta, C., Canfora, E., Chu, H., Christianson, D., Cheah, Y.-W., Poindexter, C., Chen, J., Elbashandy, A., Humphrey, M., Isaac, P., Polidori, D., Ribeca, A., van Ingen, C., Zhang, L., Amiro, B., Ammann, C., Arain, M.A., Ardö, J., Arkebauer, T., Arndt, S.K., Arriga, N., Aubinet, M., Aurela, M., Baldocchi, D., Barr, A., Beamesderfer, E., Marchesini, L.B., Bergeron, O., Beringer, J., Bernhofer, C., Berveiller, D., Billesbach, D., Black, T.A., Blanken, P.D., Bohrer, G., Boike, J., Bolstad, P.V., Bonal, D., Bonnefond, J.-M., Bowling, D.R., Bracho, R., Brodeur, J., Brümmer, C., Buchmann, N., Burban, B., Burns, S.P., Buysse, P., Cale, P., Cavagna, M., Cellier, P., Chen, S., Chini, I., Christensen, T.R., Cleverly, J., Collalti, A., Consalvo, C., Cook, B.D., Cook, D., Coursolle, C., Cremonese, E., Curtis, P.S., D'Andrea, E., da Rocha, H., Dai, X., Davis, K.J., De Cinti, B., de Grandcourt, A., De Ligne, A., De Oliveira, R.C., Delpierre, N., Desai, A.R., Di Bella, C.M., di Tommasi, P., Dolman, H., Domingo, F., Dong, G., Dore, S., Duce, P., Dufrêne, E., Dunn, A., Dušek, J., Eamus, D., Eichelmann, U., ElKhidir, H.A.M., Eugster, W., Ewenz, C.M., Ewers, B., Famulari, D., Fares, S., Feigenwinter, I., Feitz, A., Fensholt, R., Filippa, G., Fischer, M., Frank, J., Galvagno, M., Gharun, M., Gianelle, D., Gielen, B., Gioli, B., Gitelson, A., Goded, I., Goeckede, M., Goldstein, A.H., Gough, C.M., Goulden, M.L., Graf, A., Griebel, A., Gruening, C., Grünwald, T., Hammerle, A., Han, S., Han, X., Hansen, B.U., Hanson, C., Hatakka, J., He, Y., Hehn, M., Heinesch, B., Hinko-Najera, N., Hörtnagl, L., Hutley, L., Ibrom, A., Ikawa, H., Jackowicz-Korczynski, M., Janouš, D., Jans, W., Jassal, R., Jiang, S., Kato, T., Khomik, M., Klatt, J., Knohl, A., Knox, S., Kobayashi, H., Koerber, G., Kolle, O., Kosugi, Y., Kotani, A., Kowalski, A., Kruijt, B., Kurbatova, J., Kutsch, W.L., Kwon, H., Launiainen, S., Laurila, T., Law, B., Leuning, R., Li, Y., Liddell, M., Limousin, J.-M., Lion, M., Liska, A.J., Lohila, A., López-Ballesteros, A., López-Blanco, E., Loubet, B., Loustau, D., Lucas-Moffat, A., Lüers, J., Ma, S., Macfarlane, C., Magliulo, V., Maier, R., Mammarella, I., Manca, G., Marcolla, B., Margolis, H.A., Marras, S., Massman, W., Mastepanov, M., Matamala, R., Matthes, J.H., Mazzenga, F., McCaughey, H., McHugh, I., McMillan, A.M.S., Merbold, L., Meyer, W., Meyers, T., Miller, S.D., Minerbi, S., Moderow, U., Monson, R.K., Montagnani, L., Moore, C.E., Moors, E., Moreaux, V., Moureaux, C., Munger, J.W., Nakai, T., Neirynck, J., Nesic, Z., Nicolini, G., Noormets, A., Northwood, M., Nosetto, M., Nouvellon, Y., Novick, K., Oechel, W., Olesen, J.E., Ourcival, J.-M., Papuga, S.A., Parmentier, F.-J., Paul-Limoges, E., Pavelka, M., Peichl, M., Pendall, E., Phillips, R.P., Pilegaard, K., Pirk, N., Posse, G., Powell, T., Prasse, H., Prober, S.M., Rambal, S., Rannik, Ü., Raz-Yaseef, N., Reed, D., de Dios, V.R., Restrepo-Coupe, N., Reverter, B.R., Roland, M., Sabbatini, S., Sachs, T., Saleska, S.R., Sánchez-Cañete, E.P., Sanchez-Mejia, Z.M., Schmid, H.P., Schmidt, M., Schneider, K., Schrader, F., Schroder, I., Scott, R.L., Sedlák, P., Serrano-Ortíz, P., Shao, C., Shi, P., Shironya, I., Siebicke, L., Šigut, L., Silberstein, R., Sirca, C., Spano, D., Steinbrecher, R., Stevens, R.M., Sturtevant, C., Suyker, A., Tagesson, T., Takanashi, S., Tang, Y., Tapper, N., Thom, J., Tiedemann, F., Tomassucci, M., Tuovinen, J.-P., Urbanski, S., Valentini, R., van der Molen, M., van Gorsel, E., van Huissteden, K., Varlagin, A., Verfaillie, J., Vesala, T., Vincke, C., Vitale, D., Vygodskaya, N., Walker, J.P., Walter-Shea, E., Wang, H., Weber, R., Westermann, S., Wille, C., Wofsy, S., Wohlfahrt, G., Wolf, S., Woodgate, W., Li, Y., Zampedri, R., Zhang, J., Zhou, G., Zona, D., Agarwal, D., Biraud, S., Torn, M., Papale, D., 2020. The FLUXNET2015 dataset and the ONEFlux processing pipeline for eddy covariance data. *Sci. Data* 7, 225. https://doi.org/10.1038/s41597-020-0534-3

Paw U, K.T., Qiu, J., Su, H.-B., Watanabe, T., Brunet, Y., 1995. Surface renewal analysis: a new method to obtain scalar fluxes. *Agric. For. Meteorol.* 74, 119-137. https://doi.org/10.1016/0168-1923(94)02182-J

Peddinti, S.R., Kisekka, I., 2025. Evaluation of the LI-710 evapotranspiration sensor in comparison to full eddy covariance for monitoring energy fluxes in perennial and annual crops. *Agric. Water Manag.* 313, 109501. https://doi.org/10.1016/j.agwat.2025.109501

Reed, D.E., Frank, J.M., Ewers, B.E., Desai, A.R., 2018. Time dependency of eddy covariance site energy balance. *Agric. For. Meteorol.* 249, 467-478. https://doi.org/10.1016/j.agrformet.2017.08.008

Reichstein, M., Falge, E., Baldocchi, D., Papale, D., Aubinet, M., Berbigier, P., Bernhofer, C., Buchmann, N., Gilmanov, T., Granier, A., Grünwald, T., Havránková, K., Ilvesniemi, H., Janous, D., Knohl, A., Laurila, T., Lohila, A., Loustau, D., Matteucci, G., Meyers, T., Miglietta, F., Ourcival, J.-M., Pumpanen, J., Rambal, S., Rotenberg, E., Sanz, M., Tenhunen, J., Seufert, G., Vaccari, F., Vesala, T., Yakir, D., Valentini, R., 2005. On the separation of net ecosystem exchange into assimilation and ecosystem respiration: review and improved algorithm. *Glob. Change Biol.* 11, 1424-1439. https://doi.org/10.1111/j.1365-2486.2005.001002.x

Richardson, A.D., Hollinger, D.Y., Burba, G.G., Davis, K.J., Flanagan, L.B., Katul, G.G., Munger, J.W., Ricciuto, D.M., Stoy, P.C., Suyker, A.E., Verma, S.B., Wofsy, S.C., 2006. A multi-site analysis of random error in tower-based measurements of carbon and energy fluxes. *Agric. For. Meteorol.* 136, 1-18. https://doi.org/10.1016/j.agrformet.2006.01.007

Richardson, A.D., Mahecha, M.D., Falge, E., Kattge, J., Moffat, A.M., Papale, D., Reichstein, M., Stauch, V.J., Braswell, B.H., Churkina, G., Kruijt, B., Hollinger, D.Y., 2008. Statistical properties of random CO2 flux measurement uncertainty inferred from model residuals. *Agric. For. Meteorol.* 148, 38-50. https://doi.org/10.1016/j.agrformet.2007.09.001

Scott, R.L., 2010. Using watershed water balance to evaluate the accuracy of eddy covariance evaporation measurements for three semiarid ecosystems. *Agric. For. Meteorol.* 150, 219-225. https://doi.org/10.1016/j.agrformet.2009.11.002

Šigut, L., 2023. Post-process eddy covariance data with ease using R package openeddy. In, EGU General Assembly 2023. https://doi.org/10.5194/egusphere-egu23-13520

Stoy, P.C., Mauder, M., Foken, T., Marcolla, B., Boegh, E., Ibrom, A., Arain, M.A., Arneth, A., Aurela, M., Bernhofer, C., Cescatti, A., Dellwik, E., Duce, P., Gianelle, D., van Gorsel, E., Kiely, G., Knohl, A., Margolis, H., McCaughey, H., Merbold, L., Montagnani, L., Papale, D., Reichstein, M., Saunders, M., Serrano-Ortiz, P., Sottocornola, M., Spano, D., Vaccari, F., Varlagin, A., 2013. A data-driven analysis of energy balance closure across FLUXNET research sites: The role of landscape scale heterogeneity. *Agric. For. Meteorol.* 171-172, 137-152. https://doi.org/10.1016/j.agrformet.2012.11.004

Tanner, C.B., Thurtell, G.W., 1969. *Anemoclinometer measurements of Reynolds stress and heat transport in the atmospheric surface layer* (No. ECOM66G22F).

Todd, R.W., Evett, S.R., Howell, T.A., 2000. The Bowen ratio-energy balance method for estimating latent heat flux of irrigated alfalfa evaluated in a semi-arid, advective environment. *Agric. For. Meteorol.* 103, 335-348. https://doi.org/10.1016/S0168-1923(00)00139-8

Tolk, J.A., Evett, S.R., Howell, T.A., 2006. Advection Influences on Evapotranspiration of Alfalfa in a Semiarid Climate. *Agron. J.* 98, 1646-1654. https://doi.org/10.2134/agronj2006.0031

Twine, T.E., Kustas, W.P., Norman, J.M., Cook, D.R., Houser, P.R., Meyers, T.P., Prueger, J.H., Starks, P.J., Wesely, M.L., 2000. Correcting eddy-covariance flux underestimates over a grassland. *Agric. For. Meteorol.* 103, 279-300. https://doi.org/10.1016/S0168-1923(00)00123-4

van Ramshorst, J.G.V., Knohl, A., Callejas-Rodelas, J.Á., Clement, R., Hill, T.C., Siebicke, L., Markwitz, C., 2024. Lower-cost eddy covariance for CO2 and H2O fluxes over grassland and agroforestry. *Atmos. Meas. Tech.* 17, 6047-6071. https://doi.org/10.5194/amt-17-6047-2024

Volk, J.M., Huntington, J., Melton, F.S., Allen, R., Anderson, M.C., Fisher, J.B., Kilic, A., Senay, G., Halverson, G., Knipper, K., Minor, B., Pearson, C., Wang, T., Yang, Y., Evett, S., French, A.N., Jasoni, R., Kustas, W., 2023. Development of a Benchmark Eddy Flux Evapotranspiration Dataset for Evaluation of Satellite-Driven Evapotranspiration Models Over the CONUS. *Agric. For. Meteorol.* 331, 109307. https://doi.org/10.1016/j.agrformet.2023.109307

Volk, J.M., Huntington, J.L., Melton, F.S., Allen, R., Anderson, M., Fisher, J.B., Kilic, A., Ruhoff, A., Senay, G.B., Minor, B., Morton, C., Ott, T., Johnson, L., Comini de Andrade, B., Carrara, W., Doherty, C.T., Dunkerly, C., Friedrichs, M., Guzman, A., Hain, C., Halverson, G., Kang, Y., Knipper, K., Laipelt, L., Ortega-Salazar, S., Pearson, C., Parrish, G.E.L., Purdy, A., ReVelle, P., Wang, T., Yang, Y., 2024. Assessing the accuracy of OpenET satellite-based evapotranspiration data to support water resource and land management applications. *Nat. Water* 2, 193-205. https://doi.org/10.1038/s44221-023-00181-7

Wang, K., Dickinson, R.E., 2012. A review of global terrestrial evapotranspiration: Observation, modeling, climatology, and climatic variability. *Rev. Geophys.* 50, RG2005. https://doi.org/10.1029/2011RG000373

Wang, T., Verfaillie, J., Szutu, D., Baldocchi, D., 2023. Handily measuring sensible and latent heat exchanges at a bargain: A test of the variance-Bowen ratio approach. *Agric. For. Meteorol.* 333, 109399. https://doi.org/10.1016/j.agrformet.2023.109399

Wang, T.C., Senay, G.B., Verfaille, J., Szutu, D., Friedrichs, M., Eggleston, J., Baldocchi, D., 2026. Towards Affordable Wetland Evapotranspiration Monitoring Using the Variance-Bowen Ratio Method: Insights From Three Contrasting Wetlands. *Water Resour. Res.* 62, e2025WR041365. https://doi.org/10.1029/2025WR041365

Wang, W., Smith, J.A., Ramamurthy, P., Baeck, M.L., Bou-Zeid, E., Scanlon, T.M., 2016. On the correlation of water vapor and CO2: Application to flux partitioning of evapotranspiration. *Water Resour. Res.* 52, 9452-9469. https://doi.org/10.1002/2015WR018161

Webb, E.K., Pearman, G.I., Leuning, R., 1980. Correction of flux measurements for density effects due to heat and water vapour transfer. *Q. J. R. Meteorol. Soc.* 106, 85-100. https://doi.org/10.1002/qj.49710644707

Wilson, K., Goldstein, A., Falge, E., Aubinet, M., Baldocchi, D., Berbigier, P., Bernhofer, C., Ceulemans, R., Dolman, H., Field, C., Grelle, A., Ibrom, A., Law, B.E., Kowalski, A., Meyers, T., Moncrieff, J., Monson, R., Oechel, W., Tenhunen, J., Valentini, R., Verma, S., 2002. Energy balance closure at FLUXNET sites. *Agric. For. Meteorol.* 113, 223-243. https://doi.org/10.1016/S0168-1923(02)00109-0

Wutzler, T., Lucas-Moffat, A., Migliavacca, M., Knauer, J., Sickel, K., Šigut, L., Menzer, O., Reichstein, M., 2018. Basic and extensible post-processing of eddy covariance flux data with REddyProc. *Biogeosciences 15*, 5015-5030. https://doi.org/10.5194/bg-15-5015-2018

Yi, K., Senay, G.B., Fisher, J.B., Wang, L., Suvočarev, K., Chu, H., Moore, G.W., Novick, K.A., Barnes, M.L., Keenan, T.F., Mallick, K., Luo, X., Missik, J.E.C., Delwiche, K.B., Nelson, J.A., Good, S.P., Xiao, X., Kannenberg, S.A., Ahmadi, A., Wang, T., Bohrer, G., Litvak, M.E., Reed, D.E., Oishi, A.C., Torn, M.S., Baldocchi, D., 2024. Challenges and Future Directions in Quantifying Terrestrial Evapotranspiration. *Water Resour. Res.* 60, e2024WR037622. https://doi.org/10.1029/2024WR037622

Zhang, W., Nelson, J.A., Miralles, D.G., Mauder, M., Migliavacca, M., Poyatos, R., Reichstein, M., Jung, M., 2024. A New Post-Hoc Method to Reduce the Energy Imbalance in Eddy Covariance Measurements. *Geophys. Res. Lett.* 51, e2023GL107084. https://doi.org/10.1029/2023GL107084

Zheleva, D., Zamora Re, M., Tomasek, A., 2026. Eddy-covariance and LI-710 evapotranspiration measurements from paired hazelnut orchards with and without cover crops, Willamette Valley, Oregon (2024–2025) [Dataset]. Zenodo. https://doi.org/10.5281/zenodo.19740895

Supplementary Information for

Fit for purpose evapotranspiration measurements: A multi-site comparison of lower-cost approaches across croplands and shrublands

Yeonuk Kim[1,*], Todd Caldwell[1], Justin L Huntington[1], Meetpal Kukal[2], María Isabel Zamora Re[3], Dragomira Zheleva[3], Richard Jasoni[4], Christian Dunkerly[1], Murphy Gardner[1], Clarence Robison[2], Dinesh Gulati[2], Shawn Naylor[5], Christopher Pearson[1], John Volk[1], Bruno Comini de Andrade[6], Robert R. Lotspeich[7]

Affiliations

1. Division of Hydrologic Sciences, Desert Research Institute, Reno, Nevada, USA

2. Department of Soil and Water Systems, University of Idaho, Boise, Idaho, USA

3. Biological and Ecological Engineering, Oregon State University, Corvallis, Oregon, USA

4. Division of Earth and Ecosystem Sciences, Desert Research Institute, Reno, Nevada, USA

5. U.S. Geological Survey, Ohio-Kentucky-Indiana Water Science Center, Indianapolis, IN, USA

6. Independent contractor, Porto Alegre, Rio Grande do Sul, Brazil

7. U.S. Geological Survey, Water Resources Mission Area, Reston, VA, USA

* Correspondence to: Yeonuk Kim (yeonuk.kim@dri.edu)

Contents

Supplementary Text

Text S1. Comparison of daytime-only and storage-constrained energy balance corrections

We compared the conventional daytime correction of Mauder et al. (2013) with the storage-constrained approach used in this study (Equations 8 - 12) at the RRR site, which exhibited the largest surface energy imbalance among our study sites and where unresolved heat storage was therefore expected to be substantial (Figure S1).

At the half-hourly scale, the Mauder et al. (2013) correction brought daytime turbulent fluxes closer to the 1:1 relationship with available energy than our approach, with slopes of 0.964 and 0.867, respectively (Figure S1b, c). This occurred because the conventional method assigns the full daytime imbalance to daytime turbulent fluxes, whereas our approach reduces the daytime correction by treating nighttime imbalance as unresolved sub-daily heat storage. At the daily scale, however, the Mauder et al. correction produced turbulent fluxes 8% greater than available energy, while our approach achieved daily closure (slopes of 1.08 and 0.99, respectively; Figure S1f, g). Mauder-corrected latent heat flux was consequently approximately 7% higher at the half-hourly scale and 6% higher at the daily scale than estimates from our method (Figure S1d, h). Thus, enforcing closer daytime energy balance closure may overcorrect turbulent heat fluxes when nighttime energy imbalance associated with unresolved sub-daily heat storage is appreciable.

It should be noted that RRR exhibited one of the largest differences between the Mauder et al. (2013) correction and our proposed approach. At other sites, where minor heat storage terms were better constrained, the difference was generally smaller, but remained systematic. By interpreting the nighttime imbalance as unresolved sub-daily heat storage, our approach applies a more conservative correction to EC latent heat flux.

We also examined the ONEFlux energy balance correction, which calculates correction factors separately at half hourly and daily resolutions (Pastorello et al., 2020). Here, we focused on the half hourly correction and evaluated its behavior both at the native resolution and after aggregation to daily values. At an example site, SF3, the half hourly ONEFlux correction brought turbulent fluxes close to energy balance closure but produced overclosure after daily aggregation, with the regression slope increasing from 1.03 at the half hourly scale to 1.12 at the daily scale (Figure S2). This result is consistent with the overcorrection of ONEFlux-corrected turbulent fluxes after daily aggregation reported by Zhang et al. (2024). Together, these results indicate that widely used half hourly correction approaches, including those of Mauder et al. (2013) and ONEFlux, can produce overcorrection that becomes evident at the daily scale when nighttime energy imbalance is not explicitly constrained. This motivated the nighttime storage constraint used in our approach.

Text S2. Precision and accuracy of collocated LI-710 sensors at the Red Rock Road shrubland site

Six LI-COR LI-710 evapotranspiration sensors (SDI-12 addresses Add0–Add5) were temporarily deployed in a collocated cluster at the Red Rock Road (RRR) semiarid shrubland site, alongside the reference eddy covariance (EC) tower and permanent LI-710 (RRR LI-710). The six units (add0 to add5) were mounted on two towers, three per tower, in an inverted-T arrangement: a 2 m crossbar carrying the left and right units, and a 1 m stem extending forward toward the 250° predominant wind to the center unit. Closest sonic-to-sonic separation is therefore 1.4 m, with 2.0 m along each crossbar. The results were tested for a wind-direction-locked wake bias between neighbors. The scatter in the wake-risk sectors was equal to or lower than elsewhere for four of the six units and only marginally higher for the two left-position units (Figure S9) and no wind-direction-locked bias was detectable.

The concurrent six-unit record spans 2026-03-03 20:00 to 2026-03-20 13:00 (Pacific Standard Time) or 17 days, 803 half-hourly periods. The manufacturer's documented screening workflow was followed for the LI-710 fluxes (Barker, 2025). A half-hour period was dropped for a unit if the 16-bit diagnostic code was non-zero, the data-quality variable was non-zero, or the ET fell outside the range ($-0.10 < ET < 0.8$ mm). No records were gap-filled. Neither precipitation nor probable-dew conditions (nighttime ambient RH ≥ 95%) were observed during the test period. This screening left 732 of 803 half-hours (91%). This precision mask was used for unit-to-unit comparison, none of which involves the EC record.

The precision analysis (between units) includes all fluxes (λE, H, ET) and ancillary measurements of air temperature (AirTC), relative humidity (RH) and barometric pressure (Atm_press) (Table S2). Two temperature/humidity pairs appear in Table S2 and the distinction is not obvious. The ambient measurements (AirTC, RH_710) are directly comparable to a conventional weather station; it is the pair used throughout this analysis. The cell pair (cell_temp, cell_RH) is an internal sensor describing conditions inside the measurement cell. The cell_temp tends to be ~5°C warmer (and the cell_RH lower) from heat generated by the air pump. High cell_RH (>90%) or low cell_T (<0°C) will shut down the instrument.

The permanent RRR LI-710 was mounted on a crossarm ~3 m from the EC and ~6 m from the cluster. Within the analysis window, it overlaps 685 of the 803 half-hours (85%), complete except for a 2.5-day outage from 2026-03-06 03:30 to 2026-03-08 15:00, and 480 periods survive quality control; a 30% loss against roughly 9% for the cluster units; however, its full record extends well beyond this experiment, from 2024-11-12 to 2026-03-31. No energy-balance closure correction is applied anywhere in this analysis.

We separate the analysis into precision (between units) and accuracy (against EC). The analysis window is 2026-03-03 20:00:00 to 2026-03-20 13:00:00, i.e., 17 days, 803 half-hourly periods, the concurrent six-unit record (Figure S7). We used a precision mask for the LI-710 cluster based on the data-quality flag and ET range, rain plus buffer, and dew: 732 of 803 records were retained. An accuracy mask was also used on the EC data quality control flags, but only 1 record was removed and 731 retained. The stationarity and integral turbulence characteristic (SSITC) flag was deliberately excluded from the accuracy mask at RRR. At the other EC sites, SSITC filtering was retained as part of the standard quality-control procedure. Following conventional policy of SSTIC flag ≤ 1 at RRR, only 52 of 803 periods survived, discarding 93% of data during the analysis window. Periods flagged had higher mean friction velocity and wind speed (0.31 and 2.21 m s^{-1}) than periods that pass (0.15–0.19 and 0.7–1.1 m s^{-1}). The

SSITC failures are normally associated with low-turbulence, decoupled conditions, not well-mixed ones. The reference relationship is likely mismatched for this terrain, rather than a real per-period quality signal, and is not used to exclude data.

For precision, each unit in the cluster was compared against the leave-one-out mean of the other units at the same timestamp. Add5, an obvious outlier, is excluded from the reference pool for all variables (Figure S7). Add5 had a +6.91 °C temperature offset and a humidity slope of 0.62 in comparison to the pool. Add5 was returned to the manufacturer and found to have faulty calibration in the firmware. Each sensor was referenced against the mean of the other four, and Add5 against the mean of all five.

Mean precision and ranges are presented in Table 4, while the per-unit precision for each variable is presented here in Table S4. Precision is also reported as a function of flux magnitude, binned on the absolute leave-one-out mean at 0, 25, 50, 100, 150, 250, 500 W m^{-2}, rather than as a single number (Figure S10).

Accuracy was assessed against EC for both fluxes, and separately for flux partitioning via evaporative fraction, EF = $\lambda E/(\lambda E + H)$, which was used in place of the Bowen ratio because the latter is unstable near LE ≈ 0. Partitioning was restricted to daytime periods with net radiation above 75 W m^{-2} and a combined flux clear of the noise floor. The permanent LD-EC installation (RRR LI-710) was on the EC tower 6 m from the temporary cluster. It was reported in the accuracy comparison but excluded from the precision analysis and from the ensemble, because it does not share a similar footprint. Mean accuracy and ranges are presented in Table 5, while the per-unit precision for each variable is presented here in Table S5.

The cumulative sums of ET over surviving 30-minute periods are presented in Figure S8. The divergence between units amplifies the negative bias in LI-710 LE flux, but also differing data availability following the precision and accuracy masks. Over this rain-free 17-day period, the EC accumulated 20 mm of total ET, while the LI-710 averaged only 17 mm.

There are obvious limitations to this comparison. Seventeen days, one season, one biome, in early March at a semiarid shrubland site bounds the flux range sampled. Precision here is instrument repeatability; not total field uncertainty as spatial sampling error was removed by design. The benchmark ET from the EC is not error free. We should note that this test was ancillary to our primary study. The experiment was scheduled for 30+ days, but delays and the forthcoming growing season closed the testing window.

Text S3. Sensitivity of VBR estimates to sonic temperature variance

Sonic temperature differs from air temperature because the speed of sound is affected by water vapor. Consequently, fluctuations in sonic temperature T_s include a humidity contribution, and the standard deviation of sonic temperature σ_{T_s} is not strictly identical to that of air temperature σ_T. Previous field studies, however, have shown that the two variances are generally similar (Liu et al., 2001). Across the present network, direct high-frequency reconstruction of air temperature was possible at sites equipped with IRGASON systems, where sonic temperature and water vapor were measured synchronously within the same integrated measurement system. These sites therefore provided an opportunity to evaluate the use of σ_{T_s} as a practical proxy for σ_T in the VBR calculation.

At each IRGASON site, high-frequency air temperature was reconstructed by correcting sonic temperature for the effect of water-vapor fluctuations. Half-hourly air-temperature standard deviation was then calculated from the corrected high-frequency series and used in the original VBR formulation. These VBR estimates were compared with otherwise identical estimates in which σ_{T_s} was substituted for σ_T. Agreement between the two implementations was evaluated using the coefficient of determination (R^2), root-mean-square deviation (RMSD), and mean bias of the resulting latent heat flux estimates (Table S3).

Differences between the two implementations were small across all evaluated sites. R^2 ranged from 0.964 to 0.998, RMSD ranged from 2.21 to 19.0 W m^2, and mean bias ranged from 0.332 to 0.738 W m^2. The RMSD associated with using sonic-temperature variance was substantially smaller than the discrepancies observed among the ET methods in the main intercomparison. It was also smaller than the MDS-based random uncertainty estimated for VBR at all sites except the two OSU orchard sites, where it was only moderately larger. Systematic differences remained minimal at all sites, as indicated by mean biases below 1 W m^2. These results indicate that the use of σ_{T_s} as a proxy for σ_T introduces relatively minor uncertainty compared with the broader methodological uncertainty evaluated in this study. We therefore considered σ_{T_s} a suitable practical proxy for σ_T for the network-wide VBR implementation (i.e., VBR-Ts).

Supplementary Figures

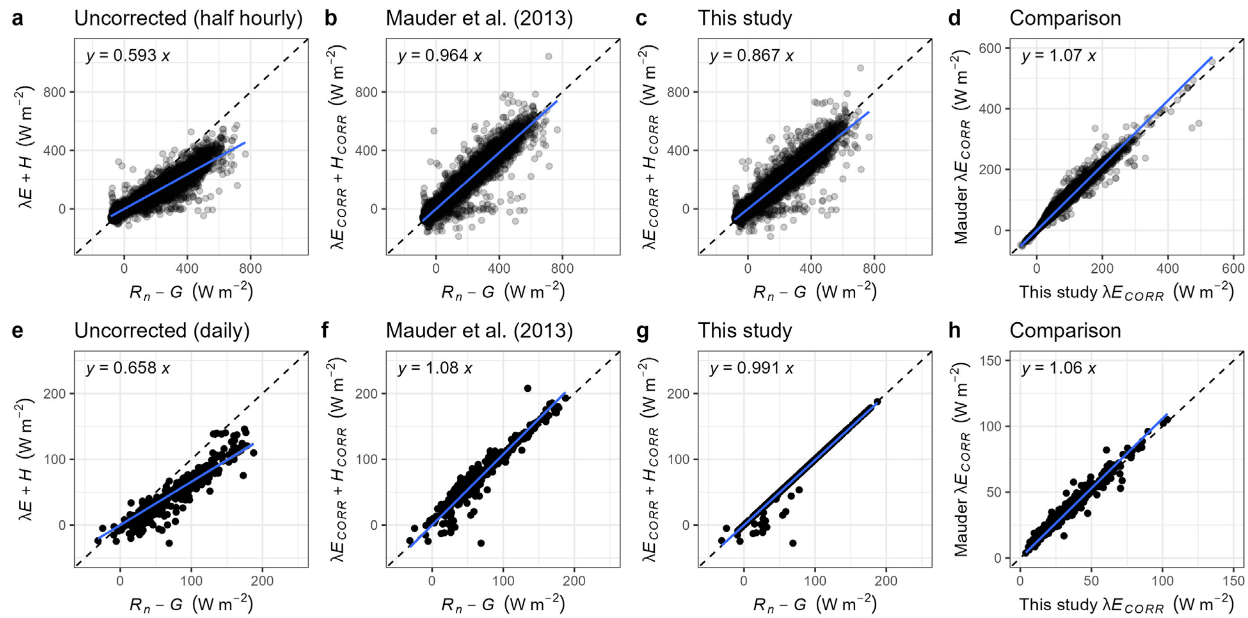

Figure S1. Comparison of the conventional daytime energy-balance correction of Mauder et al. (2013) with the storage-constrained correction used in this study at the RRR site.

Panels (a–d) show half-hourly values, and panels (e–h) show daily mean fluxes. Uncorrected turbulent heat fluxes are compared with available energy ($R_n - G$) in (a) and (e). Panels (b) and (f) show latent and sensible heat fluxes corrected using the Mauder et al. (2013) approach, which forces daytime closure while leaving nighttime fluxes unchanged. Panels (c) and (g) show the correction used in this study, in which nighttime energy imbalance is treated as apparent heat storage and used to constrain the amount of available energy assigned to daytime turbulent fluxes. Panels (d) and (h) directly compare corrected latent heat fluxes from the two approaches. Blue lines show zero-intercept ordinary least-squares regressions, with equations reported in each panel; dashed lines indicate the 1:1 relationship.

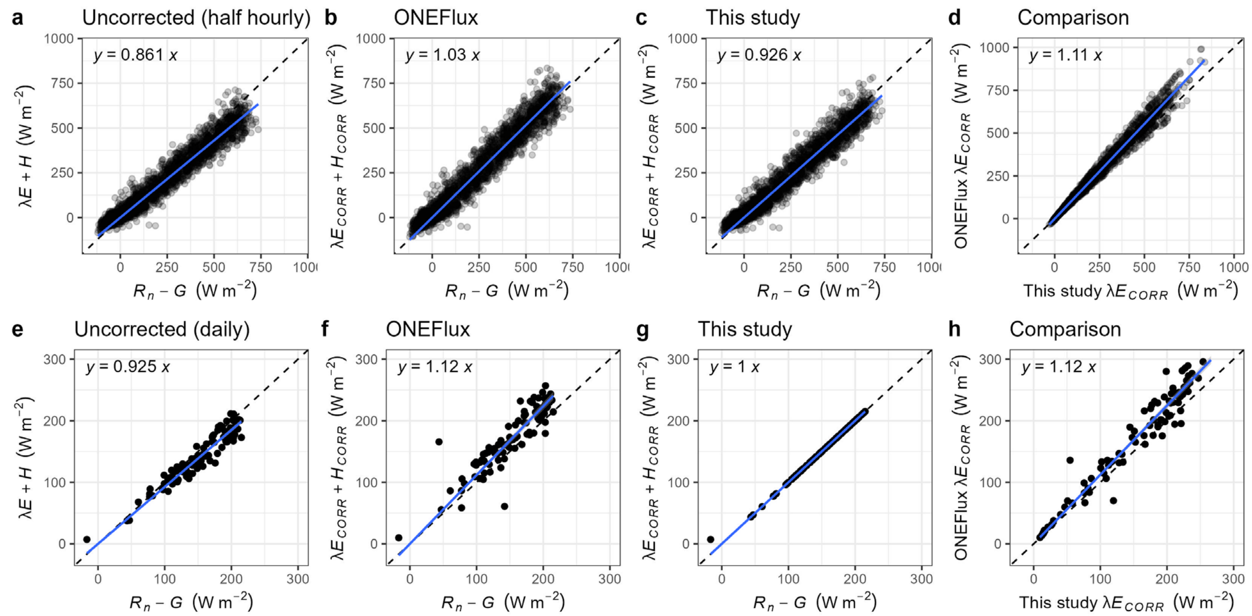

Figure S2. Comparison of half hourly ONEFlux energy-balance correction of Pastorello et al. (2020) with the storage-constrained correction used in this study at the SF3 site.

Panels (a–d) show half-hourly values, and panels (e–h) show daily aggregated fluxes from half-hourly values. Uncorrected turbulent heat fluxes are compared with available energy ($R_n - G$) in (a) and (e). Panels (b) and (f) show latent and sensible heat fluxes corrected using the ONEFlux approach. Panels (c) and (g) show the correction used in this study, in which nighttime energy imbalance is treated as apparent heat storage and used to constrain the amount of available energy assigned to daytime turbulent fluxes. Panels (d) and (h) directly compare corrected latent heat fluxes from the two approaches. Blue lines show zero-intercept ordinary least-squares regressions, with equations reported in each panel; dashed lines indicate the 1:1 relationship.

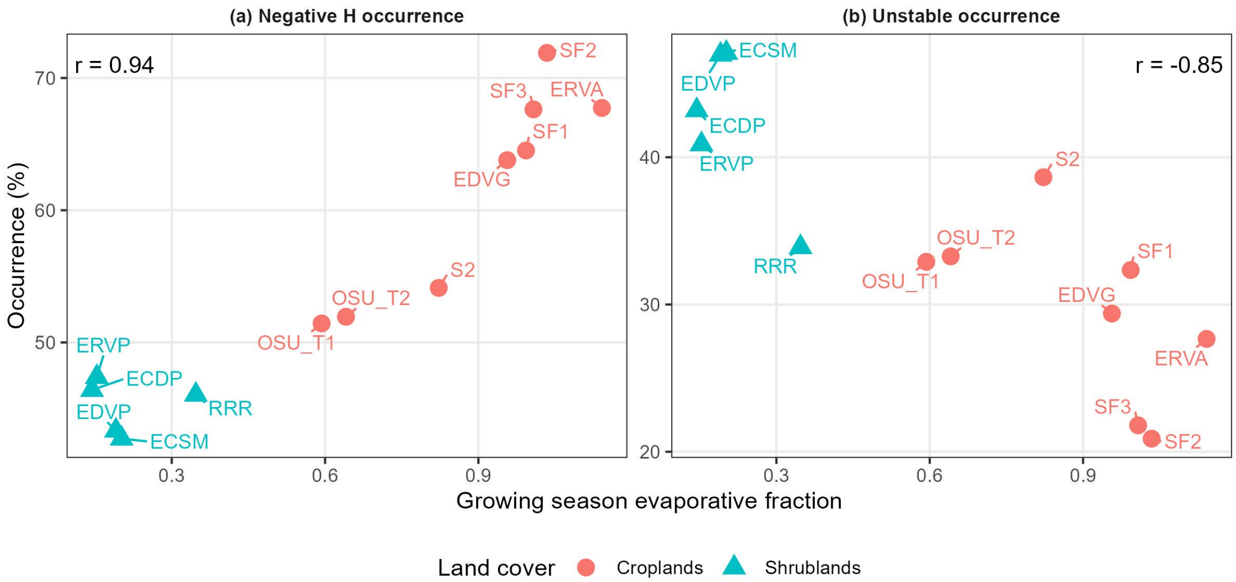

Figure S3. Relationships between growing season evaporative fraction (EF) and (a) negative sensible heat flux occurrence and (b) unstable atmospheric condition occurrence across study sites.

Occurrence was calculated from growing season half-hourly observations, with negative sensible heat flux defined $H < 0$ as and unstable conditions as $\xi < -0.04$. Symbols and colors distinguish cropland and shrubland sites, site labels identify individual sites and indicate the Pearson correlation coefficient (r) across all sites.

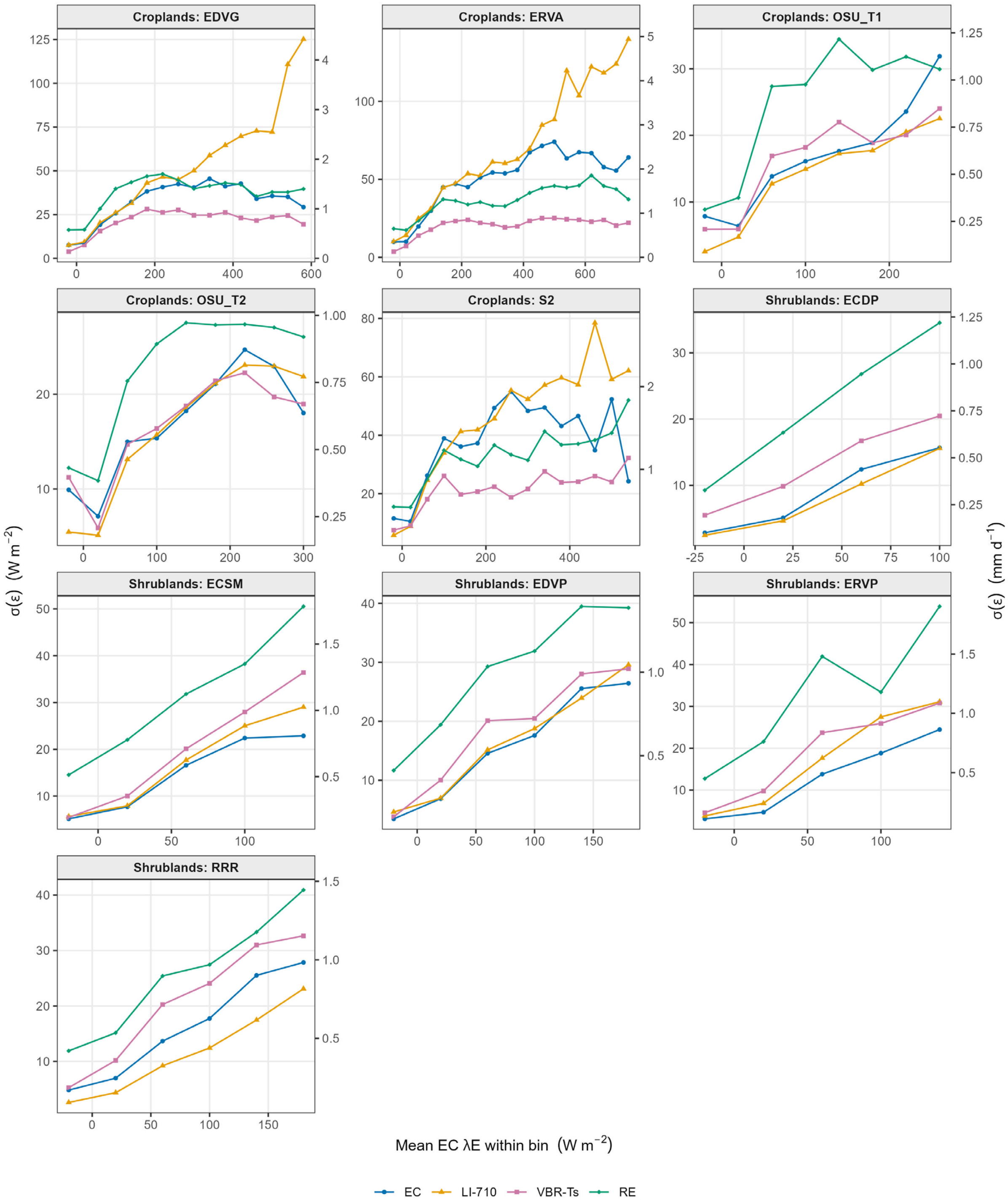

Figure S4. Site-specific dependence of half-hourly random uncertainty on eddy-covariance latent heat flux.

At each site, observations were grouped into equal-width bins according to measured EC latent heat flux. Symbols indicate random uncertainty, $\sigma(\varepsilon)$, within each bin for EC, LI-710, VBR-Ts, and RE. The x-coordinate represents the mean EC λE within each bin. The secondary y-axis expresses uncertainty as an equivalent ET rate.

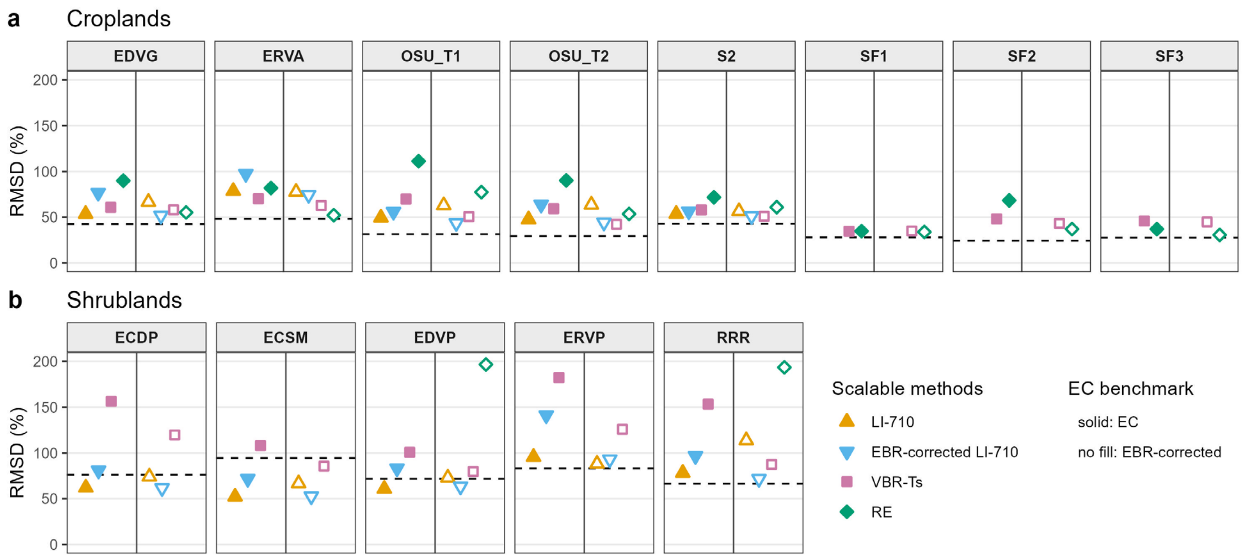

Figure S5. Relative site-level agreement of lower-cost ET methods with EC benchmarks at the half-hourly timescale.

Root-mean-square deviation (RMSD) was normalized by the mean ET magnitude of the corresponding EC benchmark and expressed as a percentage for (a) cropland and (d) shrubland sites. Symbols represent LI-710, energy balance ratio (EBR)-corrected LI-710, VBR-Ts, and RE estimates. Filled symbols show percent RMSE relative to measured EC, normalized by mean measured EC ET, whereas open symbols show percent RMSD relative to EBR-corrected EC, normalized by mean EBR-corrected EC ET. Values exceeding 200% (e.g., RE estimates at several shrubland sites) fall outside the displayed range and are omitted for visual clarity.

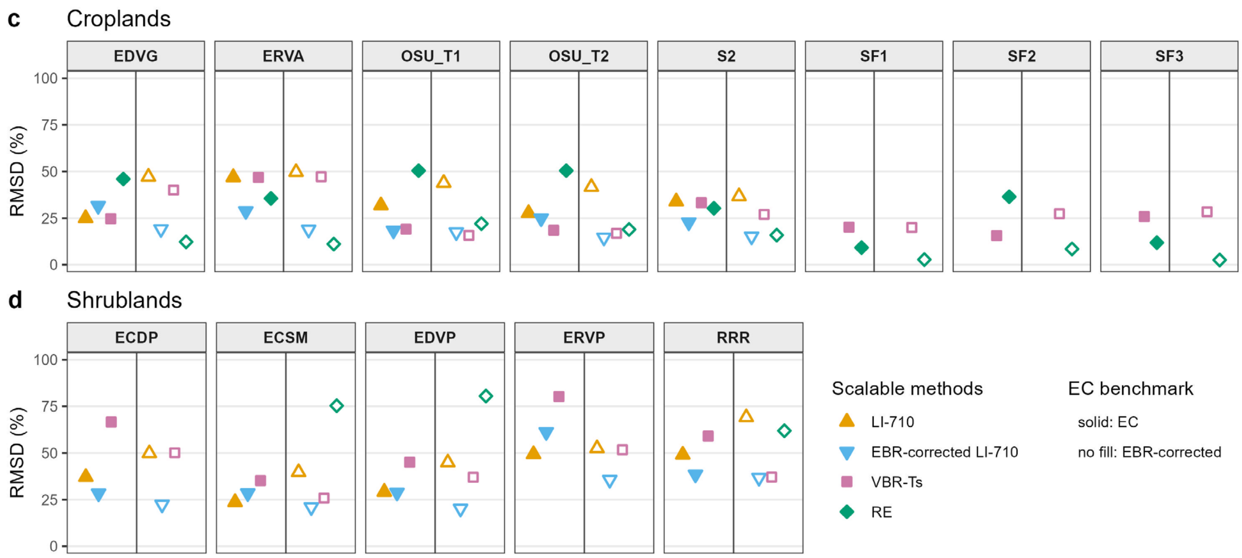

Figure S6. Relative site-level agreement of lower-cost ET methods with EC benchmarks at the daily timescale.

Root-mean-square deviation (RMSD) was normalized by the mean daily ET magnitude of the corresponding EC benchmark and expressed as a percentage for (a) cropland and (d) shrubland sites. Filled symbols show percent RMSE relative to measured EC, normalized by mean measured EC ET, whereas open symbols show percent RMSD relative to EBR-corrected EC, normalized by mean EBR-corrected EC ET. Values exceeding 100% (e.g., RE estimates at several shrubland sites) fall outside the displayed range and are omitted for visual clarity.

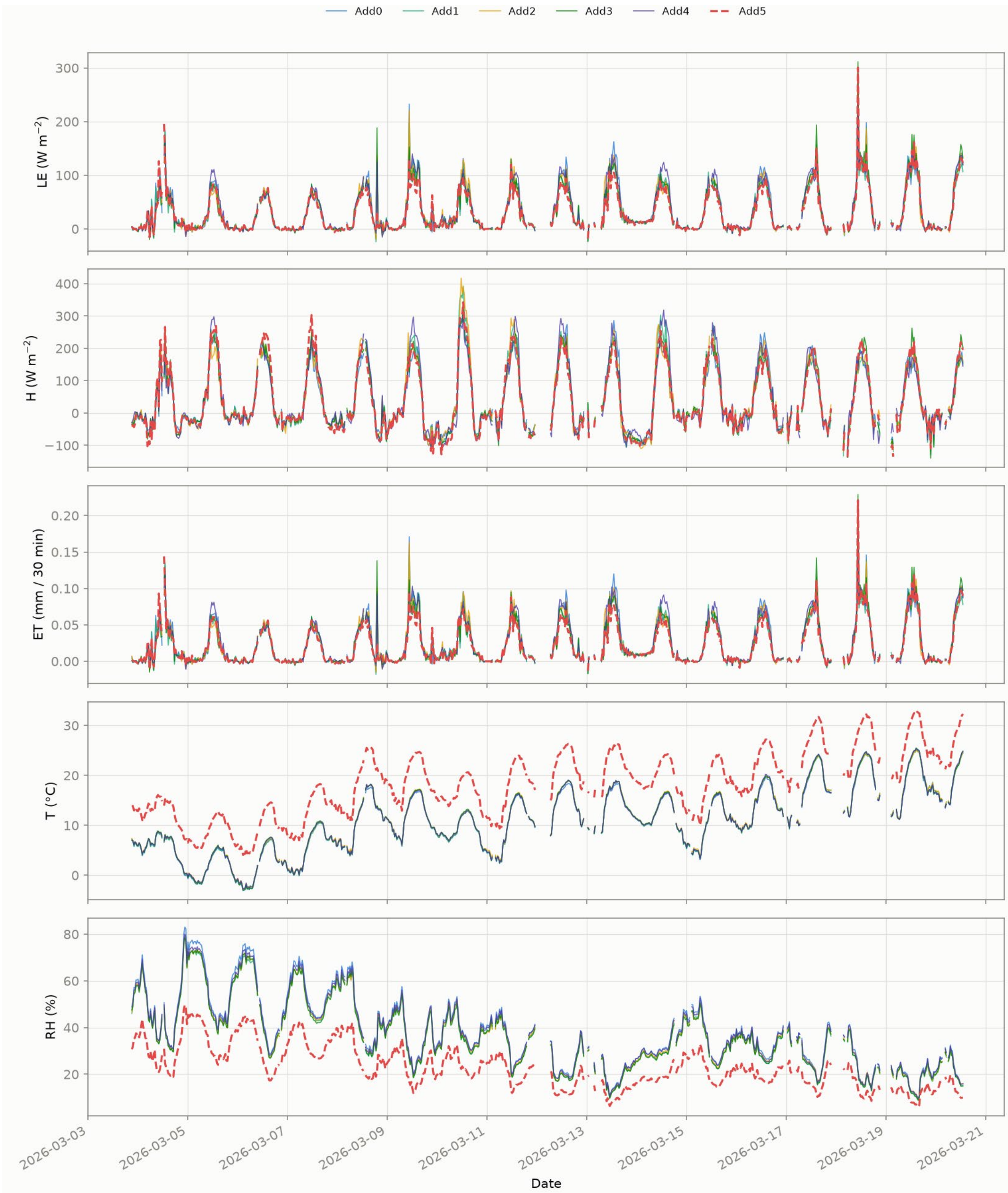

Figure S7. Time series of fluxes from the side-by-side LI-710 accuracy and precision test at RRR. Half-hourly, quality-controlled time series of all six units over the 17-day window. The outlier (Add5) was excluded from the ensemble. Its offset is visible in the temperature and humidity panels.

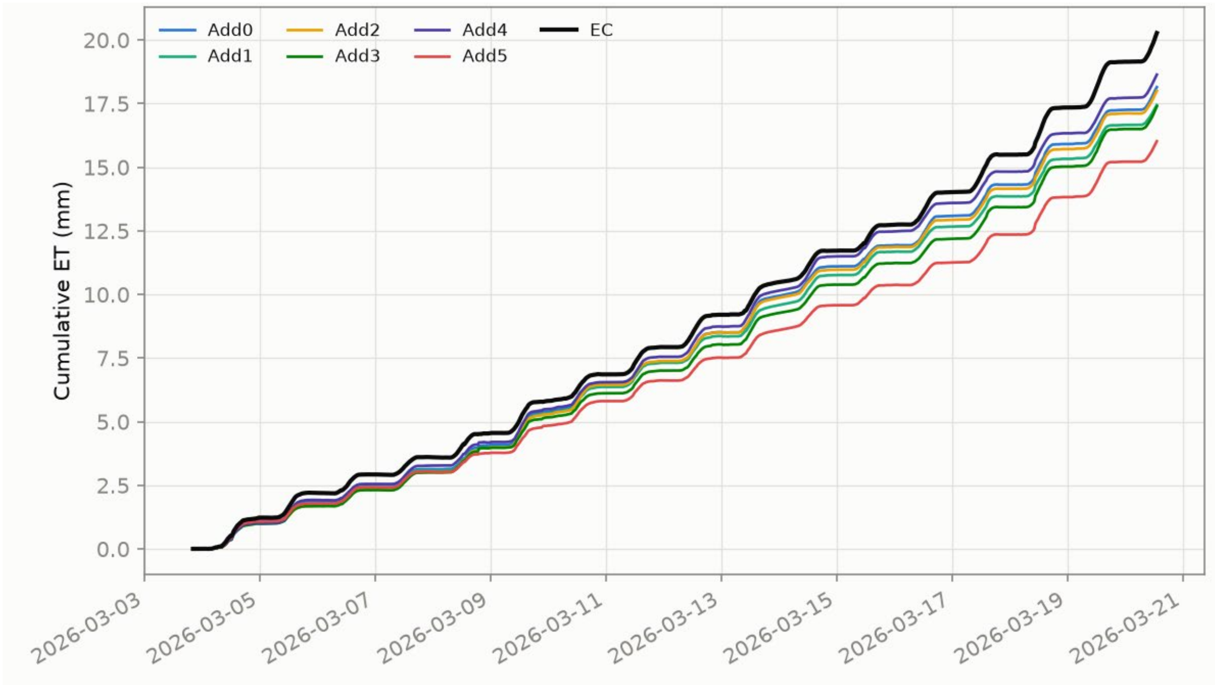

Figure S8. Cumulative evapotranspiration over the 17-day window, per unit and for EC.

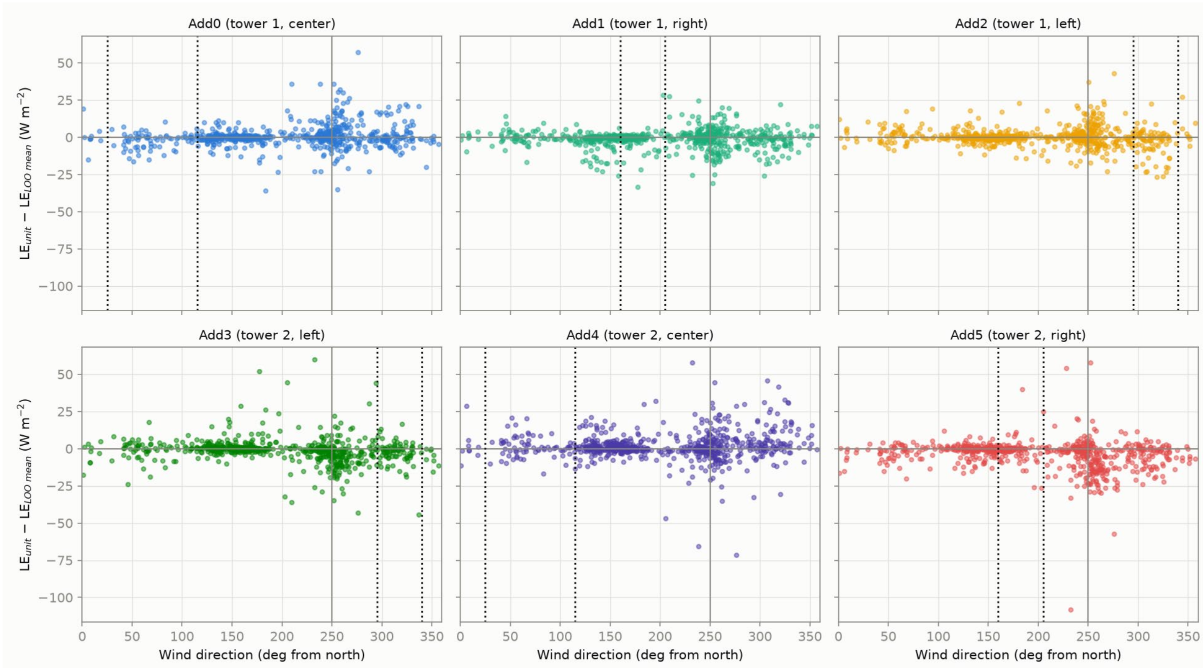

Figure S9. Deviation from the reference against wind direction, by unit. The solid line marks the predominant wind direction; dotted lines mark that unit's own neighbor-wake bearings.

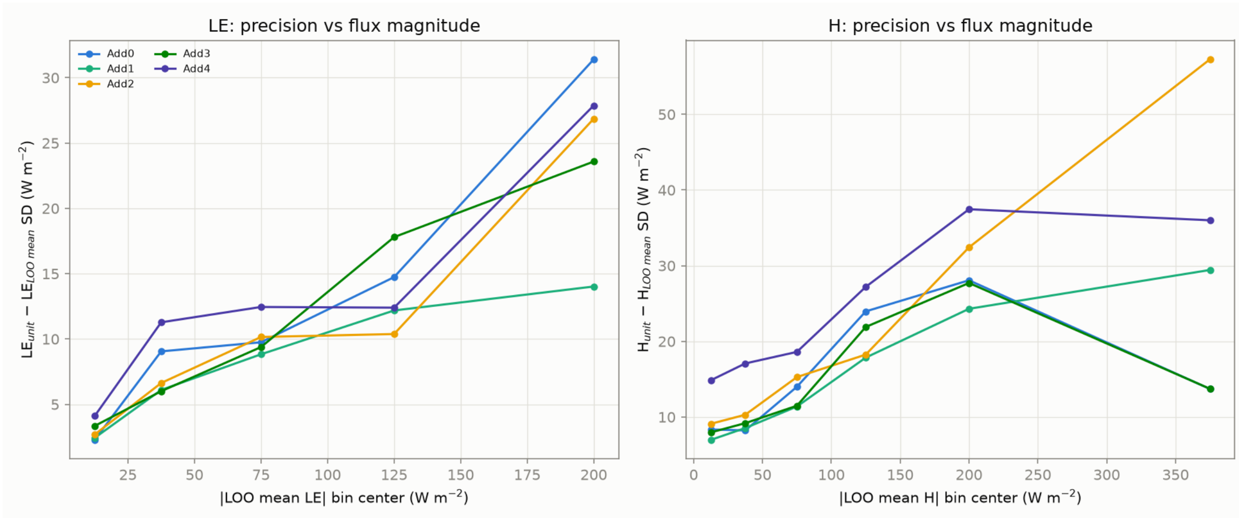

Figure S10. Between-unit residual standard deviation binned by leave-one-out (LOO) mean flux magnitude, for LE (left) and H (right).

Supplementary Tables

Table S1. Instrumentation and deployment configurations at each study site.

Site ID	EC and Lower-cost ET	Net Radiometer and Soil Heat Flux Plates	Soil Temperature and Moisture	Additional Sensors
ERVP	IRGASON LI-710	CNR4 4 HFP01 at 8 cm	2 TCAV 2 CS655 depths 0~8 cm	HMP155 humidity and temperature probe/ RM Young 05103 anemometer/ TE525 tipping bucket/ Pluvio2 bulk precipitation
ECDP	IRGASON LI-710	CNR4 6 HFP01 at 8 cm	3 TCAV 3 CS655 depths 0~8 cm	HMP155 humidity and temperature probe/ RM Young 05103 anemometer/ TE525 tipping bucket/ Pluvio2 bulk precipitation/ Teros 12 and 54 soil sensors
EDVP	IRGASON LI-710	CNR4 6 HFP01 at 8 cm	3 TCAV 3 CS655 depths 0~8 cm	HMP155 humidity and temperature probe/ RM Young 05103 anemometer/ TE525 tipping bucket/ Pluvio2 bulk precipitation/ Teros 12 and 54 soil sensors
ECSM	IRGASON LI-710	CNR4 6 HFP01 at 5 cm	3 TCAV 3 CS655 depths 0~5 cm	HMP155 humidity and temperature probe/ RM Young 05103 anemometer/ TE525 tipping bucket/ Pluvio2 bulk precipitation/ Teros 12 and 54 soil sensors
RRR	LI7500 CSAT LI-710 ATMOS 51	CNR4 4 HFP01 at 8 cm	2 TCAV 2 CS655 depths 0~5 cm	HMP155 humidity and temperature probe/ RM Young 05103 anemometer/ TE525 tipping bucket
EDVG	IRGASON LI-710	CNR4 4 HFP01 at 8 cm	3 TCAV 3 CS655 depths 0~8 cm	HMP155 humidity and temperature probe/ RM Young 05103 anemometer/ TE525 tipping bucket/ SG400 bulk precipitation
ERVA	IRGASON LI-710	CNR4 4 HFP01 at 8 cm	2 TCAV 2 CS655 depths 0~8 cm	HMP155 humidity and temperature probe/ RM Young 05103 anemometer/ TE525 tipping bucket
S2	LI7500 CSAT LI-710	CNR4 3 HFP01 at 8 cm	2 TCAV 2 CS655 depths 0~8 cm	HMP155 humidity and temperature probe/ RM Young 05103 anemometer/ TE525 tipping bucket
OSU_ T1	IRGASON LI-710	NR01 3 HFP01 at 16 cm	3 TCAV at 4,8,12,16 cm 3 CS655 at 8 cm depths 0~x cm	HygroVue 10 temperature and humidity probe/TE525 tipping bucket/ Teros 10, 12 and 21 sensors
OSU_ T2	IRGASON LI-710	NR01 3 HFP01 at 16 cm	3 TCAV at 4,8,12,16 cm 3 CS655 at 8 cm depths 0~x cm	HygroVue 10 temperature and humidity probe/TE525 tipping bucket/ Teros 10, 12 and 21 sensors
SF1	LI7500DS WindMaste ATMOS 51	SN500 2 HFP01SC at 8 cm	1 TCAV at depths 2 cm and 5 cm 2 CS655 at depth 5 cm	HygroVue 5 temperature and humidity probe/TE525MM tipping bucket/ Teros 54 sensor (depths 15, 30, 45, and 60 cm)
SF2	LI7500DS WindMaster / ATMOS51	NR01 2 HFP01SC at 8 cm	1 TCAV at depths 2 cm and 5 cm 2 CS655 at depth 5 cm	HygroVue 5 temperature and humidity probe/TE525MM tipping bucket/ Teros 54 sensor (depths 15, 30, 45, and 60 cm)
SF3	LI7500DS WindMaster	SN500 2 HFP01SC at 8 cm	1 TCAV at depths 2 cm and 5 cm 2 CS655 at depth 5 cm	HygroVue 5 temperature and humidity probe/TE525MM tipping bucket/ Teros 54 sensor (depths 15, 30, 45, and 60 cm)

Table S2. Standard output variables, units and description of the 30-minute output from the LI-710 limited diagnostic eddy covariance sensor.

Variable	Units	Description
ET_710	mm / 30 min	Evapotranspiration
LE_710	W m^{-2}	Latent heat flux
H_710	W m^{-2}	Sensible heat flux
Atm_press	kPa	Ambient (barometric) pressure
AirTC	°C	Ambient air temperature
RH_710	%	Ambient relative humidity
seq_num	#	Measurement sequence number
sample_count	#	High-frequency samples per 30-min averaging period
diag	0-65535	16-bit diagnostic code
pump_voltage	V	Pump motor voltage
cell_pressure	kPa	Optical cell pressure
cell_RH	%	Optical cell relative humidity
cell_temp	°C	Optical cell temperature
enclosure_RH	%	Sensor enclosure relative humidity
flow	cm^3 min^{-1}	Pump flow rate
input_vol	V	Sensor supply voltage
data_qc	%	Percentage of raw points discarded in processing
abs_hum_amb	g m^{-3}	Ambient absolute humidity
RH_710_amb	%	Ambient RH, secondary/derived channel
SVP_amb	kPa	Saturation vapor pressure, ambient
VPD	kPa	Vapor pressure deficit
Atm_Press_2	kPa	Secondary ambient pressure channel
air_temp_ns	°C	Air temperature, alternate/non-sonic path
dew_point_temp	°C	Dew point temperature
tilt	deg (0-180)	Sensor tilt from vertical

Table S3. Comparison of VBR latent heat flux estimates calculated using sonic-temperature and humidity-corrected air-temperature variances at IRGASON sites. Agreement was evaluated using R^2, RMSD, and mean bias.

Land cover	**Site**	**R^2**	**RMSD (W m^{-2})**	**Mean bias (W m^{-2})**
Croplands	EDVG	0.997	6.51	0.332
Croplands	ERVA	0.998	5.61	0.398
Croplands	OSU_T1	0.964	18.0	0.377
Croplands	OSU_T2	0.971	19.0	0.447
Shrublands	ERVP	0.971	5.33	0.459
Shrublands	ECDP	0.996	2.21	0.711
Shrublands	EDVP	0.993	3.47	0.695
Shrublands	ECSM	0.996	3.05	0.738

Bias was calculated as VBR latent heat flux based on humidity-corrected air temperature minus VBR latent heat flux based on sonic temperature.

Table S4. Per-unit precision against the leave-one-out mean, all variables (n = 732 half-hours). Offset and residual standard deviation (SD) are in each variable's units. Add5* was removed from the reference pool, so it is compared against the mean of the other five while each pool member is compared against the other four.

Unit	Variable	Reference units in pool	Slope	Offset	Residual SD	Residual MAD
Add0	H (W m^{-2})	4	0.933	0.716	16.708	10.866
Add1	H (W m^{-2})	4	1.036	-0.064	14.821	9.904
Add2	H (W m^{-2})	4	1.021	-0.689	19.459	12.409
Add3	H (W m^{-2})	4	1.000	-1.690	16.308	10.582
Add4	H (W m^{-2})	4	1.065	-0.508	24.668	18.048
Add5*	H (W m^{-2})	5	1.032	-3.611	17.365	11.749
Add0	LE (W m^{-2})	4	1.044	-0.969	7.354	2.566
Add1	LE (W m^{-2})	4	0.973	-0.210	6.186	2.580
Add2	LE (W m^{-2})	4	1.018	-0.427	6.562	2.576
Add3	LE (W m^{-2})	4	1.001	-1.279	8.083	2.964
Add4	LE (W m^{-2})	4	1.016	1.165	9.580	3.989
Add5*	LE (W m^{-2})	5	0.912	-0.577	8.208	2.752
Add0	P (kPa)	4	1.000	-0.036	0.008	0.007
Add1	P (kPa)	4	1.003	-0.351	0.007	0.007
Add2	P (kPa)	4	1.003	-0.284	0.015	0.015
Add3	P (kPa)	4	0.996	0.422	0.012	0.013
Add4	P (kPa)	4	0.998	0.171	0.005	0.005
Add5*	P (kPa)	5	0.998	0.200	0.010	0.011
Add0	RH (%)	4	1.046	-0.142	0.357	0.374
Add1	RH (%)	4	0.988	-0.372	0.420	0.420
Add2	RH (%)	4	0.980	0.373	0.382	0.369
Add3	RH (%)	4	0.985	-0.477	0.360	0.285
Add4	RH (%)	4	1.003	0.583	0.300	0.260
Add5*	RH (%)	5	0.622	0.190	0.309	0.256
Add0	T (°C)	4	0.997	-0.146	0.146	0.156
Add1	T (°C)	4	1.003	-0.076	0.177	0.197
Add2	T (°C)	4	0.995	0.185	0.125	0.119
Add3	T (°C)	4	1.004	0.014	0.163	0.145
Add4	T (°C)	4	1.002	0.015	0.136	0.130
Add5*	T (°C)	5	1.036	6.914	0.188	0.214

Table S5. Per-unit accuracy against the eddy covariance fluxes (latent heat, LE, and sensible heat, H) and daytime evaporative fraction (EF), as measured (unclosed).

Unit	Flux	n	Slope	Intercept	MBE	RMSD (flux) or SD (EF)
Add0	LE (W m^{-2})	731	0.900	-0.26	-4.01	16.10
Add1	LE (W m^{-2})	731	0.851	0.30	-5.28	16.94
Add2	LE (W m^{-2})	731	0.884	0.09	-4.25	15.82
Add3	LE (W m^{-2})	731	0.864	-0.37	-5.45	15.98
Add4	LE (W m^{-2})	731	0.890	1.13	-3.00	14.15
Add5	LE (W m^{-2})	731	0.781	0.23	-7.96	17.22
RRR LI-710	**LE (W m^{-2})**	**480**	**0.746**	**-0.66**	**-8.34**	**17.82**
Add0	H (W m^{-2})	731	0.866	-4.78	-11.69	29.78
Add1	H (W m^{-2})	731	0.942	-5.82	-8.82	24.22
Add2	H (W m^{-2})	731	0.932	-6.32	-9.81	27.93
Add3	H (W m^{-2})	731	0.915	-7.00	-11.36	26.58
Add4	H (W m^{-2})	731	0.965	-6.45	-8.24	27.26
Add5	H (W m^{-2})	731	0.943	-9.35	-12.29	27.49
RRR LI-710	**H (W m^{-2})**	**480**	**0.840**	**-3.63**	**-7.55**	**22.06**
Add0	EF	302	1.149	-0.034	0.0185	0.0887
Add1	EF	301	1.141	-0.056	-0.0060	0.0826
Add2	EF	302	1.163	-0.049	0.0081	0.0839
Add3	EF	300	1.008	-0.014	-0.0113	0.0762
Add4	EF	301	1.290	-0.108	-0.0057	0.1098
Add5	EF	301	1.084	-0.053	-0.0237	0.0763
RRR LI-710	**EF**	**158**	**1.072**	**-0.048**	**-0.0204**	**0.0651**